

SIMULATION OF OPTICAL FIBER COMMUNICATION SYSTEM WITH POLARIZATION MODE DISPERSION

by

Bin Lu

B.Eng., Dalian University of Technology, 1996

A Thesis Submitted in Partial Fulfilment of
the Requirements for the Degree of

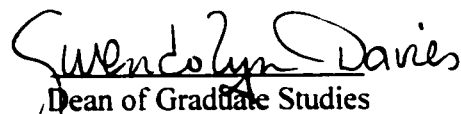
Master of Science in Engineering

in the Department of Electrical and Computer Engineering

Supervisor: Brent R. Petersen, BEng, MSc, PhD, ECE, Asst Prof

Examining Board: Bruce G. Colpitts, BScE, MScE, PhD, PEng, ECE, Prof, Chair
John M. DeDourek, BS, MS, Computer Science, Prof
Richard J. Tervo, BSc, MSc, PhD, PEng, ECE, Prof
David H. Thorne, BScE, MScE, PEng, ECE

This thesis is accepted.


Swendolyn Davies
Dean of Graduate Studies

THE UNIVERSITY OF NEW BRUNSWICK

September, 2000

© Bin Lu, 2000

This thesis is dedicated to my parents,

Yongwei Lu and Xiaoyun Ding,

and sisters, Jing Lu and Ying Lu.

ABSTRACT

This thesis is about the simulation of optical fiber communication systems with the effect of PMD (Polarization Mode Dispersion) and the application of adaptive channel equalizers, CPI (Cross Polarization Interference) cancellers and echo cancellers which are used to mitigate PMD.

The basic structure of this system is that two QAM signals are transmitted through a long optical fiber with PMD and they are received by a coherent receiver which consists of adaptive electrical channel equalizers and adaptive electrical CPI cancellers. The echo in a bidirectional transmission system is studied and adaptive echo cancellers are used to cancel it.

The objective of this thesis is to create the system structure, to simulate the optical fiber channel with PMD, to simulate the adaptive channel equalizers, CPI cancellers and echo cancellers and to evaluate the system performance.

ACKNOWLEDGEMENTS

I would like to express my profound gratitude and high regards to professor Brent R. Petersen. His encouragement, friendship and suggestions during the course of this research have played a vital role.

I also would like to express the deepest feeling of gratitude to my parents, Yong Wei Lu and Zhao Yun Ding for their support and love.

LIST OF CONTENTS

Abstract	iii
Acknowledgements	iv
List of Contents	v
List of Tables	vii
List of Figures	viii
List of Symbols	x
List of Abbreviations and Acronyms	xvi
Chapter 1. Introduction	1
1.1 Introduction to the Research	1
1.2 Thesis Contributions	3
1.3 Thesis Outline	4
Chapter 2. System Simulation Model	7
2.1 System Model	7
2.2 Baseband Simulation and Coherent Demodulation	13
2.3 Baseband System Model	15
2.3 System Development Tools: MATLAB [®] and SIMULINK [®]	18
Chapter 3. Polarization Mode Dispersion	19
3.1 What is PMD?	19
3.1.1 Birefringence and PMD	19
3.1.2 Mode Coupling in Long Fiber	21
3.2 Principal States of Polarization	22
3.3 Waveplate Model	26
3.4 Computer Simulation of PMD	28
3.5 Channel Simulation using MATLAB [®] and SIMULINK [®]	31
Chapter 4. Adaptive Channel Equalizers and CPI Cancellers	33
4.1 Adaptive Channel Equalization Technique	33
4.1.1 Fundamentals of Equalization	33
4.1.2 Adaptive Equalization	35

4.1.3 Adaptive Equalization Categorization and Algorithm	36
4.2 Channel Equalization and CPI Cancellation	39
4.3 Simulation of Channel Equalizers and CPI Cancellers	46
4.3.1 Simulation Structure of Channel Equalizers and CPI Cancellers	46
4.3.2 Performance of Channel Equalizers and CPI Cancellers	48
Chapter 5. System Performance	50
5.1 Eye Pattern	50
5.2 Bit Error Rate Evaluation	51
Chapter 6. Bidirectional Transmission System	59
6.1 Bidirectional Transmission System	59
6.1.1 Fiber Coupler	60
6.1.2 Rayleigh Backscatter	61
6.2 Echo Cancellation	63
6.3 Power Budget	64
6.3.1 Power Budget of the System without Echo Cancellers	65
6.3.2 Power Budget of the System with Echo Cancellers	66
6.4 Simulation of Echo Cancellers Using SIMULINK®	67
Chapter 7. Conclusions	69
7.1 Conclusions	69
7.2 Future Work	70
References	71
Appendix A. SIMULINK® Simulation Models	75
Appendix B. MATLAB® Source Code	89

LIST OF TABLES

Table 5.1	J_{min} (dB) when DGD is 10 ps	53
Table 5.2	J_{min} (dB) when DGD is 100 ps	54
Table 5.3	J_{min} (dB) when DGD is 500 ps	56
Table 6.1	WD1515 series: 1538/1558nm Bidirectional Coupler	61
Table A.1	Parameters of System Model	75
Table A.2	Parameters of Transmitter_A/B	76
Table A.3	Parameters of Transmitter.....	77
Table A.4	Parameters of Channel	78
Table A.5	Parameters of Impulse Response	80
Table A.6	Parameters of Gaussian Noise	81
Table A.7	Parameters of Baseband Demodulation.....	82
Table A.8	Parameters of Adaptive Channel Equalizers, CPI Cancellers and Echo Cancellers	84
Table A.9	Parameters of Normalized LMS Adaptive Filter.....	85
Table A.10	Parameters of Decision Circuit.....	86
Table A.11	Parameters of Performance Meter.....	87
Table A.12	Parameters of Square Error Trend.....	88

LIST OF FIGURES

Figure 2.1	Passband System Model	8
Figure 2.2	Impulse Response of RC Filter.....	12
Figure 2.3	Baseband System Model	16
Figure 3.1	PMD and DGD	20
Figure 3.2	PDF of $\Delta\tau$	25
Figure 3.3	Waveplate Model	27
Figure 3.4	Magnitudes of Frequency Response	29
Figure 3.5	Phases of Frequency Response	29
Figure 3.6	Magnitudes of Impulse Response	30
Figure 3.7	Phases of Impulse Response	30
Figure 3.8	Interferometric Measurement of the 10-ps PMD Emulator	31
Figure 3.9	Optical Fiber Channel Simulation	32
Figure 3.10	Simulation of Baseband Impulse Responses	32
Figure 4.1	Equalization	34
Figure 4.2	Categorization of Adaptive Equalization	36
Figure 4.3	Linear LMS Transversal Equalizer	37
Figure 4.4	Channel Equalizers and CPI Cancellers	39
Figure 4.5	Vertical Channel Equalizers and CPI Cancellers	41
Figure 4.6	LMS Adaptive Filter	47
Figure 4.7	Adaptive Channel Equalizers and CPI Cancellers	48
Figure 4.8a	J (dB) when $\mu=0.2$	49
Figure 4.8b	J (dB) when $\mu=0.4$	49
Figure 4.8c	J (dB) when $\mu=0.6$	49
Figure 4.9a	J (dB) when Filter Length=16	49
Figure 4.9b	J (dB) when Filter Length=8	49
Figure 5.1	Fully Open Eye Pattern	50
Figure 5.2	Eye Pattern (SNR=30)	51
Figure 5.3	Eye Pattern (SNR=15)	51
Figure 5.4	BER Plot	58
Figure 6.1	Bidirectional Transmission System	59
Figure 6.2	Fiber Coupler	60
Figure 6.3	A Possible Backscatter Plot	62
Figure 6.4	Echo Cancellation	63
Figure 6.5	Structure of Echo Cancellers	64
Figure 6.6	Power Budget	64
Figure 6.7	Simulation of Echo Cancellers	67
Figure 6.8	Eye Pattern without Echo Cancellers	68
Figure 6.9	Eye Pattern with Echo Cancellers	68
Figure A.1	System Model	71
Figure A.2	Transmitter_A	72
Figure A.3	Transmitter	73

Figure A.4	Channel	74
Figure A.5	Optical Fiber Channel with PMD	75
Figure A.6	Impulse response	76
Figure A.7	Gaussian Noise	77
Figure A.8	Baseband Demodulation	78
Figure A.9a	Receiver with Echo Cancellers	79
Figure A.9b	Receiver without Echo Cancellers	79
Figure A.10a	Adaptive Channel Equalizers and CPI Cancellers	80
Figure A.10b	Echo Cancellers	80
Figure A.11	Normalized LMS Adaptive Filter	81
Figure A.12	Decision Circuit	82
Figure A.13	Performance Meter	83
Figure A.14	Square Error Trend	84

LIST OF SYMBOLS

$\mathbf{a}(n)$	real part of the tap weight $\mathbf{c}(n)$. See Eqs. (4.20, 4.21).
$\mathbf{A}_h(n)$	input PAM signal in the horizontal channel.
$\mathbf{A}_v(n)$	input PAM signal in the vertical channel.
$\mathbf{b}(n)$	imaginary part of tap weight $\mathbf{c}(n)$. See Eqs. (4.20, 4.21).
B	bit rate.
B_w	bandwidth of the message signal.
c	light speed. See Eq. (3.1).
c_n	filter coefficients.
$\mathbf{c}(n)$	estimated of the equalizer tap weights at step n . See Eq. (4.13).
$c(t)$	impulse response of the equalizer. See Fig. (4.2).
$\mathbf{c}_{vv}(n), \mathbf{c}_{hh}(n)$	channel equalizers. See Fig. (4.4).
$\mathbf{c}_{vh}(n), \mathbf{c}_{hv}(n)$	CPI cancellers. See Fig. (4.4).
$\hat{\mathbf{c}}_{vv}(n)$	estimated tap-weight of the equalizer $\mathbf{c}_{vv}(n)$. See Eq. (4.44).
$\hat{\mathbf{c}}_{vh}(n)$	estimated tap-weight of the CPI canceller $\mathbf{c}_{vh}(n)$. See Eq. (4.45).
c^*, c	complex coefficients of PSPs. See Eq. (3.9).
$C(f)$	Fourier transform of $c(t)$.
$d(n)$	“desired” signal. See Eq. (4.8).
$d(\bullet)$	differential of \bullet .
D_k	phase retarder. See Eq. (3.17) and Fig. (3.3).
$e(n)$	estimated error. See Eq. (4.8).
$\mathbf{e}(n)$	estimated error vector. See Eq. (4.18).
E	input signal power. See Eq. (5.1).
$E(\bullet)$	mathematical expectation of \bullet
$\mathbf{E}_a(\omega)$	input optical field vector. See Eqs. (3.6, 3.7).
$E_a(\omega)$	amplitude of the input PSPs in frequency domain. See Eq. (3.7).
$E_b(\omega)$	amplitude of the output PSPs in frequency domain. See Eq. (3.8).
$\bar{E}_a(\omega)$	complex unit vector specifying the PSPs. See Eq. (3.7).
$\bar{E}_b(\omega)$	complex unit vector specifying the PSPs. See Eq. (3.8).
$E_a(t)$	amplitude of the time-varying input field. See Eq. (3.9).
$E_b(t)$	amplitude of the time-varying output field. See Eq. (3.9).
$\mathbf{E}_b(\omega)$	output optical field in frequency domain. See Eqs. (3.6, 3.8).
\bar{E}_+, \bar{E}_-	unit vectors specifying the two output PSPs. See Eq. (3.9).
f_c	carrier frequency. See Eq. (2.3).
f_s	sampling frequency.
$f(t)$	receiver filter. See Eqs. (2.10, 2.11) and Figs. (2.1, 2.2).
$f_a(t)$	overall complex baseband impulse response of the transmitter, channel and matched filter. See Fig. (4.1).
$F_a(f)$	Fourier transform of $f_a(t)$. See Fig. (4.1).
$g(t)$	transmitter filter. See Eqs. (2.2, 2.11) and Figs. (2.1, 2.2).
$g_a(t)$	combined impulse response of the transmitter, channel, matched filter and

	equalizer. See Eq. (4.3) and Fig. (4.1).
h	Planck's constant, 6.63×10^{-34} J/Hz. See Eq. (6.8).
$\mathbf{h}(t)$	matrix of the baseband impulse responses of the optical channel. See Eq. (4.11).
$h_b(t)$	complex baseband impulse response. See Eq. (3.21).
$\mathbf{h}_p(t)$	matrix of the passband channel impulse responses. See Eq. (2.4).
$h_{bhh}(t)$	baseband horizontal to horizontal impulse response. See Eq. (2.5).
$h_{bhv}(t)$	baseband horizontal to vertical impulse response. See Eq. (2.5).
$h_{bvh}(t)$	baseband vertical to horizontal impulse response. See Eq. (2.5).
$h_{bvv}(t)$	baseband vertical to vertical impulse response. See Eq. (2.5).
$\mathbf{h}_{hh}(t)$	matrix of the baseband horizontal to horizontal channel impulse responses. See Eq. (2.24).
$\mathbf{h}_{hv}(t)$	matrix of the baseband horizontal to vertical channel impulse responses. See Eq. (2.23).
$h_{ihh}(t)$	in-phase of passband horizontal to horizontal impulse response. See Eq. (2.5).
$h_{ihv}(t)$	in-phase of passband horizontal to vertical impulse response. See Eq. (2.5).
$h_{ivh}(t)$	in-phase of passband vertical to horizontal impulse response. See Eq. (2.5).
$h_{ivv}(t)$	in-phase of passband vertical to vertical impulse response. See Eq. (2.5).
$h_{p hh}(t)$	passband horizontal to horizontal impulse response. See Eq. (2.4) and Fig. (2.1).
$h_{p hv}(t)$	passband horizontal to vertical impulse response. See Eq. (2.4) and Fig. (2.1).
$h_{p vh}(t)$	passband vertical to horizontal impulse response. See Eq. (2.4) and Fig. (2.1).
$h_{p vv}(t)$	passband vertical to vertical impulse response. See Eq. (2.4) and Fig. (2.1).
$h_{q hh}(t)$	quadrature of passband horizontal to horizontal impulse response. See Eq. (2.5).
$h_{q hv}(t)$	quadrature of passband horizontal to vertical impulse response. See Eq. (2.5).
$h_{q vh}(t)$	quadrature of passband vertical to horizontal impulse response. See Eq. (2.5).
$h_{q vv}(t)$	quadrature of passband vertical to vertical impulse response. See Eq. (2.5).
$\mathbf{h}_{vh}(t)$	matrix of the baseband vertical to horizontal channel impulse responses. See Eq. (2.22).
$\mathbf{h}_{vv}(t)$	matrix of the baseband vertical to vertical channel impulse responses. See Eq. (2.21).
$H(\omega)$	transfer matrix of the fiber channel in the waveplate model. See Eq. (3.20).
j	imaginary number, satisfying $j^2 = -1$.

J_{min}	minimum MSE. See Eq. (5.10).
$\mathbf{J}(n)$	mean-squared error vector. See Eq. (4.19).
l_c	coupling length.
L	fiber length.
$M_k(\omega)$	DGD generator. See Eqs. (3.16, 3.17) and Fig. (3.3).
M_s	system loss.
n_f	effective index of refraction for fast mode. See Eq. (3.1).
n_s	effective index of refraction for slow mode. See Eq. (3.1).
n_1, n_2	random Gaussian noises. See Eq. (5.2).
N	number of the transmitter or receiver filter taps. See Eq. (2.2).
N_k	transfer matrix of the segment k in a single mode fiber. See Eq. (3.17).
N_p	receiver sensitivity (average number of photos per bit).
$p(\Delta\tau)$	probability density function of DGD. See Eq. (3.12).
P_b	bit error rate.
P_u	power in the starting mode. See Eq.(3.3).
$P_b(l_c)$	average power in the orthogonal polarization mode. See Eq.(3.3).
P_{ct}	crosstalk. See Eq. (6.3).
P_{dir}	directivity. See Eq. (6.4).
P_{el}	excess loss. See Eq. (6.1).
P_i	optical power launched into the fiber. See Eq. (6.6).
P_{il}	insertion loss. See Eq. (6.2).
P_{rb}	Rayleigh backscattered optical power. See Eq. (6.6).
P_{rec}	received sensitivity (dBm). See Eq. (6.8).
P_{rsl}	Rayleigh scatter loss.
P_s	symbol error probability for 4-level QAM signal. See Eq. (5.4).
P_{sr}	split ratio. See Eq. (6.5).
P_{total}	total power in the fiber. See Eq.(3.3)
P_0	power of Transmitter_B. See Fig. (6.6).
P_1	power of Transmitter_A. See Fig. (6.6).
P_2	signal power after Coupler_A. See Fig. (6.6).
P_3	signal power received by Coupler_B. See Fig. (6.6).
P_4	signal power received by Receiver_B. See Fig. (6.6).
P_5	echo signal power due to coupler crosstalk and the Rayleigh scatter. See Fig. (6.6).
$\mathbf{P}_{vv}(n)$	cross-correlation vector between the input vector to the equalizer $\mathbf{u}_v(n)$ and the desired response $x_v(n)$. See Eq. (4.29).
$\hat{\mathbf{P}}_{vv}(n)$	instantaneous estimate of $\mathbf{P}_{vv}(n)$. See Eq. (4.40).
$\mathbf{Q}_{vv}(n)$	cross-correlation vector between the input vector to the equalizer $\mathbf{u}_v(n)$ in the vertical polarization channel and the input vector in the vertical polarization channel $\mathbf{u}_h(n)$. See Eq. (4.31).
$\hat{\mathbf{Q}}_{vv}(n)$	instantaneous estimate of $\mathbf{Q}_{vv}(n)$. See Eq. (4.42).
$Q(\bullet)$	Q-function of \bullet .
r	filter rolloff factor. See Eq. (2.11) and Fig. (2.2).

R_t	phase rotator. See Eq. (3.7).
$\mathbf{R}_{vv}(n)$	auto-correlation matrix of the input vector to the equalizer $\mathbf{u}_v(n)$. See Eq. (4.30).
$\hat{\mathbf{R}}_{vv}(n)$	instantaneous estimate of $\mathbf{R}_{vv}(n)$. See Eq. (4.41).
$\mathbf{s}_{bh}(t)$	baseband signal vector in horizontal channel. See Eq. (2.19) and Fig. (2.3).
$\mathbf{s}_{bv}(t)$	baseband signal vector in vertical channel. See Eq. (2.19) and Fig. (2.3).
$s_h(t)$	modulated signal after the modulator in the horizontal channel. See Eq. (2.3) and Fig. (2.1).
$s_{ih}(t)$	in-phase signal after the transmitter filter in the horizontal channel. See Eq. (2.2) and Figs. (2.1, 2.3).
$s_{iv}(t)$	in-phase signal after the transmitter filter in the vertical channel. See Eq. (2.2) and Figs. (2.1, 2.3).
$s_{qh}(t)$	quadrature signal after the transmitter filter in the horizontal channel. See Eq. (2.2) and Figs. (2.1, 2.3).
$s_{qv}(t)$	quadrature signal after the transmitter filter in the vertical channel. See Eq. (2.2) and Figs. (2.1, 2.3).
$s_v(t)$	modulated signal after the modulator in the vertical channel. See Eq. (2.3) and Fig. (2.1).
S	fraction of captured optical power. See Eq. (6.6).
$S_{bv}(t)$	complex baseband waveform of the modulated signal in the vertical channel. See Eq. (2.13).
$\hat{\mathbf{s}}$	three-component unit Stokes vector. See Eq. (3.10).
T	transmitter filter sampling time. See Eq. (2.2).
$\mathbf{T}(\omega)$	optical fiber complex transfer matrix. See Eq. (3.4).
$u(n)$	discrete baseband input signal to the equalizer. See Fig. (4.3).
$\mathbf{u}(n)$	K dimensional input discrete signal vector at step n . See Eq. (4.9).
$\mathbf{u}(t)$	output signal vector of the fiber channel. See Eqs. (2.6, 4.12).
$\mathbf{u}_{bh}(t)$	received baseband signal vector in the horizontal channel. See Eq. (2.25) and Fig. (2.3).
$u_{b,ih}(t)$	received baseband in-phase signal in the horizontal channel. See Eq. (2.25) and Fig. (2.3).
$u_{b,iv}(t)$	received baseband in-phase signal in the vertical channel. See Eq. (2.25) and Fig. (2.3).
$u_{b,qh}(t)$	received baseband quadrature signal in the horizontal channel. See Eq. (2.25) and Fig. (2.3).
$u_{b,qv}(t)$	received baseband quadrature signal in the vertical channel. See Eq. (2.25) and Fig. (2.3).
$\mathbf{u}_{bv}(t)$	received baseband signal vector in vertical channel. See Eq. (2.25) and Fig. (2.3).
$u_h(t)$	output of the horizontal channel. See Eqs. (2.6, 4.11).
$u_v(t)$	output of the vertical channel. See Eqs. (2.6, 4.11).
$\mathbf{u}_v(n), \mathbf{u}_h(n)$	input signal vectors to the equalizer in the vertical and horizontal channels.

	See Eq. (4.15) and Fig. (4.4).
$u_1(\omega), u_2(\omega)$	complex quantities of the transfer matrix, $\mathbf{T}(\omega)$.
$v(t)$	Gaussian noise signal. See Eq. (2.8) and Fig. (2.1).
v_g	different group velocity. See Eq. (3.2).
$v_h(t)$	Gaussian noise signal in the horizontal channel. See Eq. (2.8) and Fig. (2.1).
$v_v(t)$	Gaussian noise signal in the vertical channel. See Eq. (2.8) and Fig. (2.1).
w_0	angular carrier frequency. See Eq. (3.21).
W_o	input optical pulse width. See Fig. (6.6).
$\mathbf{x}(n)$	“desired” signal vector. See Eq. (4.17).
$\mathbf{x}_h(n)$	input QAM signal vector for the horizontal channel. See Eq. (2.1) and Fig. (2.1).
$x_{ih}(n)$	in-phase signal in the horizontal polarization channel. See Eq. (2.1) and Fig. (2.1).
$x_{iv}(n)$	in-phase signal in the vertical polarization channel. See Eq. (2.1) and Fig. (2.1).
$x_{qh}(n)$	quadrature signal in the horizontal polarization channel. See Eq. (2.1) and Fig. (2.1).
$x_{qv}(n)$	quadrature signal in the vertical polarization channel. See Eq. (2.1) and Fig. (2.1).
$\mathbf{x}_v(n)$	input QAM signal vector for the vertical channel. See Eq. (2.1) and Fig. (2.1).
$y(n)$	output of the adaptive equalizer. See Eq. (4.7).
$\mathbf{y}(n)$	output signal vector. See Eq. (4.10) and Fig. (4.4).
$y_{eq}(t)$	output of the equalizer. See Fig. (4.1).
$y_h(t)$	output of receiver in the horizontal channel. See Eq. (2.9) and Fig. (2.1).
$y_{ih}(t)$	demodulated in-phase signal in the horizontal channel. See Eq. (2.10) and Fig. (2.1).
$y_{iv}(t)$	demodulated in-phase signal in the vertical channel. See Eq. (2.10) and Fig. (2.1).
$y_{qh}(t)$	demodulated quadrature signal in the horizontal channel. See Eq. (2.10) and Fig. (2.1).
$y_{qv}(t)$	demodulated quadrature signal in the vertical channel. See Eq. (2.10) and Fig. (2.1).
$y_v(t)$	output of the receiver in the vertical channel. See Eq. (2.9) and Fig. (2.1).
$\mathbf{Z}_h(t)$	received PAM signals in the horizontal channel. See Fig. (2.1).
$\mathbf{Z}_v(t)$	received PAM signals in the vertical channel. See Fig. (2.1).
α	average differential group delay time. See Eq. (3.12).
α_f	fiber loss.
β_f	propagation constant for the fast mode. See Eq. (3.1) and Fig. (3.1).
β_s	propagation constant for the slow mode. See Eq. (3.1) and Fig. (3.1).
γ	received SNR. See Eq. (5.5).
γ_r	Rayleigh scattering coefficient. See Eq. (6.6).
γ_s	system SNR. See Eq. (5.12).

γ_a	attenuation coefficient. See Eq. (6.6).
$\Delta\beta$	birefringence. See Eq. (3.1).
Δn_{eff}	differential index of fraction. See Eq. (3.1).
$\Delta\tau$	DGD. See Eq. (3.2) and Fig. (3.1).
$\Delta\tau_{rms}$	rms value of the differential group delay $\Delta\tau$. See Eq. (3.14).
$\nabla_{vh}(J_v(n))$	gradient of $J_v(n)$ to $\mathbf{c}_{vh}(n)$. See Eq. (4.23).
$\nabla_{vv}(J_v(n))$	gradient of $J_v(n)$ to $\mathbf{c}_{vv}(n)$. See Eq. (4.22).
θ_k, φ_k	independent uniformly distributed random variables, distributed from $-\pi$ to π . See Eqs. (3.18, 3.19).
λ	wavelength.
μ	step-size, an adaptation constant. See Eq. (4.8).
σ_c^2	variance of the channel Gaussian noise.
σ_1^2	variance of n_1 .
σ_2^2	variance of n_2 .
τ_k	Maxwellian distributed DGD. See Eq. (3.16).
τ, τ_1	arrival times in the two polarization states. See Eq. (3.9).
$\langle \tau \rangle$	average DGD in each segment of a fiber. See Eq. (3.15).
ϕ_h	initial phases in the horizontal channel. See Eq. (2.18).
ϕ_v	initial phases in the vertical channel. See Eq. (2.17).
ψ	polarization-independent phase. See Eq. (3.4).
π	Ludolphian number, 3.1415926 ...
ω	angular frequency.
ω_0	central angular frequency.
φ_v, φ_h	phase of the optical field. See Eqs. (3.7.3.8).
Ω	dispersion vectors, indicates rate and direction of rotation. See Eq. (3.10).
\bullet^H	Hermitian transpose of \bullet .
\bullet^T	matrix transpose of \bullet .
\bullet'	complex conjugate of \bullet .
$\bullet * \blacklozenge$	convolution of \bullet and \blacklozenge .
$\bullet \times \blacklozenge$	multiplication of \bullet and \blacklozenge .
$\langle \bullet \rangle$	average of \bullet .
$ \bullet $	absolute value of \bullet .

LIST OF ABBREVIATION AND ACRONYMS

BER	Bit Error Rate
CPI	Cross Polarization Interference
DFT⁻¹	inverse Discrete Fourier Transformation
DGD	Differential Group Delay
DSP	Digital Signal Processing
EDFA	Erbium-Doped Fiber Amplifier
FIR	Finite Impulse Response
IF	Intermediate Frequency
IM-DD	Intensity Modulation with Direct Detection
ISI	Inter-Symbol Interference
LMS	Least Mean Square
LTE	Linear Transversal Equalizer
MSE	Mean Squared Error
OTDR	Optical Time Domain Reflectometry
PAM	Pulse Amplitude Modulation
PDF	Probability Density Function
PMD	Polarization Mode Dispersion
PN	Pseudonoise
PSPs	Principal States of Polarization
QAM	Quadrature Amplitude Modulation
RLS	Recursive Least Squares
RMS	Root Mean Square
SNR	Signal Noise Ratio
ZF	Zero Forcing

Chapter 1

Introduction

1.1 Introduction to the Research

Optical fiber communication systems have attracted more attention in the recent years, because of the outstanding advantage of optical fibers. The most significant merit of an optical fiber is its enormous bandwidth. An optical fiber communication system uses a very high carrier frequency, around 200 THz [2], which yields a far greater potential bandwidth than a cable system; coaxial cables have a bandwidth up to approximately 500 MHz [1]. In optical systems, this carrier frequency is usually expressed as a wavelength, 1.55 μm . This enormous bandwidth provides the potential to transmit signals at a very high speed.

At present, however, this potential bandwidth cannot be fully utilized. A significant reason is the fiber dispersion. Usually, the fiber dispersion includes inter-mode dispersion, intra-mode dispersion and PMD [2]. In a single mode fiber, inter-mode dispersion is absent. In the systems used today, intra-mode dispersion is not a significant problem. PMD is the main limitation that confines the optical fiber transmission systems from utilizing the bandwidth effectively.

An EDFA (Erbium-Doped Fiber Amplifier) can regenerate weak signals, but it makes the dispersion worse since the dispersion effects accumulate over the multiple amplifier stages. Therefore, the current task of optical fiber communication system

design is to solve the fiber dispersion problem, especially PMD. There are many techniques developed for PMD compensation in both the optical domain and the electrical domain [2]. Early strategies to reduce PMD were focused on reducing the intrinsic PMD of the fiber by altering the manufacturing process [60,61]. This led to the low and stable values of PMD in the new generation of single-mode fibers being manufactured [62]. More recent efforts have been examining ways in which lightwave systems can be designed to better accommodate otherwise unacceptable levels of PMD and thus make full use of the existing embedded fiber base. Such strategies include reduction of ISI (Inter-Symbol Interference) by electronic equalization in the receiver [40,41,43], and optical equalization using an automatic polarization controller at the receiver or transmitter [42,59].

Winters proposed a strategy for PMD compensation using optical equalization [42]. He used a polarization controller to adjust the polarization into a fiber to one of the PSPs (Principal States of Polarization) of the fiber. The receiver detects only one of the PSPs to eliminate first-order PMD. A method to track the changing PSPs using a gradient search algorithm was also presented in his paper. The advantage of optical techniques is that they can be bit rate independent, while for electrical techniques, the complexity and difficulty will increase dramatically as the bit rate increases. With the development of high speed DSP (Digital Signal Processing) and Si/SiGe epitaxial transistors [64,65], an electrical equalizer operating at 10 GHz may be realized [51]. A high speed electrical equalizer becomes an attractive solution for PMD mitigation due to its compact and cost effective implementation.

Based on previous research, the intent of this thesis is to construct a simulation model of an optical fiber communication system, including simulating the optical fiber channel with PMD as well as the electrical channel equalizers and CPI cancellers to compensate PMD.

1.2 Thesis Contributions

This thesis proposes a novel optical fiber transmission system where two 4-QAM (Quadrature Amplitude Modulation) signals are transmitted separately over vertical and horizontal polarization channels. This strategy has a clear advantage, more system capacity and higher bit rate. However, it also causes CPI between the two signals in the two polarization channels. Actually, CPI is the result of PMD due to the power coupling. PMD and CPI can be compensated using electrical adaptive filters.

The simulation of PMD in an optical fiber channel is an important part of this thesis. By applying the theory of PSPs [45,52] and the waveplate model [42,57,59], the frequency responses and baseband impulse responses are obtained. The complex baseband impulse responses are the backbone to construct the simulation of the optical fiber channel. Gaussian noise signals are also added to represent the thermal noise in the channel and the front end of the receiver.

This thesis proposes the combination of channel equalizers and CPI cancellers which are applied to compensate the PMD and CPI in an optical fiber communication system. It shows the potential application of electrical adaptive equalizers and CPI cancellers in an optical fiber communication system and demonstrates a bright future for

this strategy. The structure of the channel equalizers and cancellers is described and analyzed. The contribution that the equalizers and CPI cancellers offer is demonstrated by the performance improvement they create.

The system performance such as the eye pattern and bit error rate are presented. The bit error rate is an important parameter to measure the performance of an optical fiber communication system. It shows the PMD, CPI and the noise effects on the optical fiber communication system as well as and the contribution of adaptive channel equalizers and CPI cancellers in the receiver. Also, the bit error rate reveals the relation between PMD and the received SNR (Signal Noise Ratio), and helps us determine the requirement for PMD and the noise tolerance.

As a further study, bidirectional transmission through a single fiber is also presented. The crosstalk in the coupler and the backscatter [1] in the fiber causes a returned echo in this system. To eliminate this echo, echo cancellers in the receiver might be used. The power penalties when there are echo cancellers and no echo cancellers [19,28] are compared to show the contribution of the echo cancellers.

1.3 Thesis Outline

The outline of the thesis is as follows:

Chapter 2: The system simulation model is constructed. Signal format, transmitter, channel and receiver structures are defined. The requirements of the baseband simulation model are proposed and explained. Finally, the simulation tools, MATLAB® and

SIMULINK[®], are introduced.

- Chapter 3** PMD concepts and the PSPs are discussed first. Based on the theory of PSPs, a waveplate model is presented, which is used to simulate the frequency responses and complex baseband impulse responses. The computer simulation of PMD is achieved by using the complex baseband impulse responses. The method of simulation using MATLAB[®] and SIMULINK[®] is also shown in this chapter.
- Chapter 4:** At first, the adaptive channel equalizer technique is introduced, which includes fundamental equalizer theory and the type of adaptive equalizers. Then, the method to determine the adaptive tap weights of the equalizer and CPI canceller using the normalized LMS (Least Mean Square) algorithm is derived. The adaptive channel equalizers and CPI cancellers are constructed based on these results. The performance of the adaptive equalizers and cancellers is also analyzed.
- Chapter 5:** The eye patterns of the received signals are shown in this chapter. The system bit error rate curve is also shown. The discussion of the system performance is presented.
- Chapter 6:** Bidirectional transmission in a single fiber is proposed. The coupler crosstalk and Rayleigh backscatter as well as their effect on the echo are introduced. Then, the power penalty is calculated, and

the implementation with or without an echo cancellers is discussed.

Chapter 7: The conclusion of this research and the future work are presented.

Chapter 2

System Simulation Model

2.1 System Model

In this thesis, 4-state QAM signals are launched onto a fiber. The benefit of this modulation scheme is good spectral efficiency. A dually polarized digital optical fiber transmission system with two independent QAM input signals is constructed [21-26]. One QAM signal is transmitted over a horizontal channel and the other is transmitted over a vertical channel. This system is shown in Fig. (2.1).

The input signals $A_h(n)$ and $A_v(n)$ are 4 level PAM (Pulse Amplitude Modulation) signals. They are uniformly distributed random integer signals ranging from 1 to 4. These PAM signals are then converted to QAM signals $x_v(n)$ and $x_h(n)$, by mapping,

$$\mathbf{x}_v(n) = \begin{bmatrix} x_{iv}(n) \\ x_{qv}(n) \end{bmatrix}, \quad \mathbf{x}_h(n) = \begin{bmatrix} x_{ih}(n) \\ x_{qh}(n) \end{bmatrix}, \quad (2.1)$$

where $x_v(n)$, $x_h(n)$ are QAM signal vectors in the vertical and horizontal channels.

$x_{iv}(n)$ is the in-phase signal in the vertical polarization channel,

$x_{qv}(n)$ is the quadrature signal in the vertical polarization channel,

$x_{ih}(n)$ is the in-phase signal in the horizontal polarization channel, and

$x_{qh}(n)$ is the quadrature signal in the horizontal polarization channel.

$x_{iv}(n)$, $x_{qv}(n)$, $x_{ih}(n)$ and $x_{qh}(n)$ are the values of $1+j$, $-1+j$, $1-j$ and $-1-j$. And j is the imaginary number, satisfying $j^2 = -1$.

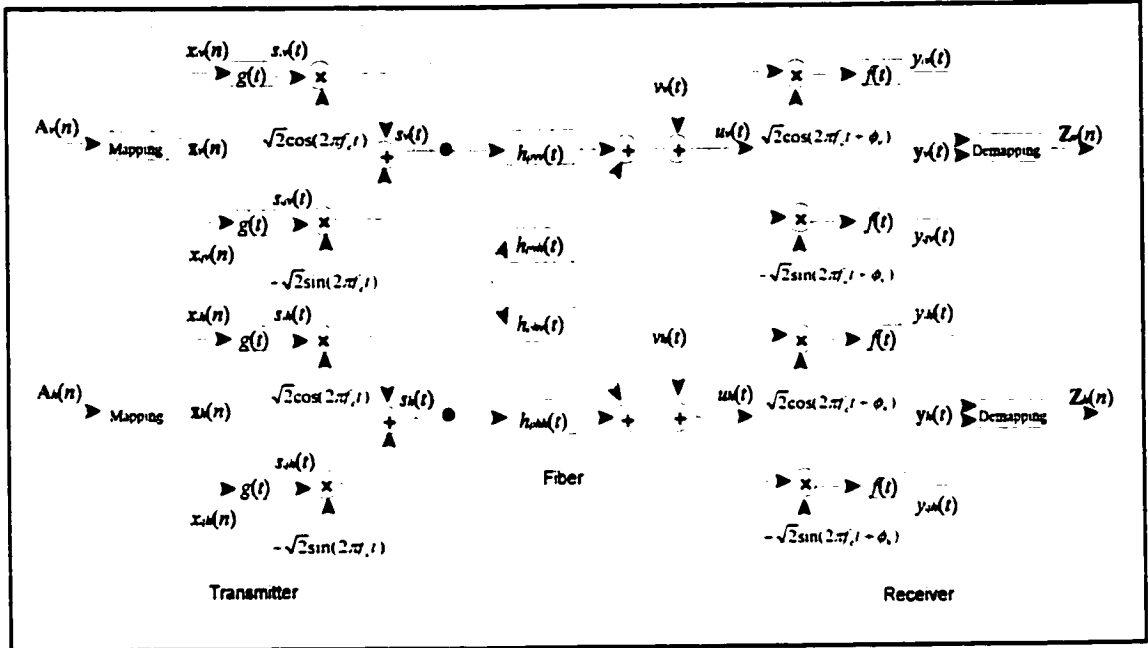


Figure 2.1 Passband System Model

The signals after transmitter filter, $g(t)$, are $s_{ih}(t)$, $s_{qh}(t)$, $s_{iv}(t)$ and $s_{qv}(t)$,

$$\begin{aligned}
 s_{iv}(t) &= \sum_{n=0}^{N-1} x_{iv}(n)g(t-nT), \\
 s_{qv}(t) &= \sum_{n=0}^{N-1} x_{qv}(n)g(t-nT), \\
 s_{ih}(t) &= \sum_{n=0}^{N-1} x_{ih}(n)g(t-nT), \\
 s_{qh}(t) &= \sum_{n=0}^{N-1} x_{qh}(n)g(t-nT),
 \end{aligned} \tag{2.2}$$

where $s_{iv}(t)$ is the in-phase signal after transmitter filter in the vertical channel,

$s_{qv}(t)$ is the quadrature signal after transmitter filter in the vertical channel,

$s_{ih}(t)$ is the in-phase signal after transmitter filter in the horizontal channel,
 $s_{qh}(t)$ is the quadrature signal after transmitter filter in the horizontal channel,
 $g(t)$ is the transmitter filter, which can be selected by the designer to satisfy the
 limitations on transmitted power and bandwidth,
 T is the transmitter filter signaling rate or symbol period, and
 N is the number of transmitter filter taps.

The above signals are then passed to modulators. The modulated signals are $s_v(t)$ and $s_h(t)$,

$$\begin{aligned}
 s_v(t) &= \sqrt{2} \left[s_{iv}(t) \cos(2\pi f_c t) - s_{qv}(t) \sin(2\pi f_c t) \right], \\
 s_h(t) &= \sqrt{2} \left[s_{ih}(t) \cos(2\pi f_c t) - s_{qh}(t) \sin(2\pi f_c t) \right],
 \end{aligned} \tag{2.3}$$

where $s_v(t)$ is the modulated signal after the modulator in the vertical channel.

$s_h(t)$ is the modulated signal after the modulator in the horizontal channel. and
 f_c is the carrier frequency.

The optical fiber channel is characterized by a matrix $\mathbf{h}_p(t)$ with four passband
 impulse responses,

$$\mathbf{h}_p(t) = \begin{bmatrix} h_{p_{vv}}(t) & h_{p_{vh}}(t) \\ h_{p_{hv}}(t) & h_{p_{hh}}(t) \end{bmatrix}, \tag{2.4}$$

where $h_{p_{vv}}(t)$ is the passband vertical to vertical impulse response,

$h_{p_{hh}}(t)$ is the passband horizontal to horizontal impulse response,

$h_{p_{vh}}(t)$ is the passband vertical to horizontal impulse response, and

$h_{p_{hv}}(t)$ is the passband horizontal to vertical impulse response.

In Eq. (2.4), the passband channel impulse responses are related to the baseband channel impulse responses by,

$$\begin{aligned}
h_{pvv}(t) &= 2\text{Re}\left[h_{bvv}(t)e^{j2\pi f_c t}\right] = 2\left[h_{ivv}(t)\cos(2\pi f_c t) - h_{qv v}(t)\sin(2\pi f_c t)\right], \\
h_{pvh}(t) &= 2\text{Re}\left[h_{bvh}(t)e^{j2\pi f_c t}\right] = 2\left[h_{ivh}(t)\cos(2\pi f_c t) - h_{qv h}(t)\sin(2\pi f_c t)\right], \\
h_{phv}(t) &= 2\text{Re}\left[h_{bhv}(t)e^{j2\pi f_c t}\right] = 2\left[h_{ihv}(t)\cos(2\pi f_c t) - h_{qh v}(t)\sin(2\pi f_c t)\right], \\
h_{pvh}(t) &= 2\text{Re}\left[h_{bhv}(t)e^{j2\pi f_c t}\right] = 2\left[h_{ihh}(t)\cos(2\pi f_c t) - h_{qh h}(t)\sin(2\pi f_c t)\right],
\end{aligned} \tag{2.5}$$

where $\text{Re}[\bullet]$ denotes the real part of \bullet . The subscripts of $h(t)$ in Eq. (2.5) are of the form $s_1 s_2 s_3$. The first subscript, s_1 is one of “ p ”, “ b ”, “ i ” or “ q ”, denoting the type of impulse response, “passband”, “complex baseband”, “in-phase baseband” or “quadrature baseband”, respectively. The second and the third subscripts, s_2 and s_3 , will be either “ v ” or “ h ”, denoting “horizontal” and “vertical” respectively. The subscript s_3 denotes the input to the channel and the subscript s_2 denotes the output of the channel.

Having known the modulated signals and channel responses, the output of the channel, $\mathbf{u}(t)$, can be obtained [25],

$$\mathbf{u}(t) = \begin{bmatrix} u_v(t) \\ u_h(t) \end{bmatrix} = \begin{bmatrix} s_v(t) * h_{pvv}(t) + s_h(t) * h_{phv}(t) \\ s_v(t) * h_{pvh}(t) + s_h(t) * h_{pvh}(t) \end{bmatrix} + \mathbf{v}(t), \tag{2.6}$$

where $*$ denotes convolution,

$$s(t) * h(t) = \int_{-\infty}^{\infty} h(t - \tau) s(\tau) d\tau, \tag{2.7}$$

$u_v(t)$ is the output of the vertical channel,

$u_h(t)$ is the output of the horizontal channel, and

$\mathbf{v}(t)$ is the Gaussian noise signal vector with the components in both vertical and

horizontal channels, $v_v(t)$ and $v_h(t)$,

$$\mathbf{v}(t) = \begin{bmatrix} v_v(t) \\ v_h(t) \end{bmatrix}. \quad (2.8)$$

The noise signals $v_v(t)$ and $v_h(t)$ are zero mean uncorrelated with variances of σ_c^2 .

In the receiver, $\mathbf{u}(t)$ is first demodulated and then passed through receiver filters.

The outputs of the receiver are $y_v(t)$ and $y_h(t)$,

$$\mathbf{y}_v(t) = \begin{bmatrix} y_{iv}(t) \\ y_{qv}(t) \end{bmatrix}, \quad \mathbf{y}_h(t) = \begin{bmatrix} y_{ih}(t) \\ y_{qh}(t) \end{bmatrix}, \quad (2.9)$$

and we have,

$$\begin{aligned} y_{iv}(t) &= \sqrt{2} [u_v(t) \cos(2\pi f_c t + \phi_v)] * f(t), \\ y_{qv}(t) &= -\sqrt{2} [u_v(t) \sin(2\pi f_c t + \phi_v)] * f(t), \\ y_{ih}(t) &= \sqrt{2} [u_h(t) \cos(2\pi f_c t + \phi_h)] * f(t), \\ y_{qh}(t) &= -\sqrt{2} [u_h(t) \sin(2\pi f_c t + \phi_h)] * f(t), \end{aligned} \quad (2.10)$$

where $y_{iv}(t)$ is the demodulated in-phase signal in the vertical channel.

$y_{qv}(t)$ is the demodulated quadrature signal in the vertical channel,

$y_{ih}(t)$ is the demodulated in-phase signal in the horizontal channel,

$y_{qh}(t)$ is the demodulated quadrature signal in the horizontal channel,

ϕ_v and ϕ_h are the phase offsets between the transmitter and the receiver in the

vertical and horizontal channels.

$f(t)$ is the receiver filter that is used to cut off the frequency components near $2f_c$

and preserve the desired component near zero.

The PAM signals $\mathbf{Z}_v(n)$ and $\mathbf{Z}_h(n)$ for the vertical and horizontal channels can be obtained

by demapping the received QAM signals $y_v(t)$ and $y_h(t)$. $Z_v(t)$ and $Z_h(t)$ are similar in structure to $A_v(t)$ and $A_h(t)$.

In digital transmission, signals are often represented by ideal steps, and they have infinite bandwidth. To restrict the spectrum of the source signal, an RC (Raised Cosine) filter is commonly used [11]. In this system, the RC filter is divided into two parts, one is the transmitter filter $g(t)$ and the other is the receiver filter $f(t)$. Each part is the square root of the magnitude response of the RC filter in the frequency domain. The impulse response of $g(t)$ and $f(t)$ is [11],

$$g(t) = f(t) = \frac{4r}{\pi\sqrt{T}} \frac{\cos\left((1+r)\pi\frac{t}{T}\right) + \frac{\sin\left((1-r)\pi\frac{t}{T}\right)}{4r\frac{t}{T}}}{\left(1 - \left(4r\frac{t}{T}\right)^2\right)}, \quad (2.11)$$

where r is the rolloff factor, $0 \leq r \leq 1$.

The impulse response of RC filter is shown in Fig. (2.2) [11].

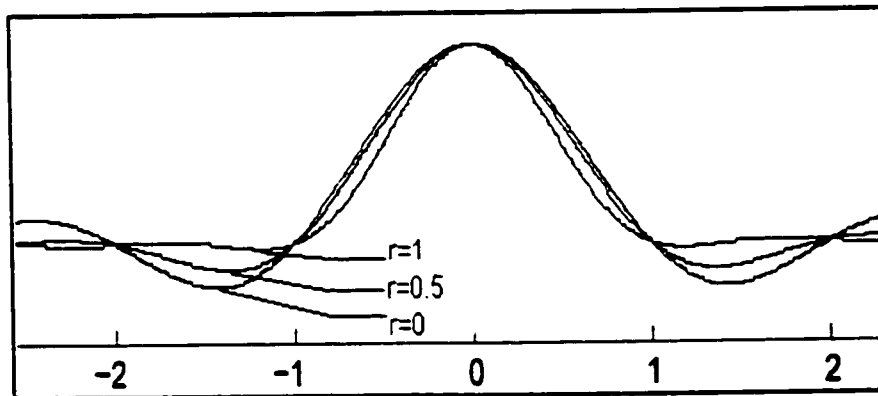


Figure 2.2 Impulse Response of RC Filter

2.2 Baseband Simulation and Coherent Demodulation

The previous section described the passband model where the carrier frequency f_c was introduced in the model. According to Nyquist's baseband sampling theorem, it requires that a simulation sampling frequency f_s must be at least twice the maximum frequency being modeled. Since the optical carrier frequency is usually very high, around 200 THz, modeling passband communication systems involves high computational loads. To alleviate this problem, baseband simulation techniques are used.

Baseband simulation, also known as the low-pass equivalent method, uses the complex envelope of a passband signal. As an example, consider the vertical channel in Fig. (2.1). The equation for modulating the in-phase signal $s_{iv}(t)$ and the quadrature signal $s_{qv}(t)$ by the carrier frequency is [5,11],

$$s_v(t) = \sqrt{2} \left[s_{iv}(t) \cos(2\pi f_c t) - s_{qv}(t) \sin(2\pi f_c t) \right], \quad (2.12)$$

which is equivalent to,

$$s_v(t) = \sqrt{2} \operatorname{Re} \left\{ \left[s_{iv}(t) + j s_{qv}(t) \right] e^{j(2\pi f_c t)} \right\} = \sqrt{2} \operatorname{Re} \left\{ S_{bv}(t) e^{j(2\pi f_c t)} \right\}, \quad (2.13)$$

where $S_{bv}(t)$ is called the complex baseband waveform,

$$S_{bv}(t) = s_{iv}(t) + j s_{qv}(t). \quad (2.14)$$

The high frequency component f_c disappeared in this expression. Baseband simulation models the complex baseband waveform $S_{bv}(t)$ only. Let B_w be the bandwidth of the message signal. The baseband simulation requires the simulation sampling rate to be

larger than $2B_w$. In the baseband simulation, the signal bandwidth is always assumed to be much smaller than the carrier frequency, or $B_w \ll f_c$. Note, the output of a baseband modulator and the input to a baseband demodulator are complex signals.

Demodulation can be divided into two methods, coherent and noncoherent demodulation [11]. Coherent demodulation requires the knowledge of the frequency and phase to recover the received message signal. Noncoherent demodulation permits the recovery of the message signal without knowing the frequency and phase.

The coherently demodulated signal in the vertical channel is, $y_v(t)$,

$$\begin{aligned} y_v(t) &= y_{iv}(t) + jy_{qv}(t) \\ &= \sqrt{2} \left[u_v(t) \cos(2\pi f_c t + \phi_v) - j(u_v(t) \sin(2\pi f_c t + \phi_v)) \right] * f(t) \\ &= \sqrt{2} \left[u_v(t) e^{-j(2\pi f_c t + \phi_v)} \right] * f(t). \end{aligned} \quad (2.15)$$

Suppose,

$$u_v(t) = \sqrt{2} \left[u_{biv}(t) \cos(2\pi f_c t) - u_{bqv}(t) \sin(2\pi f_c t) \right], \quad (2.16)$$

we can get,

$$\begin{aligned} y_v(t) &= \sqrt{2} \left\{ \left[\sqrt{2} (u_{biv}(t) \cos(2\pi f_c t) - u_{bqv}(t) \sin(2\pi f_c t)) \right] e^{-j(2\pi f_c t + \phi_v)} \right\} * f(t) \\ &= 2 \left\{ \left[\begin{aligned} &u_{biv}(t) \cos^2(2\pi f_c t) - u_{bqv}(t) \sin(2\pi f_c t) \cos(2\pi f_c t) - \\ &j(u_{biv}(t) \cos(2\pi f_c t) \sin(2\pi f_c t)) + j(u_{bqv}(t) \sin^2(2\pi f_c t)) \end{aligned} \right] e^{-j\phi_v} \right\} * f(t) \\ &= (u_{biv}(t) + ju_{bqv}(t)) e^{-j\phi_v}, \end{aligned} \quad (2.17)$$

where $u_{biv}(t)$ is the received baseband in-phase signal in the vertical channel, and

$u_{bqv}(t)$ is the received baseband quadrature signal in the vertical channel.

Similar to $y_v(t)$, the received signal in horizontal channel, $y_h(t)$, is,

$$y_h(t) = \left(u_{bih}(t) + ju_{bqh}(t) \right) e^{-j\phi_h}, \quad (2.18)$$

where $u_{bih}(t)$ is the received baseband in-phase signal in the horizontal channel, and $u_{bqh}(t)$ is the received baseband quadrature signal in the horizontal channel.

2.3 Baseband System Model

Because of the benefit of baseband simulation, the passband model which is shown in Fig. (2.1) can be transformed to a baseband model. A baseband model is constructed which includes a transmitter, a receiver and a channel, they are shown in Fig. (2.3).

In the baseband model, the complex signals can be expressed as the matrix forms.

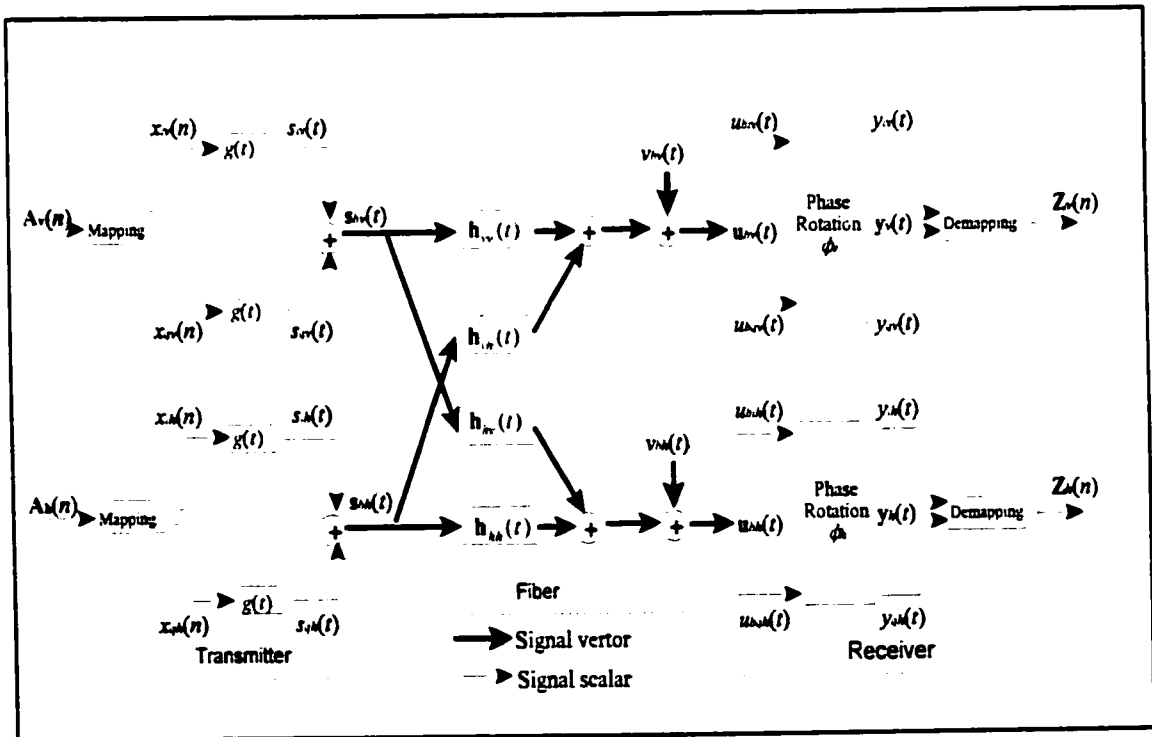


Figure 2.3 Baseband System Model

Thus, in the transmitter, the baseband modulated signals $\mathbf{s}_{bv}(t)$ and $\mathbf{s}_{bh}(t)$ are,

$$\begin{aligned}\mathbf{s}_{bv}(t) &= \begin{bmatrix} s_{iv}(t) \\ s_{qv}(t) \end{bmatrix}, \\ \mathbf{s}_{bh}(t) &= \begin{bmatrix} s_{ih}(t) \\ s_{qh}(t) \end{bmatrix},\end{aligned}\tag{2.19}$$

where $\mathbf{s}_{bv}(t)$ is the baseband signal vector in the vertical channel, and

$\mathbf{s}_{bh}(t)$ is the baseband signal vector in the horizontal channel.

Corresponding to the passband channel impulse responses in Eqs. (2.4, 2.5), the baseband impulse responses are expressed in a matrix form,

$$\mathbf{h}(t) = \begin{bmatrix} \mathbf{h}_{vv}(t) & \mathbf{h}_{vh}(t) \\ \mathbf{h}_{hv}(t) & \mathbf{h}_{hh}(t) \end{bmatrix},\tag{2.20}$$

where $\mathbf{h}(t)$ is the overall baseband complex impulse response matrix,

$\mathbf{h}_{vv}(t)$ is the baseband impulse response matrix, from the vertical to the vertical channel.

$$\mathbf{h}_{vv}(t) = \begin{bmatrix} h_{ivv}(t) & h_{qv v}(t) \\ -h_{qv v}(t) & h_{ivv}(t) \end{bmatrix},\tag{2.21}$$

$\mathbf{h}_{vh}(t)$ is the baseband impulse response matrix, from the vertical to the horizontal channel,

$$\mathbf{h}_{vh}(t) = \begin{bmatrix} h_{ivh}(t) & h_{qv h}(t) \\ -h_{qv h}(t) & h_{ivh}(t) \end{bmatrix},\tag{2.22}$$

$\mathbf{h}_{hv}(t)$ is the baseband impulse response matrix, from the horizontal to the vertical channel,

$$\mathbf{h}_{hv}(t) = \begin{bmatrix} h_{ihv}(t) & h_{qhv}(t) \\ -h_{qhv}(t) & h_{ihv}(t) \end{bmatrix}, \text{ and} \quad (2.23)$$

$\mathbf{h}_{hh}(t)$ is the baseband impulse response matrix, from the horizontal to the horizontal channel,

$$\mathbf{h}_{hh}(t) = \begin{bmatrix} h_{ihh}(t) & h_{qhh}(t) \\ -h_{qhh}(t) & h_{ihh}(t) \end{bmatrix}. \quad (2.24)$$

In the receiver, the received baseband signal vectors $\mathbf{u}_{bv}(t)$ and $\mathbf{u}_{bh}(t)$ are,

$$\mathbf{u}_{bv}(t) = \begin{bmatrix} u_{biv}(t) \\ u_{bqv}(t) \end{bmatrix}, \quad \mathbf{u}_{bh}(t) = \begin{bmatrix} u_{bih}(t) \\ u_{bqh}(t) \end{bmatrix}. \quad (2.25)$$

From Eqs. (2.17, 2.18), we have,

$$\mathbf{y}_v(t) = \begin{bmatrix} y_{iv}(t) \\ y_{qv}(t) \end{bmatrix} = \begin{bmatrix} \cos \phi_v & -\sin \phi_v \\ \sin \phi_v & \cos \phi_v \end{bmatrix} \begin{bmatrix} u_{biv}(t) \\ u_{bqv}(t) \end{bmatrix}, \text{ and} \quad (2.26)$$

$$\mathbf{y}_h(t) = \begin{bmatrix} y_{ih}(t) \\ y_{qh}(t) \end{bmatrix} = \begin{bmatrix} \cos \phi_h & -\sin \phi_h \\ \sin \phi_h & \cos \phi_h \end{bmatrix} \begin{bmatrix} u_{bih}(t) \\ u_{bqh}(t) \end{bmatrix}. \quad (2.27)$$

Thus, in the baseband model, there is a phase rotation between $\mathbf{u}_{bv}(t)$ and $\mathbf{y}_v(t)$, $\mathbf{u}_{bh}(t)$ and $\mathbf{y}_h(t)$ which can be expressed as a matrix. Therefore, the baseband system model is constructed as that shown in Fig. (2.3) which is used as a foundation of the whole simulation system.

2.3 System Development Tools: MATLAB[®] and SIMULINK[®]

MATLAB[®] is a high-performance language for technical computing [13]. It integrates computation, visualization, and programming in an easy-to-use environment where problems and solutions are expressed in familiar mathematical notation. The Signal Processing Toolbox is a collection of tools built on MATLAB[®] [14]. This toolbox supports a wide range of signal processing operations, from waveform generation to filter design and implementation, parametric modeling, and spectral analysis [15,16].

SIMULINK[®] is a software package in MATLAB[®] for modeling, simulating, and analyzing dynamical systems [10]. It supports linear and nonlinear systems, modeled in continuous time, sampled time, or a hybrid of the two. SIMULINK[®] is a powerful tool for real-time simulation. The communications Toolbox and DSP Blockset are the most useful tools for simulation of telecommunication systems. The Communications Toolbox is a collection of computation functions and simulation blocks for research, development, system design, analysis, and simulation in the communications area [11]. The DSP Blockset is a collection of block libraries which have been designed specifically for DSP applications, and include operations such as classical, multirate, and adaptive filtering, complex and matrix arithmetic, transcendental and statistical operations, convolution, and Fourier transforms [12].

Chapter 3

Polarization Mode Dispersion

3.1 What is PMD?

3.1.1 Birefringence and PMD

In single-mode fibers there are two different polarization modes, the fast mode and the slow mode, due to birefringence which is caused by internal or external stresses or by non-perfect circularity of the fiber core. Each polarization mode has its own propagation constant β_s and β_f , which are shown in Fig. (3.1). Usually the state of polarization of an arbitrary optical field can be represented by the vector sum of the field components aligned with the two polarization modes.

The difference in propagation constants is called birefringence [3].

$$\Delta\beta = |\beta_s - \beta_f| = \left| \frac{\omega n_s}{c} - \frac{\omega n_f}{c} \right| = \frac{\omega}{c} \Delta n_{eff}, \quad (3.1)$$

where $\Delta\beta$ is birefringence,

β_s is the propagation constant of the slow mode,

β_f is the propagation constant of the fast mode,

Δn_{eff} is the differential index of refraction,

n_s is the effective index of refraction of the slow mode,

n_f is the effective index of refraction of the fast mode,

c is the speed of light, 3×10^8 m/s,

ω is the angular frequency, and

$|\bullet|$ denotes the absolute value of \bullet .

The birefringence, $\Delta\beta$, is related to the different group velocity v_g ,

$$v_g = \left(\frac{d(\Delta\beta)}{d\omega} \right)^{-1},$$

where $d(\bullet)$ denotes the differential of \bullet .

The different group velocities of the modes limit the bandwidth of the optical fiber communication system, because they cause pulse broadening. Thus the difference in the group delays of the fast and slow modes is,

$$\Delta\tau = v_g L = \left(\frac{\Delta n_{eff}}{c} - \frac{\omega}{c} \frac{d\Delta n_{eff}}{d\omega} \right) L, \quad (3.2)$$

where $\Delta\tau$ is also called the differential group delay (DGD), and L is the fiber length.

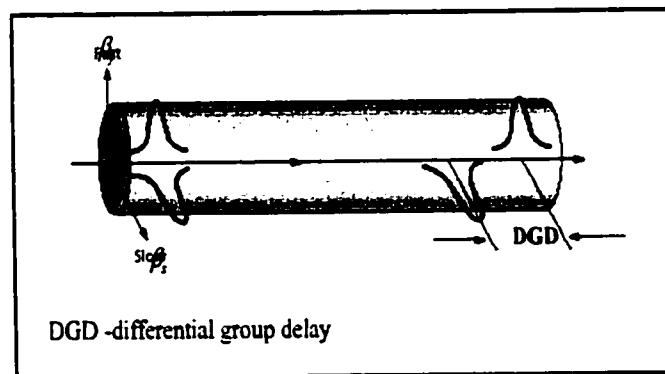


Figure 3.1 PMD and DGD [70]

Because of the existence of birefringence, if the input pulse excites both polarization components, it becomes broader at the fiber output since the two components disperse along the fiber because of the DGD, see Fig. (3.1). This phenomenon is called

Polarization Mode Dispersion (PMD). And the delay between the two components is called the DGD.

3.1.2 Mode coupling in long fiber

In Eq. (3.2), for a specific Δn_{eff} , DGD is proportional to the fiber length, L .

However, this phenomenon occurs only in short fiber. In long-distance optical fiber transmission systems, there is a polarization mode coupling due to power of one polarization mode leaking into the other mode. The mode coupling is a random process, but the average power will grow with the distance.

A coupling length, l_c is defined to be the length at which the average power in the orthogonal polarization mode, $P_b(l_c)$, is within $1/e^2$ of the power in the starting mode, P_a [2,66],

$$\frac{\langle P_a \rangle - \langle P_b(l_c) \rangle}{P_{total}} = \frac{1}{e^2}, \quad (3.3)$$

where P_{total} is the total power in the fiber, and

$\langle \bullet \rangle$ stands for the ensemble average of \bullet .

The coupling length, l_c can be used to distinguish between a long fiber and a short fiber. When a fiber length is less than l_c , it can be considered to be a short-length fiber. In a short-length fiber, the polarization effects are deterministic and PMD grows linearly with the fiber length. When a fiber length is much larger than l_c , we can regard it as a long-length fiber. In a long-length fiber, the fiber shows a statistical variation in the polarization due to both PMD and mode coupling. Also, the DGD becomes proportional to the square root of the fiber length [57].

3.2 Principal States of Polarization

Poole proposed a well known model, “Principal States of Polarization”, in 1986 to describe PMD [52]. It revealed that “in any linear optical transmission medium that has no polarization-dependent loss there exist orthogonal input states of polarization for which the corresponding output states of polarization are orthogonal and show no dependence on wavelength to first order”. Such states are called principal states of polarization (PSPs).

Under the assumptions of this model, the linear medium can be described by a complex transfer matrix $\mathbf{T}(\omega)$ [67],

$$\mathbf{T}(\omega) = e^{(-\alpha_r L + j\psi(\omega, L))} \begin{bmatrix} u_1(\omega) & u_2(\omega) \\ -u_2^*(\omega) & -u_1^*(\omega) \end{bmatrix}, \quad (3.4)$$

where α_r is the fiber loss,

$\psi(\omega, L)$ is the polarization-independent phase,

$u_1(\omega)$ and $u_2(\omega)$ are complex quantities, and they satisfy the relation,

$$|u_1(\omega)|^2 + |u_2(\omega)|^2 = 1, \text{ and} \quad (3.5)$$

•' denotes complex conjugate of •.

Suppose the input optical field vector is $\mathbf{E}_a(\omega)$, and the output optical field is $\mathbf{E}_b(\omega)$. The relationship between these optical fields is,

$$\mathbf{E}_b(\omega) = \mathbf{T}(\omega) \mathbf{E}_a(\omega), \quad (3.6)$$

and the optical field $\mathbf{E}_a(\omega)$ and $\mathbf{E}_b(\omega)$ can be expressed in the form [2],

$$\mathbf{E}_a(\omega) = E_a(\omega) e^{j\theta_a} \bar{\mathbf{E}}_a(\omega), \quad (3.7)$$

$$\mathbf{E}_b(\omega) = E_b(\omega)e^{j\varphi_b} \bar{\mathbf{E}}_b(\omega), \quad (3.8)$$

where $E_a(\omega)$ is the amplitude of the input PSPs in frequency domain,

$E_b(\omega)$ is the amplitude of the output PSPs in frequency domain,

φ_a is the phase of the input PSPs in frequency domain,

φ_b is the phase of the output PSPs in frequency domain,

$\bar{\mathbf{E}}_a(\omega)$ is the complex unit vector specifying the input PSPs, and

$\bar{\mathbf{E}}_b(\omega)$ is the complex unit vector specifying the output PSPs.

The Eq. (3.6) is a frequency model used to describe the PSPs. The important contribution of this model is that it points out the property of polarization invariance with frequency for the first order, that an optical pulse aligned with a principal state at the input of a fiber will emerge at the output with its spectral components all having the same state of polarization [52]. This means that the only distortion in the pulse is the phase distortion and it will not change the shape of the pulse.

Because of the existence of PSPs, any input signal can be expressed as the sum of two states. In either of these polarization states there is no pulse shape distortion, but the two states have different time delays. Thus we also describe the model in the time domain as [54],

$$\mathbf{E}_b(t) = c_+ E_a(t - \tau_+) \bar{\mathbf{E}}_+ + c_- E_a(t - \tau_-) \bar{\mathbf{E}}_-, \quad (3.9)$$

where $\mathbf{E}_b(t)$ is the output PSPs in the time domain,

$E_a(t)$ are the amplitudes of the time-varying input PSPs in the time domain,

c_+ , c_- are complex coefficients, which are the fraction of the power of the input

signal into each of the PSPs,

\vec{E}_+, \vec{E}_- are unit vectors specifying the two output PSPs, and

τ_+, τ_- are the arrival times in the two polarization states.

The difference of the arrival times is DGD, $\Delta\tau = \tau_+ - \tau_-$, which shows two different PSPs cause the pulse broadening at the output of a fiber. Eq. (3.9) describes the first-order effect of PMD in time domain [45], which is shown to induce a dual splitting of the initial pulse. In short fibers, the principal states correspond to the polarization modes of the fiber. In the long fiber spans, these states are determined by the cumulative effects of the birefringence over the entire span [2].

In frequency domain, the polarization mode dispersion is manifested as a frequency dependent state of polarization at the output of a fiber [54,55]. Over a narrow frequency range, it takes the form of a rotation of the polarization on the Poincaré sphere,

$$\frac{d\hat{s}}{d\omega} = \Omega \times \hat{s}, \quad (3.10)$$

where \hat{s} is the three-component unit Stokes vector, representing the states of polarization of the output on the Poincaré sphere,

Ω indicates the rate and direction of rotation, and is usually referred to as

dispersion vector, and

$\bullet \times \blacklozenge$ denotes the multiplication of \bullet and \blacklozenge .

The relationship between the frequency domain and the time domain behaviors is that the rate of rotation, $|\Omega|$, is equal to the differential group delay time experienced by spectrally narrow pulses having polarization aligned at the input with two orthogonal PSPs [55],

$$|\Omega| = \Delta\tau. \quad (3.11)$$

Using the theory of PSPs, the statistical properties of DGD were studied. The PDF (Probability Density Function) of DGD, $p(\Delta\tau)$, has been proven to be a Maxwellian distribution [58],

$$p(\Delta\tau) = \begin{cases} \sqrt{\frac{2}{\pi}} \frac{\Delta\tau^2}{\alpha^3} e^{-\frac{\Delta\tau^2}{2\alpha^2}} & \Delta\tau \geq 0, \\ 0 & \text{otherwise,} \end{cases} \quad (3.12)$$

where α is the average differential group delay time,

$$\alpha = \frac{2\sqrt{2}}{\sqrt{3\pi}} \Delta\tau_{rms}, \text{ and} \quad (3.13)$$

$\Delta\tau_{rms}$ is the rms value of the DGD,

$$\Delta\tau_{rms} = \langle \Delta\tau^2 \rangle = \langle \Omega_1^2 + \Omega_2^2 + \Omega_3^2 \rangle, \quad (3.14)$$

where Ω_1 , Ω_2 and Ω_3 are dispersion vectors which have independent Gaussian distributions with zero mean and identical variance [56]. Therefore, to generate a Maxwellian distributed variable, first we should generate three independent Gaussian random variables, then take the square root of sum of three squared Gaussian random variables.

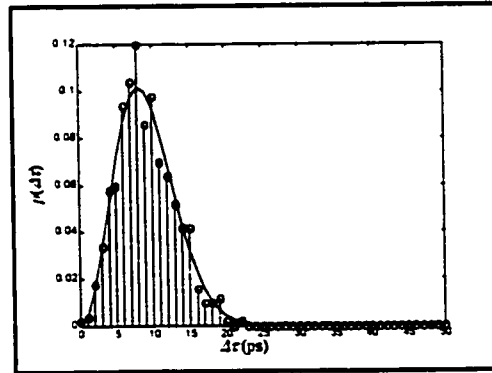


Figure 3.2 PDF of $\Delta\tau$

Fig. (3.2) shows a probability distribution of the random Maxwellian distributed DGDs in every segment of a fiber whose average DGD through the whole fiber is 100 ps, and the number of segments, K , is 100. Thus, the average DGD in each segment, $\langle \tau \rangle$ is,

$$\langle \tau \rangle = \frac{\alpha}{\sqrt{K}} = 10 \text{ ps} . \quad (3.15)$$

3.3 Waveplate Model

The waveplate model is a practical and effective approach to measure and simulate the first-order PMD in a long single mode fiber and was discussed in papers [57,59]. According to the theory of PSPs, a fiber which is polarization loss independent, excited by one of its PSPs defined at the optical angular frequency ω , behaves as a simple delay. Thus if we suppose the input field is an input reference frame which consists of two orthogonal input PSPs, and the output field is an output reference frame which consists of two orthogonal output PSPs, then the phase shift of a fiber can be described by a Jones matrix, $M_k(\omega)$ which we call the “DGD generator”,

$$M_k(\omega) = \begin{bmatrix} e^{j\omega\tau_k} & 0 \\ 0 & e^{-j\omega\tau_k} \end{bmatrix} \quad k = 1, 2, \dots, K, \quad (3.16)$$

where τ_k is the differential time delay of one segment, and

K is the number of fiber segments.

Considering the existence of mode coupling which causes random rotations, we should add a phase rotator and phase retarder. Thus each segment of a single mode fiber can be simulated as a combination of a DGD generator $M_k(\omega)$, a phase rotator R_k and phase retarder D_k which is shown in Fig (3.3),

$$N_k(\omega) = D_k R_k M_k(\omega) \quad k = 1, 2, \dots, K, \quad (3.17)$$

$$D_k = \begin{bmatrix} e^{j\varphi_k} & 0 \\ 0 & e^{-j\varphi_k} \end{bmatrix}, \quad (3.18)$$

$$R_k = \begin{bmatrix} \cos\theta_k & \sin\theta_k \\ -\sin\theta_k & \cos\theta_k \end{bmatrix}, \quad (3.19)$$

where $N_k(\omega)$ is the transfer matrix of the segment k in a single mode fiber, and θ_k and φ_k are independent uniformly distributed random variables, distributed from $-\pi$ to π .

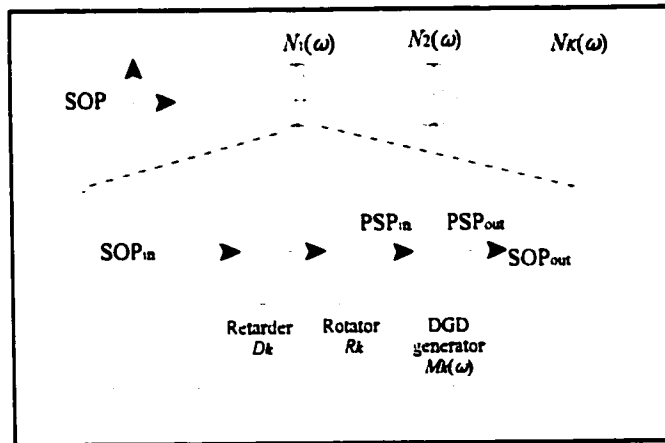


Figure 3.3 Waveplate Model

The overall transfer matrix, $H(\omega)$, is the concatenation of all the segments shown in Fig. (3.3),

$$H(\omega) = e^{\beta(\omega)} \prod_{k=1}^K N_k(\omega), \quad (3.20)$$

where $\beta(\omega)$ is determined by the polarization-independent phase shift and the fiber loss.

3.4 Computer Simulation of PMD

Based on the waveplate model, a computer simulation is used to get both frequency responses and impulse responses.

The waveplate model provides the frequency transfer response $H(\omega)$ with central frequency, $f_c = c/\lambda_c$, where the central wavelength, λ_c , is 1.55 μm . In the digital simulation performed in this thesis, to balance the computing speed and the accuracy, we used 128 frequency points in the frequency domain, which means the sampling frequency, f_s , is $128 \times B$, where B is the signal bit rate. Thus a passband frequency is in the range from $f_c - f_s/2$ to $f_c + f_s/2$.

In this simulation, the bit rate, B , is 2.5 GHz, the DGD is 100 ps, and K is 100 segments. Fig. (3.4) shows the magnitudes of the frequency responses, $H(\omega)$, and Fig. (3.5) shows the phases of these frequency responses.

Our objective is to get the baseband impulse responses of the optical fiber channel with PMD. To achieve this objective, the passband frequency responses should be shifted to baseband. Then the baseband impulse responses can be obtained from,

$$h_b(t) = \text{DFT}^{-1} [H(\omega - \omega_0)], \quad (3.21)$$

where $h_b(t)$ is the complex baseband impulse response,

DFT⁻¹ denotes inverse discrete Fourier transformation, and

ω_0 is the central angular frequency.

Thus we can get four complex baseband impulse responses, $h_{bv}(t)$, $h_{bv}(t)$, $h_{bh}(t)$ and $h_{bh}(t)$. Fig. (3.6) shows the magnitudes of impulse responses, and Fig. (3.7) shows phases of impulse responses.

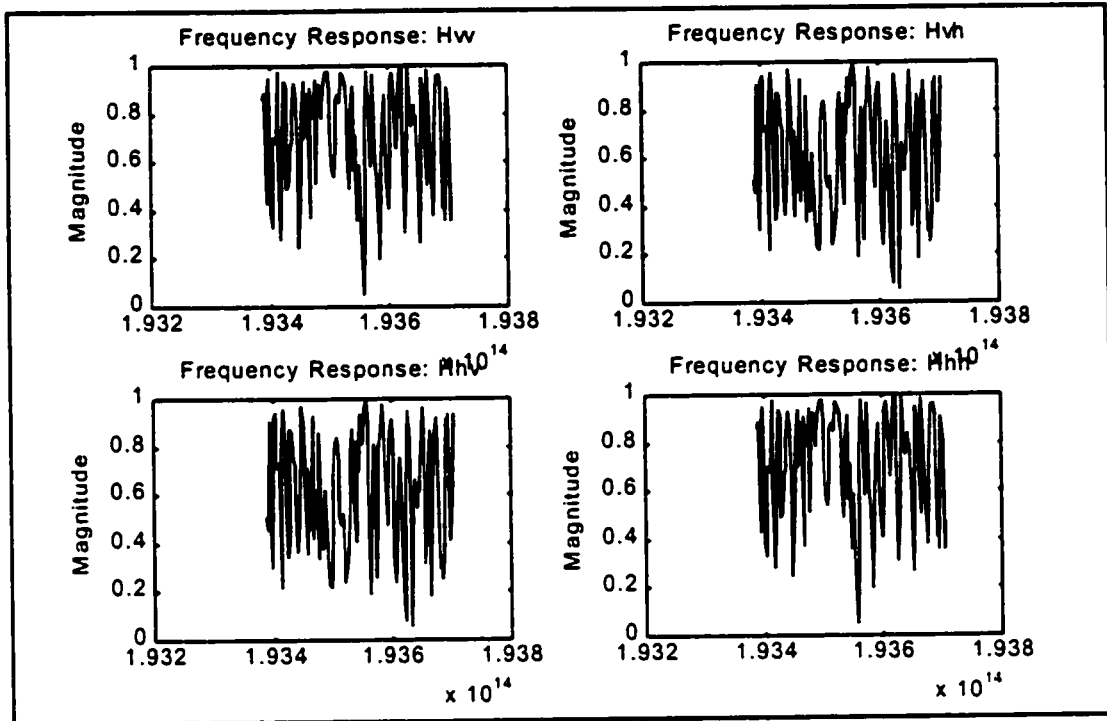


Figure 3.4 Magnitudes of Frequency Responses

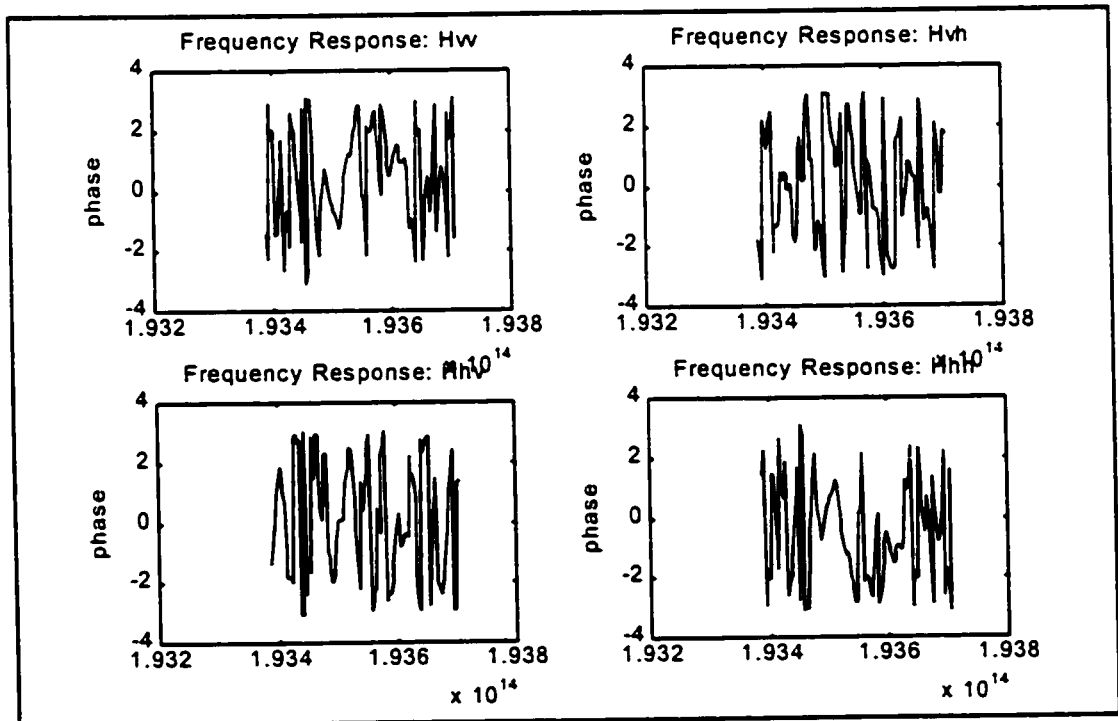


Figure 3.5 Phases of Frequency Responses

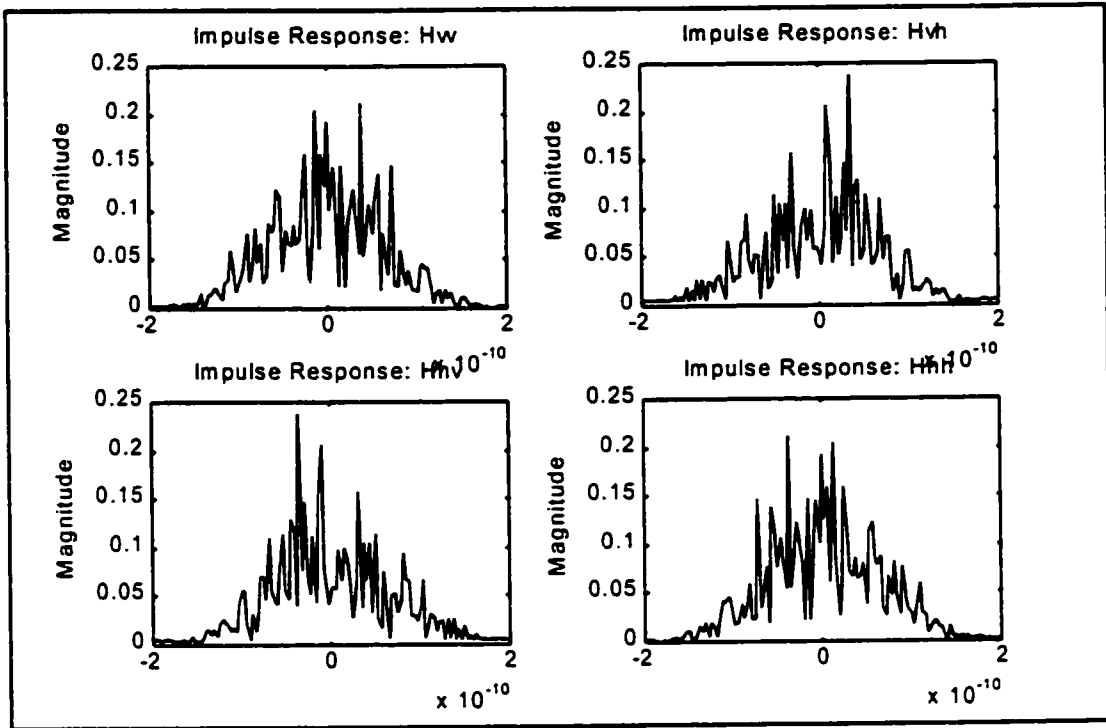


Figure 3.6 Magnitudes of Impulse Responses

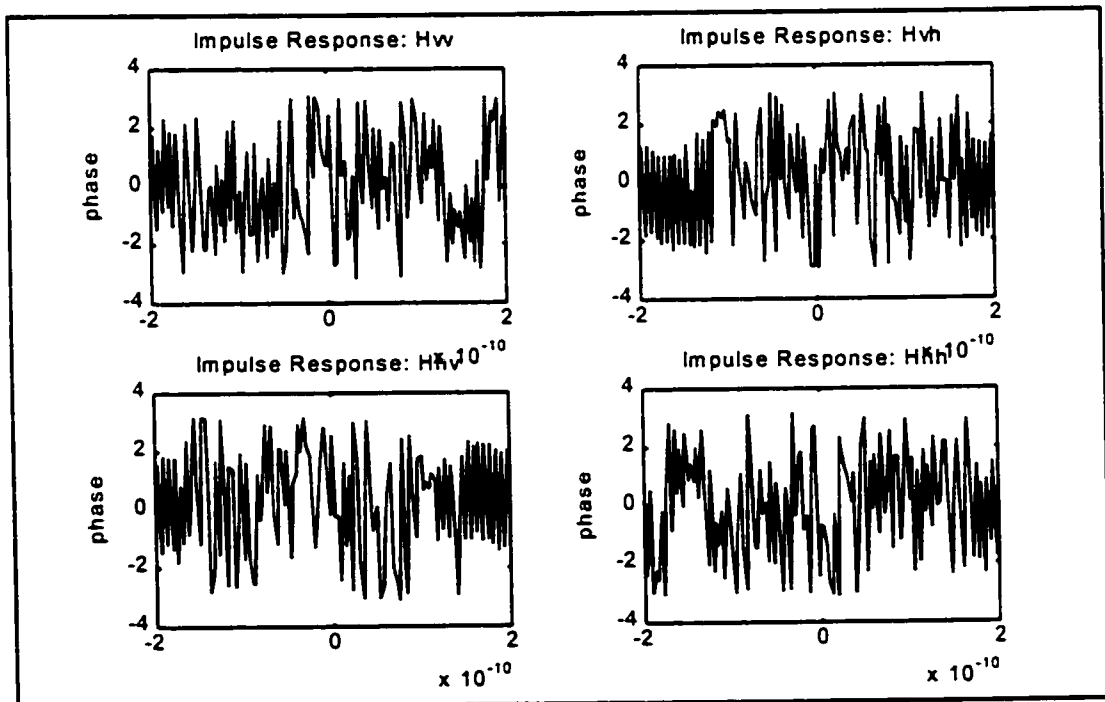


Figure 3.7 Phases of Impulse Responses

Fig. (3.8) shows the interferometric measurement of PMD ($\lambda = 1.3 \mu\text{m}$) of a 10 ps emulator in a IM-DD (Intensity Modulation with Direct Detection) transmission system [68]. Although it is a different type of transmission system, wavelength, and value of PMD (10 ps or 100 ps), there is a qualitative agreement between the measurement and the simulation.

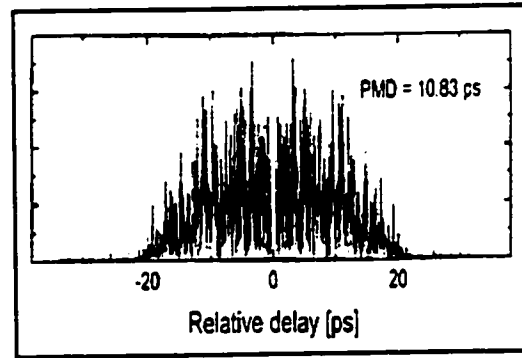


Figure 3.8 Interferometric Measurement of the 10-ps PMD Emulator [68]

3.5 Channel Simulation using MATLAB^c and SIMULINK^c

Based on the waveplate model and the baseband impulse responses, the optical fiber channel simulation is constructed in Fig. (3.9). It is just the implementation of the fiber model in Fig. (2.3).

In Fig. (3.9), V_{in} and H_{in} represent the inputs to the vertical and horizontal channels, and V_{out} and H_{out} represent the outputs of the vertical and horizontal channels. The impulse responses are complex, and the implementation of these impulse responses is shown in Fig. (3.10). A complex impulse response is comprised of four real impulse responses. Convolution of the input signals in Fig. (3.10) with these real impulse responses is realized by calling the MATLAB^c function, *filter()*, as in

$$y(t) = filter(h_y(t), x(t)), \quad (3.22)$$

where $y(t)$ is the output of fiber channel,

$h_y(t)$ is the real or imaginary part of baseband channel impulse response, which

can be one of $h_{vv}(t)$, $h_{vv}(t)$, $h_{vh}(t)$, $h_{vh}(t)$, $h_{iv}(t)$, $h_{iv}(t)$, $h_{ih}(t)$ or $h_{hh}(t)$,

$x(t)$ is the input signal vector, and

$filter()$ is a MATLAB[®] function.

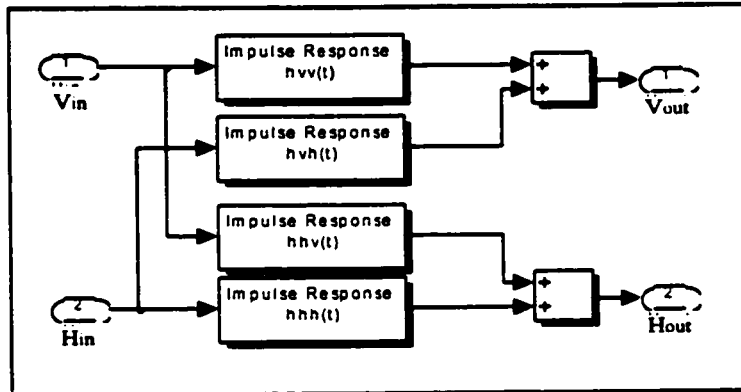


Figure 3.9 Optical Fiber Channel Simulation

In Fig. (3.10), S-Function, a SIMULINK[®] block, is used to call a MATLAB[®] function. The purpose of the “Buffer” and “Unbuffer” block is to convert scalars and vectors.

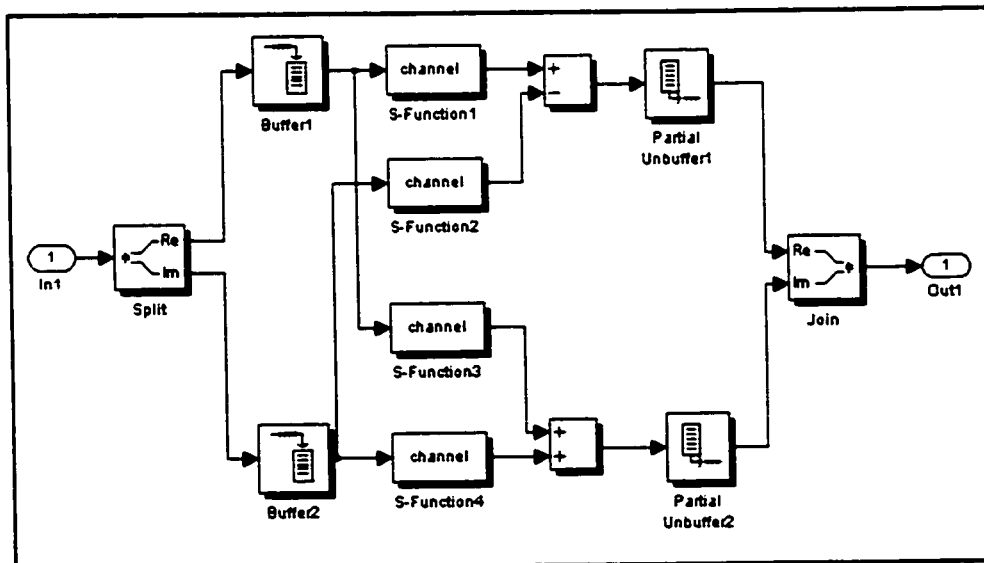


Figure 3.10 Simulation of Baseband Impulse Responses

Chapter 4

Adaptive Channel Equalizers and CPI Cancellers

4.1 Adaptive Channel Equalization Technique

4.1.1 Fundamentals of Equalization

The transmission of digital data through a linear communication channel usually suffers deterioration due to two major limits, ISI and additive thermal noise. ISI is caused by multipath in a bandlimited time dispersion channel which distorts the transmitted signal, causing bit errors at the receiver. In an optical fiber, the factors that can cause ISI are inter-mode dispersion, chromatic dispersion, and PMD.

Equalization is a technique to overcome ISI. Since the fading channel is usually random and time varying, equalizers must track the time varying characteristics of the fading channel, and this kind of equalizer is called adaptive equalizer which provides precise control over the time response of the channel.

Fig. (4.1) shows a communication system with an adaptive equalizer $c(t)$ [5]. $x(t)$ is the data input, and $f_a(t)$ is the overall complex baseband impulse response of the transmitter, channel and matched filter. The signal received by the equalizer is,

$$y(t) = x(t) * f_a(t) + v(t), \quad (4.1)$$

where $v(t)$ is the baseband Gaussian noise signal.

If the impulse response of equalizer is $c(t)$, then the output of the equalizer is

$y_{eq}(t)$,

$$\begin{aligned} y_{eq}(t) &= y(t) * c(t) \\ &= x(t) * f_a(t) * c(t) + v(t) * c(t) \\ &= x(t) * g_a(t) + v(t) * c(t), \end{aligned} \quad (4.2)$$

where $g_a(t)$ is the combined impulse response of the transmitter, channel, matched filter

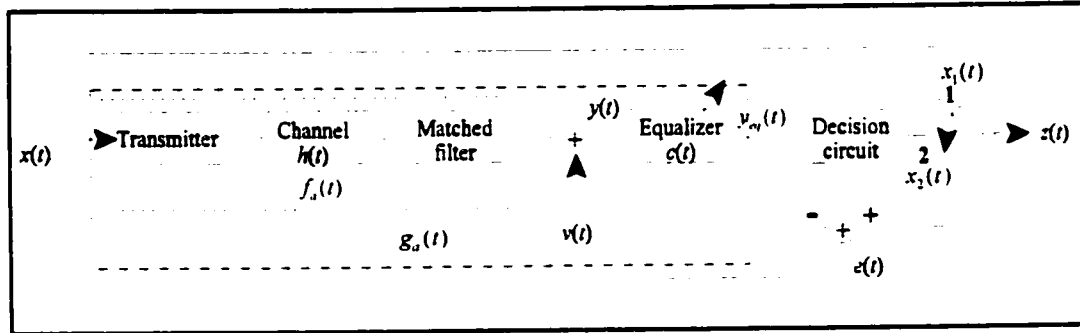


Figure 4.1 Equalization

and equalizer,

$$g_a(t) = f_a(t) * c(t). \quad (4.3)$$

The complex impulse response of equalizer $c(t)$ can be expressed as a transversal FIR filter with coefficients c_n ,

$$c(t) = \sum_{n=0}^{N-1} c_n \delta(t - nT). \quad (4.4)$$

where N is the number of filter taps.

Ideally, the desired output of equalizer, $y_{eq}(t)$, should be equal to the original input $x(t)$. If $v(t)$ is equal to zero, then to force $y_{eq}(t)$ equal to $x(t)$, Eq. (4.3) is used to get

$$g_a(t) = f_a(t) * c(t) = \delta(t). \quad (4.5)$$

In frequency domain, Eq. (4.5) can be expressed as,

$$F_a(f)C(f) = 1, \quad (4.6)$$

where $F_a(f)$ is the Fourier transform of $f_a(t)$, and

$C(f)$ is the Fourier transform of $c(t)$.

The result we get in Eq. (4.6) shows that when the baseband noise $v(t)$ is ignored, the equalizer filter $C(f)$ actually is an inverse filter of $F_a(f)$ which is the frequency response of the combination of fiber channel, transmitter and matched filter.

4.1.2 Adaptive Equalization

The characteristic of the time varying optical fiber channel requires the use of an adaptive equalizer. An adaptive equalizer needs the knowledge of the desired input so as to compare it with the output of the equalizer to get the error signal which is used in the adaptive algorithm. However, because of the different locations of transmitter and receiver, it is difficult to get the original data input to the transmitter in the receiver. There are two methods which can generate a “desired” signal as that in the transmitter [7].

1. The first method is called training. In this method, before data transmission, a sequence of PN (pseudonoise) signals are sent from transmitter as test signals. In the receiver, this PN signal is pre-stored and it is the same as that in the transmitter. The PN signal is called a training sequence, and the time to transmit the training sequence is called the training period. In the training period, the adaptive equalizer can adjust its filter coefficients and reaches a steady state where the smallest error is achieved. After the training period, the filter coefficients are fixed. Sometimes, the training sequence will be resent periodically to allow the adaptive equalizer to adapt to the time-varying channel. In Fig. (4.1), when the switch is switched to “1”, it means the receiver is using the

training sequence, $x_1(t)$.

2. The second method is called decision-directed. Usually this method is used along with the training method. In the training method, the equalizer is adapted using a training sequence. When the training period is over, the equalizer will be adapted using the decision-directed method at the receiver. After the training period, the error and ISI are very small. Therefore, the decisions made by the receiver are correct enough to be used as a replica of the desired signal. This means that the adaptive equalizer is able to improve the tap weight settings by virtue of the correlation procedure built into its feedback control loop. In Fig. (4.1), after the training period, the switch is then switched to "2" from "1", and $x_2(t)$ is used to estimate the error $e(t)$, which will be used to update the tap weights.

4.1.3 Adaptive Equalization Categorization and Algorithm

The general categorization of adaptive equalization techniques according to the types, structures and algorithms is shown in Fig. (4.2) [5].

Equalizer				
Linear	Type	Nonlinear		
		DFE	ML Symbol Detector	MLSE
Structure				
Transversal	Lattice	Transversal	Lattice	Equalizer
Zero Forcing LMS RLS	Gradient RLS	LMS RLS	Gradient RLS	LMS RLS
Algorithm				

Figure 4.2 Categorization of Adaptive Equalization [5]

Equalizers can be divided into two general categories, linear and nonlinear equalizers. In Fig. (4.1), there is no feedback from the output of receiver, $z(t)$, thus it is a linear equalizer. On the other hand, if $z(t)$ is fed back in order to control the equalizer, the equalizer is nonlinear.

In this thesis, a discrete LTE (Linear Transversal Equalizer) structure is used which is shown in Fig. (4.3). A discrete LTE is made up of K tapped delay lines which have a symbol period T_s , and the number of taps is K . In Fig. (4.3), the output of the LTE, $y(n)$ is,

$$y(n) = \sum_{k=0}^{K-1} c'_k(n)u(n-k), \quad (4.7)$$

where n is time index,

$u(n)$ is the baseband input signal, and

$c_k(n)$ are the complex coefficients.

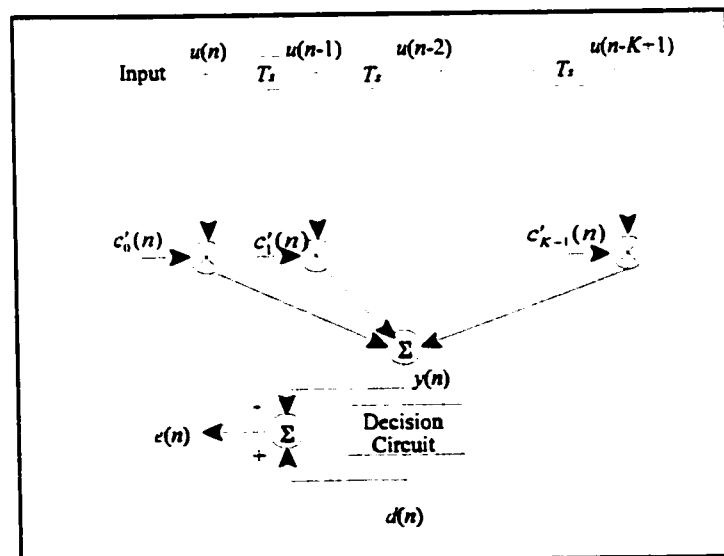


Figure 4.3 Linear LMS Transversal Equalizer

Classic adaptive equalizer algorithms include ZF (Zero Forcing), LMS (Least Mean Squares) and RLS (Recursive Least Squares). In this thesis, four linear LMS transversal adaptive filters are used as channel equalizers and CPI cancellers. The complex normalized LMS algorithm is described mathematically as [7,12],

$$\begin{aligned}
 y(n) &= \mathbf{c}^H(n)\mathbf{u}(n), \\
 e(n) &= d(n) - y(n), \\
 \mathbf{c}(n+1) &= \mathbf{c}(n) + \frac{\mu}{a + \mathbf{u}^H(n)\mathbf{u}(n)} \mathbf{u}(n)e'(n),
 \end{aligned} \tag{4.8}$$

where \bullet^H denotes Hermitian transpose of \bullet ,

$\mathbf{u}(n)$ is the K dimensional input signal vector at step n ,

$$\mathbf{u}(n) = [u(n) \ u(n-1) \ \dots \ u(n-K+1)]^T, \tag{4.9}$$

$\mathbf{c}(n)$ is the K dimensional vector of estimated of the equalizer tap weights at step n ,

$$\mathbf{c}(n) = [c_0(n) \ c_1(n) \ \dots \ c_{K-1}(n)]^T, \tag{4.10}$$

$d(n)$ is the “desired” signal,

$y(n)$ is the output of adaptive equalizer,

$e(n)$ is the estimated error,

μ is the adaptation constant, sometimes it is called step-size, and

a is a small positive constant (e^{-10}) used to overcome the potential numerical

instability in the tap weight update.

4.2 Channel Equalization and CPI Cancellation

The existence of PMD in an optical fiber introduces CPI between the dually polarized signals and ISI. This chapter contributes to realize CPI cancellation as well as ISI equalization.

Fig. (4.4) shows the discrete baseband structure of the channel equalizers and CPI cancellers, where $c_{vv}(n)$ and $c_{hh}(n)$ are the channel equalizers and we call $c_{vh}(n)$ and $c_{hv}(n)$ are the CPI cancellers.

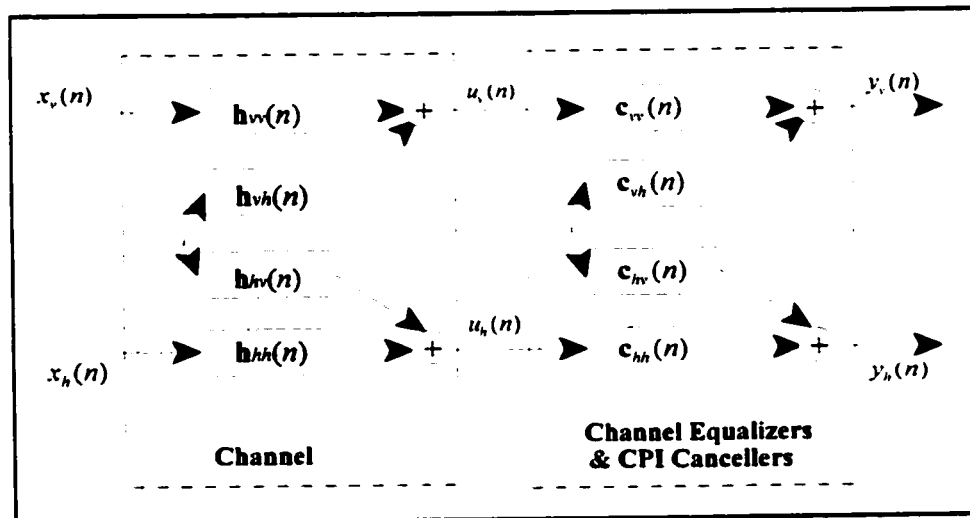


Figure 4.4 Channel Equalizers and CPI Cancellers

The complex inputs to the vertical and horizontal polarization channels are $x_v(n)$ and $x_h(n)$, and the outputs of channels are $u_v(n)$ and $u_h(n)$. Because this is a baseband model, the IF (Intermediate Frequency) stage and the modulator/demodulator are not shown. Thus the channel is followed by channel equalizers and CPI cancellers whose outputs are $y_v(n)$ and $y_h(n)$. We can express the relationship between these signals in matrix form,

$$\mathbf{u}(n) = \mathbf{h}(n) * \mathbf{x}(n) = \begin{bmatrix} \mathbf{h}_{vv}(n) & \mathbf{h}_{vh}(n) \\ \mathbf{h}_{hv}(n) & \mathbf{h}_{hh}(n) \end{bmatrix} * \begin{bmatrix} x_v(n) \\ x_h(n) \end{bmatrix} = \begin{bmatrix} u_v(n) \\ u_h(n) \end{bmatrix}, \quad (4.11)$$

$$\mathbf{y}(n) = \mathbf{c}^H(n) \mathbf{u}(n) = \begin{bmatrix} \mathbf{c}_{vv}^H(n) & \mathbf{c}_{vh}^H(n) \\ \mathbf{c}_{hv}^H(n) & \mathbf{c}_{hh}^H(n) \end{bmatrix} \begin{bmatrix} \mathbf{u}_v(n) \\ \mathbf{u}_h(n) \end{bmatrix} = \begin{bmatrix} y_v(n) \\ y_h(n) \end{bmatrix}, \quad (4.12)$$

where $\mathbf{y}(n)$ is the output signal vector,

$\mathbf{c}(n)$ is the matrix of adaptive channel equalizers and CPI cancellers,

$$\begin{aligned} \mathbf{c}_{vv}(n) &= [c_{vv0}(n) \quad c_{vv1}(n) \quad \dots \quad c_{vv(K-1)}(n)]^T, \\ \mathbf{c}_{vh}(n) &= [c_{vh0}(n) \quad c_{vh1}(n) \quad \dots \quad c_{vh(K-1)}(n)]^T, \\ \mathbf{c}_{hv}(n) &= [c_{hv0}(n) \quad c_{hv1}(n) \quad \dots \quad c_{hv(K-1)}(n)]^T, \\ \mathbf{c}_{hh}(n) &= [c_{hh0}(n) \quad c_{hh1}(n) \quad \dots \quad c_{hh(K-1)}(n)]^T, \end{aligned} \quad (4.13)$$

$u(n)$ is the fiber channel output at step n , (4.14)

$$\mathbf{u}(n) = \begin{bmatrix} u_v(n) \\ u_h(n) \end{bmatrix},$$

$\mathbf{u}(n)$ is the input signal vector to the equalizer,

$$\mathbf{u}(n) = \begin{bmatrix} \mathbf{u}_v(n) \\ \mathbf{u}_h(n) \end{bmatrix}, \quad (4.15)$$

$\mathbf{u}_v(n)$ and $\mathbf{u}_h(n)$ are the input signal vectors in vertical and horizontal channels to the equalizer,

$$\begin{aligned} \mathbf{u}_v(n) &= [u_v(n) \quad u_v(n-1) \quad \dots \quad u_v(n-K+1)]^T, \\ \mathbf{u}_h(n) &= [u_h(n) \quad u_h(n-1) \quad \dots \quad u_h(n-K+1)]^T, \end{aligned} \quad (4.16)$$

\bullet^T stands for the matrix transpose of \bullet ,

$\mathbf{x}(n)$ is the desired signal vector,

$$\mathbf{x}(n) = \begin{bmatrix} x_v(n) \\ x_h(n) \end{bmatrix}, \text{ and} \quad (4.17)$$

$\mathbf{h}(n)$ is the matrix of the complex baseband channel impulse responses, see

Eq. (2.21).

The error, $\mathbf{e}(n)$, is the difference between the desired response $\mathbf{x}(n)$ and output of the cancellers and equalizers, $\mathbf{y}(n)$,

$$\mathbf{e}(n) = \mathbf{x}(n) - \mathbf{y}(n) = \begin{bmatrix} x_v(n) - y_v(n) \\ x_h(n) - y_h(n) \end{bmatrix} = \begin{bmatrix} e_v(n) \\ e_h(n) \end{bmatrix}. \quad (4.18)$$

Next is defined the MSE (mean-squared error), $\mathbf{J}(n)$,

$$\begin{aligned} \mathbf{J}(n) &= E(\mathbf{e}(n)\mathbf{e}'(n)) = E(|\mathbf{e}(n)|^2) \\ &= \begin{bmatrix} E(e_v(n)e_v'(n)) \\ E(e_h(n)e_h'(n)) \end{bmatrix} = \begin{bmatrix} E(|e_v(n)|^2) \\ E(|e_h(n)|^2) \end{bmatrix} = \begin{bmatrix} J_v(n) \\ J_h(n) \end{bmatrix}, \end{aligned} \quad (4.19)$$

where $E(\bullet)$ denotes mathematical expectation of \bullet .

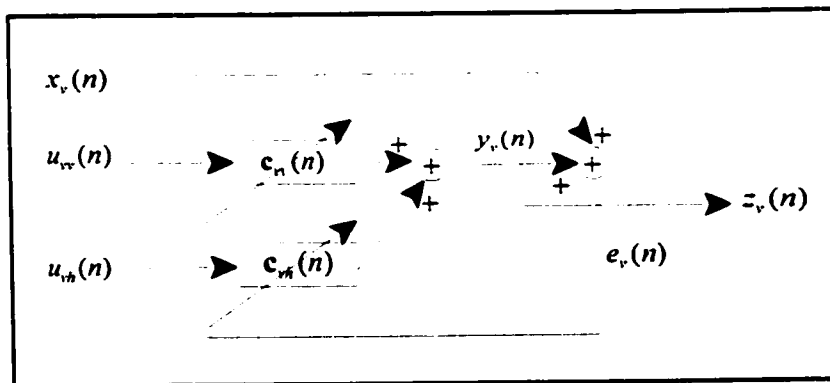


Figure 4.5 Vertical Channel Equalizer and CPI Canceller

To simplify the analysis, consider only the vertical polarization channel equalizer $\mathbf{c}_{vv}(n)$ and the CPI canceller $\mathbf{c}_{vh}(n)$ from the horizontal to the vertical channel, as shown in Fig. (4.5).

Suppose the complex filter tap weight vector for channel equalizer $\mathbf{c}_{vv}(n)$, is,

$$\mathbf{c}_{vv}(n) = \mathbf{a}_{vv}(n) + j\mathbf{b}_{vv}(n), \quad (4.20)$$

and for CPI canceller $\mathbf{c}_{vh}(n)$, it is,

$$\mathbf{c}_{vh}(n) = \mathbf{a}_{vh}(n) + j\mathbf{b}_{vh}(n), \quad (4.21)$$

where $\mathbf{a}(n)$ is the real part and $\mathbf{b}(n)$ is the imaginary part of tap weight $\mathbf{c}(n)$. The gradient of $J_v(n)$ with respect to $\mathbf{c}_{vv}(n)$ and $\mathbf{c}_{vh}(n)$ is [7],

$$\nabla_{vv}(J_v(n)) = \frac{dJ_v(n)}{d\mathbf{a}_{vv}(n)} + j \frac{dJ_v(n)}{d\mathbf{b}_{vv}(n)}, \quad (4.22)$$

$$\nabla_{vh}(J_v(n)) = \frac{dJ_v(n)}{d\mathbf{a}_{vh}(n)} + j \frac{dJ_v(n)}{d\mathbf{b}_{vh}(n)}. \quad (4.23)$$

where $\nabla_{vv}(J_v(n))$ is the gradient of $J_v(n)$ to $\mathbf{c}_{vv}(n)$, and

$\nabla_{vh}(J_v(n))$ is the gradient of $J_v(n)$ to $\mathbf{c}_{vh}(n)$.

Substituting the $J_v(n)$ of Eq. (4.19) in Eq. (4.22),

$$\nabla_{vv}(J_v(n)) = E \left[e'_v(n) \frac{de_v(n)}{d\mathbf{a}_{vv}(n)} + e_v(n) \frac{de'_v(n)}{d\mathbf{a}_{vv}(n)} + je'_v(n) \frac{de_v(n)}{d\mathbf{b}_{vv}(n)} + je_v(n) \frac{de'_v(n)}{d\mathbf{b}_{vv}(n)} \right], \quad (4.24)$$

According to Eqs. (4.12, 4.18, 4.20) [7],

$$\begin{aligned}
\frac{de_v(n)}{da_{vv}(n)} &= -\frac{dy_v(n)}{da_{vv}(n)} = -\mathbf{u}_v(n), \\
\frac{de_v(n)}{db_{vv}(n)} &= -\frac{dy_v(n)}{db_{vv}(n)} = j\mathbf{u}_v(n), \\
\frac{de'_v(n)}{da_{vv}(n)} &= -\frac{dy'_v(n)}{da_{vv}(n)} = -\mathbf{u}'_v(n), \\
\frac{de'_v(n)}{db_{vv}(n)} &= -\frac{dy'_v(n)}{db_{vv}(n)} = -j\mathbf{u}'_v(n).
\end{aligned} \tag{4.25}$$

Therefore, the final result will be,

$$\nabla_{vv}(J_v(n)) = -2E[\mathbf{u}_v(n)e'_v(n)], \tag{4.26}$$

Same as the $\nabla_{vv}(J_v(n))$, $\nabla_{vh}(J_v(n))$ is,

$$\nabla_{vh}(J_v(n)) = -2E[\mathbf{u}_h(n)e'_v(n)]. \tag{4.27}$$

To study the channel equalizer $\mathbf{c}_{vv}(n)$, expand Eq. (4.22), giving,

$$\begin{aligned}
\nabla_{vv}(J_v(n)) &= -2E[\mathbf{u}_v(n)e'_v(n)] \\
&= -2E[\mathbf{u}_v(n)(x'_v(n) - \mathbf{c}_{vv}^T(n)\mathbf{u}'_v(n) - \mathbf{c}_{vh}^T(n)\mathbf{u}'_h(n))] \\
&= -2\mathbf{P}_{vv}(n) + 2\mathbf{c}_{vv}(n)\mathbf{R}_{vv}(n) + 2\mathbf{c}_{vh}(n)\mathbf{Q}_{vv}(n),
\end{aligned} \tag{4.28}$$

where $\mathbf{P}_{vv}(n)$ is the cross-correlation vector between the input vector to the equalizer $\mathbf{u}_v(n)$

and the desired response $x_v(n)$,

$$\mathbf{P}_{vv}(n) = E[\mathbf{u}_v(n)x'_v(n)], \tag{4.29}$$

$\mathbf{R}_{vv}(n)$ is the auto-correlation matrix of the input vector to the equalizer $\mathbf{u}_v(n)$

$$\mathbf{R}_{vv}(n) = E[\mathbf{u}_v(n)\mathbf{u}_v^H(n)], \tag{4.30}$$

$\mathbf{Q}_{vv}(n)$ is the cross-correlation vector between the input vector to the equalizer

$\mathbf{u}_v(n)$ in the vertical polarization channel and the input vector in the

vertical polarization channel $\mathbf{u}_h(n)$,

$$\mathbf{Q}_{vv}(n) = E[\mathbf{u}_v(n)\mathbf{u}_h^H(n)]. \quad (4.31)$$

Similar to above, $\nabla_{vh}(J_v(n))$ can be expanded to get,

$$\nabla_{vh}(J_v(n)) = -2\mathbf{P}_{vh}(n) + 2\mathbf{Q}_{vh}(n)\mathbf{c}_{vv}(n) + 2\mathbf{R}_{vh}(n)\mathbf{c}_{vh}(n), \quad (4.32)$$

and,

$$\mathbf{P}_{vh}(n) = E[\mathbf{u}_h(n)x'_v(n)], \quad (4.33)$$

$$\mathbf{R}_{vh}(n) = E[\mathbf{u}_h(n)\mathbf{u}_v^H(n)], \text{ and} \quad (4.34)$$

$$\mathbf{Q}_{vh}(n) = E[\mathbf{u}_h(n)\mathbf{u}_h^H(n)]. \quad (4.35)$$

According to the method of steepest descent, the updated value of the tap-weight vectors for equalizer $\mathbf{c}_{vv}(n)$ and canceller $\mathbf{c}_{vh}(n)$ are,

$$\mathbf{c}_{vv}(n+1) = \mathbf{c}_{vv}(n) - \frac{1}{2}\mu\nabla_{vv}(J_v(n)), \quad (4.36)$$

and

$$\mathbf{c}_{vh}(n+1) = \mathbf{c}_{vh}(n) - \frac{1}{2}\mu\nabla_{vh}(J_v(n)), \quad (4.37)$$

where μ is called step size, an adaption constant which controls the size of the

incremental correction applied to the tap-weight vector [7]. Substituting in $\nabla_{vv}(J_v(n))$ and

$\nabla_{vh}(J_v(n))$ from Eqs. (4.28, 4.32),

$$\mathbf{c}_{vv}(n+1) = \mathbf{c}_{vv}(n) + \mu [\mathbf{P}_{vv}(n) - \mathbf{R}_{vv}(n)\mathbf{c}_{vv}(n) - \mathbf{Q}_{vh}(n)\mathbf{c}_{vh}(n)], \quad (4.38)$$

$$\mathbf{c}_{vh}(n+1) = \mathbf{c}_{vh}(n) + \mu [\mathbf{P}_{vh}(n) - \mathbf{R}_{vh}(n)\mathbf{c}_{vv}(n) - \mathbf{Q}_{vh}(n)\mathbf{c}_{vh}(n)]. \quad (4.39)$$

In Eqs. (4.38,4.39), the adaptive tap-weights for channel equalizer $\mathbf{c}_{vv}(n)$ and CPI canceller $\mathbf{c}_{vh}(n)$ are established. In reality, however, this method will not work because the exact measurement of the gradient vector $\nabla_{vv}(J_v(n))$ and $\nabla_{vh}(J_v(n))$ is impossible since it requires the correlation matrix $\mathbf{R}(n)$ and cross-correlation matrixes $\mathbf{P}(n)$ and $\mathbf{Q}(n)$. Therefore, $\nabla_{vv}(J_v(n))$ and $\nabla_{vh}(J_v(n))$ must be estimated from the available data. This idea is realized in the LMS algorithm.

In the LMS algorithm, the instantaneous estimates are used instead of the correlation matrix $\mathbf{R}(n)$ and cross-correlation matrices $\mathbf{P}(n)$ and $\mathbf{Q}(n)$, and for channel equalizer $\mathbf{c}_{vv}(n)$, they are defined by, respectively,

$$\hat{\mathbf{P}}_{vv}(n) = \mathbf{u}_v(n)x'_v(n), \quad (4.40)$$

$$\hat{\mathbf{R}}_{vv}(n) = \mathbf{u}_v(n)\mathbf{u}_v^H(n), \quad (4.41)$$

$$\hat{\mathbf{Q}}_{vh}(n) = \mathbf{u}_v(n)\mathbf{u}_h^H(n). \quad (4.42)$$

The corresponding instantaneous estimate of the gradient vector is then,

$$\hat{\nabla}_{vv}(J_v(n)) = -2\mathbf{u}_v(n)x'_v(n) + 2\mathbf{u}_v(n)\mathbf{u}_v^H(n)\hat{\mathbf{c}}_{vv} + 2\mathbf{u}_v(n)\mathbf{u}_h^H(n)\hat{\mathbf{c}}_{vh}, \quad (4.43)$$

where $\hat{\mathbf{c}}_{vv}(n)$ is the estimated tap-weight of channel equalizer $\mathbf{c}_{vv}(n)$, and $\hat{\mathbf{c}}_{vh}(n)$ is the estimated tap-weight of CPI canceller $\mathbf{c}_{vh}(n)$.

Substituting the estimated gradient vector $\hat{\nabla}_{vv}(J_v(n))$ in Eq. (4.43) for the $\nabla_{vv}(J_v(n))$ in Eq. (4.36), gives get the adaptive tap-weight in the LMS algorithm,

$$\hat{\mathbf{c}}_{vv}(n+1) = \hat{\mathbf{c}}_{vv}(n) + \mu \mathbf{u}_v(n) \left[x'_v(n) - \mathbf{u}_v^H(n) \hat{\mathbf{c}}_{vv}(n) - \mathbf{u}_h^H(n) \hat{\mathbf{c}}_{vh}(n) \right], \quad (4.44)$$

and similar to Eq. (4.43),

$$\hat{\mathbf{c}}_{vh}(n+1) = \hat{\mathbf{c}}_{vh}(n) + \mu \mathbf{u}_h(n) \left[x'_v(n) - \mathbf{u}_v^H(n) \hat{\mathbf{c}}_{vv}(n) - \mathbf{u}_h^H(n) \hat{\mathbf{c}}_{vh}(n) \right], \quad (4.45)$$

$$\hat{\mathbf{c}}_{hv}(n+1) = \hat{\mathbf{c}}_{hv}(n) + \mu \mathbf{u}_v(n) \left[x'_h(n) - \mathbf{u}_h^H(n) \hat{\mathbf{c}}_{hh}(n) - \mathbf{u}_v^H(n) \hat{\mathbf{c}}_{hv}(n) \right], \quad (4.46)$$

$$\hat{\mathbf{c}}_{hh}(n+1) = \hat{\mathbf{c}}_{hh}(n) + \mu \mathbf{u}_h(n) \left[x'_h(n) - \mathbf{u}_h^H(n) \hat{\mathbf{c}}_{hh}(n) - \mathbf{u}_v^H(n) \hat{\mathbf{c}}_{hv}(n) \right]. \quad (4.47)$$

When the input $\mathbf{u}(n)$ is large, the LMS algorithm experiences a gradient noise amplification problem [7]. Therefore, the normalized algorithm is used to overcome this problem. The normalized algorithms of Eqs. (4.41 -4.44) are,

$$\hat{\mathbf{c}}_{vv}(n+1) = \hat{\mathbf{c}}_{vv}(n) + \frac{\mu \mathbf{u}_v(n)}{\alpha + \mathbf{u}_v^H(n) \mathbf{u}_v(n)} \left[x'_v(n) - \mathbf{u}_v^H(n) \hat{\mathbf{c}}_{vv}(n) - \mathbf{u}_h^H(n) \hat{\mathbf{c}}_{vh}(n) \right], \quad (4.48)$$

$$\hat{\mathbf{c}}_{vh}(n+1) = \hat{\mathbf{c}}_{vh}(n) + \frac{\mu \mathbf{u}_h(n)}{\alpha + \mathbf{u}_h^H(n) \mathbf{u}_h(n)} \left[x'_v(n) - \mathbf{u}_v^H(n) \hat{\mathbf{c}}_{vv}(n) - \mathbf{u}_h^H(n) \hat{\mathbf{c}}_{vh}(n) \right], \quad (4.49)$$

$$\hat{\mathbf{c}}_{hv}(n+1) = \hat{\mathbf{c}}_{hv}(n) + \frac{\mu \mathbf{u}_v(n)}{\alpha + \mathbf{u}_v^H(n) \mathbf{u}_v(n)} \left[x'_h(n) - \mathbf{u}_h^H(n) \hat{\mathbf{c}}_{hh}(n) - \mathbf{u}_v^H(n) \hat{\mathbf{c}}_{hv}(n) \right], \quad (4.50)$$

$$\hat{\mathbf{c}}_{hh}(n+1) = \hat{\mathbf{c}}_{hh}(n) + \frac{\mu \mathbf{u}_h(n)}{\alpha + \mathbf{u}_h^H(n) \mathbf{u}_h(n)} \left[x'_h(n) - \mathbf{u}_h^H(n) \hat{\mathbf{c}}_{hh}(n) - \mathbf{u}_v^H(n) \hat{\mathbf{c}}_{hv}(n) \right], \quad (4.51)$$

where μ is the step size, $0 < \mu < 2$,

α is a small positive constant.

4.3 Simulation of Channel Equalizers and CPI Cancellers

4.3.1 Simulation Structure of Channel Equalizers and CPI Cancellers

Based on the Eqs. (4.48-4.51), the Normalized LMS channel equalizers or CPI cancellers can be constructed using SIMULINK^c as shown in Fig. (4.6).

Fig. (4.6) shows the model of the normalized LMS filter. In this model, the first input is $u(n)$, the second input is error $e(n)$ and the output is $y(n)$. The buffer is used to generate input signal vector $\mathbf{u}(n)$.

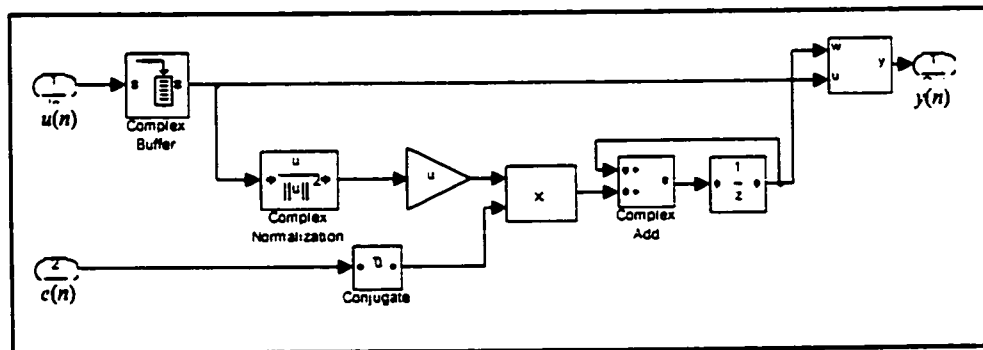


Figure 4.6 LMS Adaptive Filter

The overall adaptive equalization and cancellation system is shown in Fig. (4.7). Complex delays, z^{-31} and z^{-64} , are used to synchronize the output of the equalizer and the desired input. The factors that cause the delay include the transmitter filter, receiver filter and channel delay. So the desired input from the information generator has to be delayed by the same time. The input signals are sampled at the rate $f_s = B$ which is 128 times lower than the channel sampling rate before they go into the equalizer. Two switches are used to select the training or decision-directed method. At the beginning of this simulation, the switches are set to the training method. In every bit period, the tap-weights are adjusted to minimize the errors. After the MSE reaches the steady state,

switches are then set to decision-directed method where output signals of the decision circuits are used as the desired input.

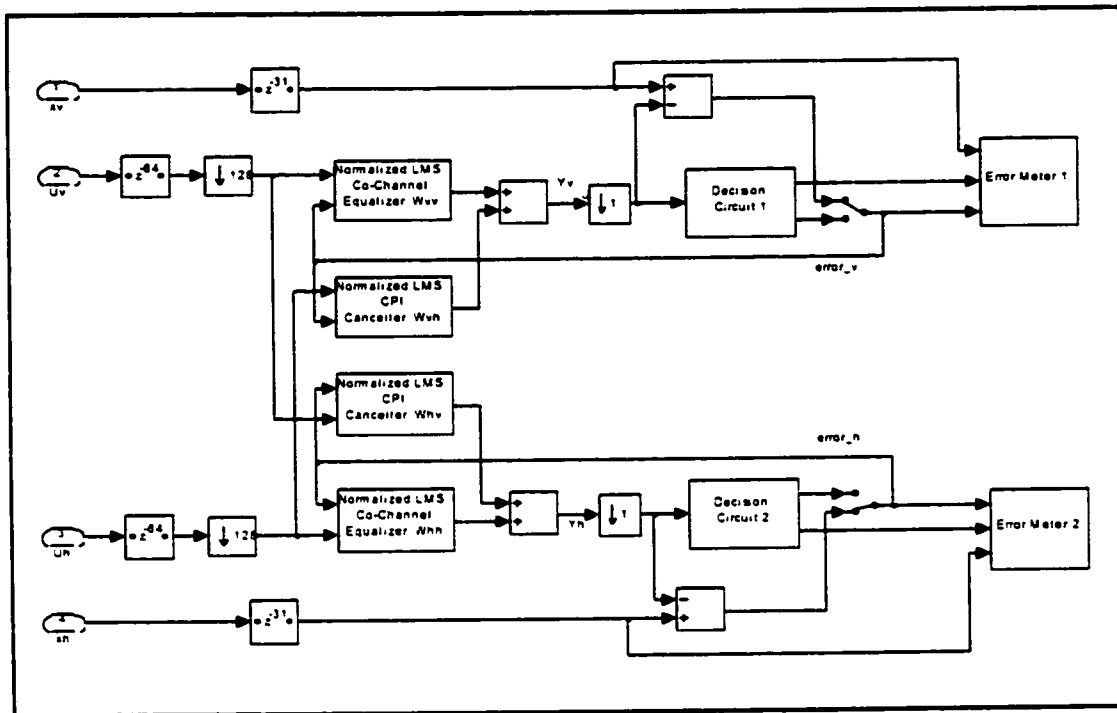


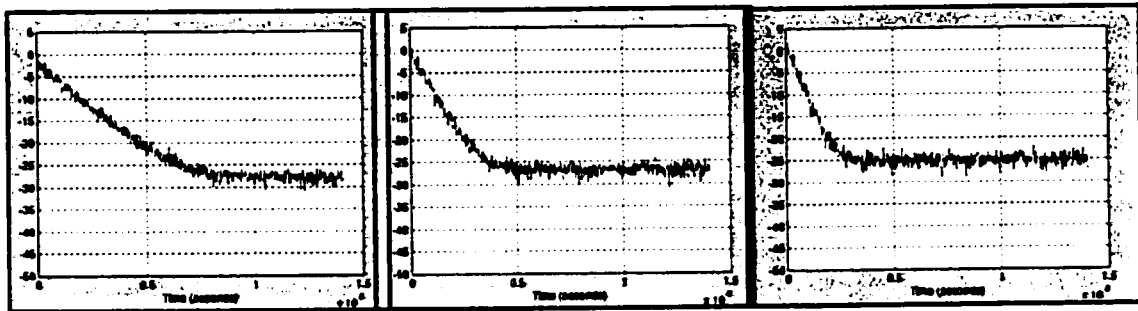
Figure 4.7 Adaptive Channel Equalizers and CPI Cancellers

4.3.2 Performance of Channel Equalizers and CPI Cancellers

From Eqs. (4.48-4.51), we can see that the value of step-size μ is very important. Fig. (4.8) shows three leaning curves with errors (dB) on the ordinates, when μ is 0.2, 0.4 and 0.6 respectively. By comparing these three cases, it is clear we have to tradeoff the training time versus the residual error. When μ is 0.2, the error is the smallest, but it takes longer time to train. When μ is 0.6, the equalizer can reach the steady state quickly, but the error is the largest. Thus we choose μ equal to 0.4, which is the best compromise.

Also, the number of taps in the equalizer and canceller is the factor that affects the performance and accuracy of the receiver. In the simulation system, we choose 8 taps for

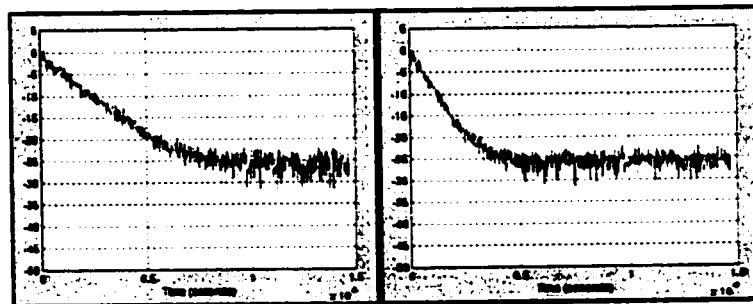
equalizers and cancellers rather than 16 taps, because when we use 8 taps, the filter takes less time to reach steady state and has smaller variance. The errors (dB) of the equalizer and canceller when number of filter number of taps is 8 and 16 are shown in Figs. (4.9a,4.9b).



**J (dB) when $\mu=0.2$
Figure 4.8 (a)**

**J (dB) when $\mu=0.4$
Figure 4.8 (b)**

**J (dB) when $\mu=0.6$
Figure 4.8 (c)**



**J (dB)
when Filter Length=16
Figure 4.9 (a)**

**J (dB)
when Filter Length=8
Figure 4.9 (b)**

Chapter 5

System Performance

5.1 Eye Pattern

The eye pattern is a convenient way to see the distortion on a channel, which is usually obtained by displaying the data pulse stream on an oscilloscope. A two level signal after an RC filter with filter rolloff factor of 0.8 in the transmitter is shown in Fig. (5.1). In this eye pattern, one symbol interval is displayed, and the central vertical line indicates the decision point where one can

get the lowest error and best BER. Thus sampling should occur at this point where eye is open the widest. If all of the lines in the traces go through the desired pulse amplitude at the decision point, then the eye is said to be fully open, such as the one in Fig (5.1).

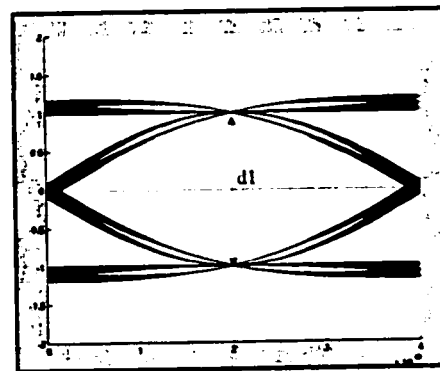


Figure 5.1 Fully Open Eye Pattern

Through the eye pattern, we can roughly measure the performance of the received signal in the receiver, which suffers from the PMD and noise. When the input SNR is 30 dB, the eye pattern in the receiver is obtained as shown in Fig (5.2). By comparing these two figures, it is clear that the width of eye pattern d_2 in Fig. (5.2) is smaller than d_1 , which indicates the latter traces deviate from the completely open eye pattern.

Fig. (5.3) is the eye pattern when input SNR is 15 dB. The width of eye pattern d_3 is

much smaller than d_2 , so the error probability is larger, because there is a smaller space to distinguish between the two levels.

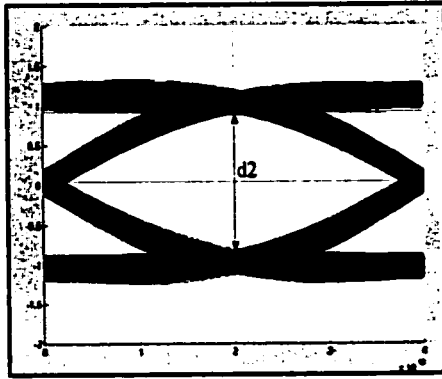


Figure 5.2 Eye Pattern (SNR=30)

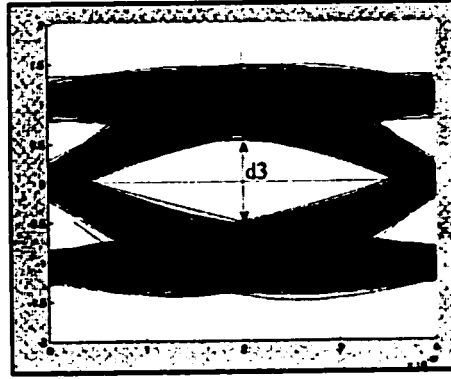


Figure 5.3 Eye Pattern (SNR=15)

5.2 Bit Error Rate Evaluation

The eye pattern is only a rough method to measure the error. To analyze accurately the performance of a telecommunication system, the bit error rate (BER) must be known.

The simplest way to measure BER is error counting, or counting the number of error bits in a period. This is simple, but it may not be accurate. Also because the BER in an optical fiber communication system is very low, usually lower than 10^{-9} , it requires a rather long time to get a satisfactory result by simulation.

An alternative way to measure BER is by calculation. Consider the case in which the transmitted signal over the vertical or horizontal channel is $s(t)$,

$$s(t) = \begin{bmatrix} \sqrt{E} \\ 0 \end{bmatrix}, \quad (5.1)$$

where E is the input signal power. The corresponding received signal in receiver, $r(t)$, is

$$r(t) = \begin{bmatrix} \sqrt{E} + n_1 \\ n_2 \end{bmatrix}, \quad (5.2)$$

where n_1 and n_2 are the error signals with zero mean and the same variance, σ^2 ,

$$\sigma^2 = \sigma_1^2 = \sigma_2^2, \quad (5.3)$$

where σ_1^2 and σ_2^2 are the variances of n_1 and n_2 , respectively. This distortion in the detected bit is due to ISI, CPI and noise. To simplify the calculations, the distortion is treated as Gaussian noise. For high signal-to-noise ratios, this assumption will produce an acceptable estimate of the BER.

Thus the symbol error probability for 4-level QAM signal is [8], P_s ,

$$P_s = 1 - \left[1 - Q\left(\sqrt{\frac{E}{2\sigma^2}}\right) \right]^2, \quad (5.4)$$

where $Q(\bullet)$ stands for Q -function, which is defined as,

$$Q(z) = \int_z^{\infty} \frac{1}{\sqrt{2\pi}} e^{-\frac{y^2}{2}} dy. \quad (5.5)$$

Suppose, the received SNR, γ , is,

$$\gamma = \frac{E}{2\sigma^2}, \quad (5.6)$$

then the symbol error probability in Eq. (5.4) is,

$$P_s = 1 - \left[1 - Q(\sqrt{\gamma}) \right]^2. \quad (5.7)$$

The relationship between bit error rate, P_b , and P_s is,

$$1 - (1 - P_b)^2 = P_s. \quad (5.8)$$

Thus, we have,

$$P_b = Q(\sqrt{\gamma}). \quad (5.9)$$

The relationship between the received SNR, γ , and minimum MSE, J_{min} , is [8],

$$\gamma = \frac{1 - J_{min}}{J_{min}} \approx \frac{1}{J_{min}}, \quad (5.10)$$

Thus, BER can be obtained by measuring the J_{min} ,

$$P_b = Q\left(\sqrt{\frac{1}{J_{min}}}\right). \quad (5.11)$$

Therefore, it is possible to measure the minimum received MSE J_{min} when the channel equalizers and CPI cancellers reach the steady state, and to get the BER according to Eq. (5.11).

In this simulation system, the channel and receiver thermal noises are treated as Gaussian noises, the input signal power is 0 dB. The signal bit rate is 2.5 GHz. The system SNR, γ_s , is from 4 to 32 dB, where,

$$\gamma_s = \frac{E}{2\sigma_c^2}, \text{ and} \quad (5.12)$$

σ_c^2 is the variance of channel Gaussian noise. The DGD is 10 ps, 100 ps and 500 ps, separately. The number of the adaptive filter taps is 8, and step-size, μ , is 0.4. The training time is longer than 3×10^{-6} sec for 10-ps PMD, 5×10^{-6} sec for 100-ps PMD and 10×10^{-6} sec for 500-ps PMD. We measure the J_{min} four times (No. 1 to No. 4) for every γ_s . Each time, the J_{min} in vertical in-phase signal, vertical quadrature signal, horizontal in-phase and horizontal quadrature signal are obtained. The experimental results of J_{min} are listed in Tables (5.1, 5.2, 5.3).

Table 5.1 J_{min} (dB) when DGD is 10 ps

γ_s (dB)	No.	J_{min} (dB) (DGD = 10 ps)					Avg. J_{min} (dB)
		Vertical In-phase	Vertical Quadrature	Horizontal In-phase	Horizontal Quadrature	Avg.	
4	1	-6.78	-7.84	-13.2	-12.7	-10.1	-10.2
	2	-12.3	-12.0	-8.50	-8.51	-10.3	
	3	-13.1	-11.9	-9.45	-7.22	-10.4	
	4	-11.8	-11.1	-7.91	-8.94	-9.94	
8	1	-13.9	-13.1	-9.76	-12.7	-12.4	-11.6
	2	-10.2	-10.5	-10.8	-9.50	-10.2	
	3	-11.3	-11.6	-10.7	-12.3	-11.4	
	4	-13.2	-13.1	-13.0	-10.8	-12.5	
12	1	-12.8	-12.8	-11.3	-12.9	-12.4	-13.5
	2	-12.3	-12.5	-14.9	-14.7	-13.6	
	3	-14.0	-15.1	-14.3	-12.8	-14.0	
	4	-14.1	-13.6	-15.8	-12.2	-13.9	
16	1	-14.0	-13.5	-11.8	-14.7	-13.5	-15.3
	2	-16.9	-16.4	-17.0	-16.2	-16.6	
	3	-13.5	-14.0	-13.0	-17.3	-14.4	
	4	-18.8	-17.1	-16.4	-13.9	-16.6	
20	1	-17.0	-17.3	-19.2	-17.3	-17.7	-18.3
	2	-17.6	-18.9	-22.6	-18.0	-19.2	
	3	-17.3	-17.0	-19.7	-16.0	-17.55	
	4	-16.9	-17.7	-18.3	-21.9	-18.7	
24	1	-24.1	-23.6	-27.7	-21.7	-24.3	-23.6
	2	-23.1	-25.5	-26.5	-30.1	-26.3	

	3	-21.3	-22.5	-26.5	-21.6	-23.0	
	4	-20.6	-20.0	-23.2	-19.1	-20.7	
28	-1	-29.5	-31.5	-32.1	-36.3	-32.3	-29.5
	2	-25.1	-26.6	-30.5	-25.6	-26.9	
	3	-27.4	-27.6	-33.1	-28.1	-29.0	
	4	-29.6	-30.8	-29.3	-29.6	-29.8	

Table 5.2 J_{min} (dB) when DGD is 100 ps

γ_s (dB)	No.	J_{min} (dB) (DGD = 100 ps)					Avg. J_{min} (dB)
		Vertical In-phase	Vertical Quadrature	Horizontal In-phase	Horizontal Quadrature	Avg.	
4	1	-9.57	-8.31	-8.22	-9.47	-8.89	-7.75
	2	-7.46	-6.77	-5.54	-5.51	-6.32	
	3	-8.27	-7.58	-7.51	-7.94	-7.83	
	4	-8.27	-7.23	-7.77	-7.43	-7.67	
8	1	-12.0	-9.05	-11.5	-8.91	-10.4	-9.13
	2	-11.2	-9.42	-10.4	-9.66	-10.2	
	3	-8.41	-7.34	-8.05	-8.77	-8.14	
	4	-8.89	-7.58	-7.70	-7.20	-7.84	
12	1	-12.6	-10.7	-11.0	-11.8	-11.5	-10.8
	2	-12.3	-10.3	-10.2	-11.9	-11.2	
	3	-11.0	-9.31	-9.57	-10.6	-10.1	
	4	-10.8	-9.89	-10.2	-10.1	-10.2	
16	1	-12.7	-10.5	-10.5	-12.5	-11.6	-12.5
	2	-14.2	-11.0	-13.2	-11.5	-12.5	

	3	-12.3	-10.4	-10.9	-11.3	-11.2	
	4	-16.5	-13.1	-13.1	-16.3	-14.8	
20	1	-19.3	-14.6	-17.7	-15.1	-16.7	-15.1
	2	-14.9	-11.3	-12.4	-13.0	-12.9	
	3	-18.6	-14.1	-16.6	-15.1	-16.1	
	4	-14.5	-14.1	-16.1	-14.0	-14.7	
24	1	-19.8	-15.1	-15.6	-18.5	-17.2	-18.2
	2	-22.0	-17.0	-19.9	-17.8	-19.2	
	3	-25.6	-20.6	-21.6	-23.6	-22.9	
	4	-19.0	-14.2	-19.0	-14.1	-16.6	
28	1	-25.1	-19.6	-25.1	-19.6	-22.4	-22.9
	2	-28.2	-22.6	-27.7	-23.1	-25.5	
	3	-24.8	-19.1	-21.1	-20.8	-21.4	
	4	-26.5	-21.2	-23.9	-22.4	-23.5	
32	1	-29.8	-24.3	-27.6	-25.1	-26.7	-28.6
	2	-29.3	-31.6	-30.6	-29.5	-30.3	
	3	-30.0	-27.5	-29.2	-27.8	-28.6	
	4	-28.5	-27.7	-26.8	-31.9	-28.7	

Table 5.3 J_{min} (dB) when DGD is 500 ps

γ_s (dB)	No.	J_{min} (dB) DGD = 500 ps					Avg. J_{min} (dB)
		Vertical In-phase	Vertical Quadrature	Horizontal In-phase	Horizontal Quadrature	Avg.	
4	1	-4.16	-4.00	-4.08	-4.10	-4.09	-4.15
	2	-4.07	-4.09	-4.06	-4.12	-4.09	

	3	-4.16	-4.19	-4.37	-4.39	-4.27	
	4	-4.17	-4.28	-4.31	-4.30	-4.27	
8	1	-7.07	-7.20	-5.68	-5.74	-6.42	-5.93
	2	-5.66	-5.73	-7.01	-7.08	-6.37	
	3	-5.60	-6.14	-7.05	-7.56	-6.59	
	4	-4.33	-4.41	-4.36	-4.31	-4.35	
12	1	-6.75	-6.88	-7.96	-7.69	-7.32	-7.74
	2	-7.76	-8.74	-10.6	-10.7	-9.46	
	3	-6.05	-6.31	-7.32	-6.98	-6.66	
	4	-7.29	-7.67	-7.77	-7.38	-7.53	
16	1	-8.80	-9.76	-10.8	-9.94	-9.84	-10.2
	2	-9.24	-10.6	-10.9	-9.60	-10.1	
	3	-8.09	-8.39	-8.21	-8.56	-8.31	
	4	-11.4	-14.1	-12.8	-12.2	-12.6	
20	1	-12.4	-14.8	-14.3	-13.6	-13.8	-12.5
	2	-9.74	-11.4	-11.4	-9.93	-10.6	
	3	-12.0	-14.5	-14.9	-12.6	-13.5	
	4	-11.4	-12.8	-13.1	-11.7	-12.2	
24	1	-11.6	-14.6	-13.2	-12.1	-12.9	-14.5
	2	-16.8	-17.8	-17.7	-17.6	-17.5	
	3	-14.2	-16.4	-14.4	-16.7	-15.4	
	4	-13.7	-14.9	-15.1	-14.1	-14.4	
28	1	-15.7	-16.4	-16.8	-16.1	-16.2	-16.2
	2	-16.2	-17.5	-17.2	-17.0	-17.0	
	3	-15.1	-16.5	-15.6	-16.9	-16.0	
	4	-14.6	-16.1	-16.2	-15.0	-15.4	

32	1	-17.4	-17.8	-18.0	-18.0	-17.8	-18.2
	2	-16.9	-17.4	-17.8	-17.3	-17.4	
	3	-19.3	-21.8	-22.4	-19.2	-20.7	
	4	-15.7	-18.4	-16.3	-17.4	-16.9	

From the above tables and Eq. (5.11), the BER plot is shown in Fig. (5.4). This figure shows the BER when DGD is 10, 100 and 500 ps. From the BER plot, to make the BER smaller than 10^{-9} , the system SNR, γ_s , should be larger than 17 dB when DGD is 10 ps, larger than 21 dB when DGD is 100 ps, and larger than 27 dB when DGD is 500 ps. Also the BER plot shows the trends of BER for these three cases. With the increase of γ_s , the plot of BER when DGD is 10 and 100 ps decrease steeply, however, when DGD is 500 ps, it decreases slowly.

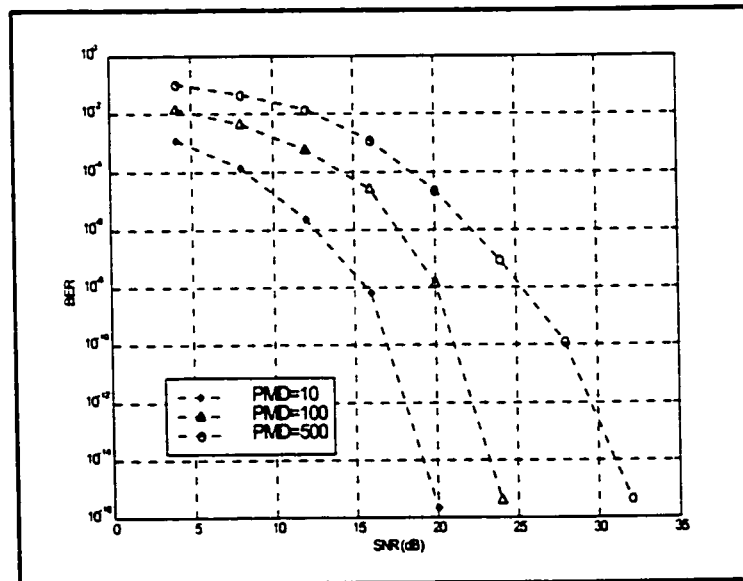


Figure 5.4 BER Plot

Chapter 6

Bidirectional Transmission System

6.1 Bidirectional Transmission System

Until now, what was discussed is an unidirectional data transmission system through a fiber. Ordinarily, to realize a duplex transmission using only one wavelength, two fibers are required, one for the forward transmission, the other for the backward transmission.

In this thesis, a different strategy, a bidirectional transmission system is presented. In this strategy, a transceiver is used, which consists a transmitter, a receiver and a coupler. This strategy is shown in Fig. (6.1).

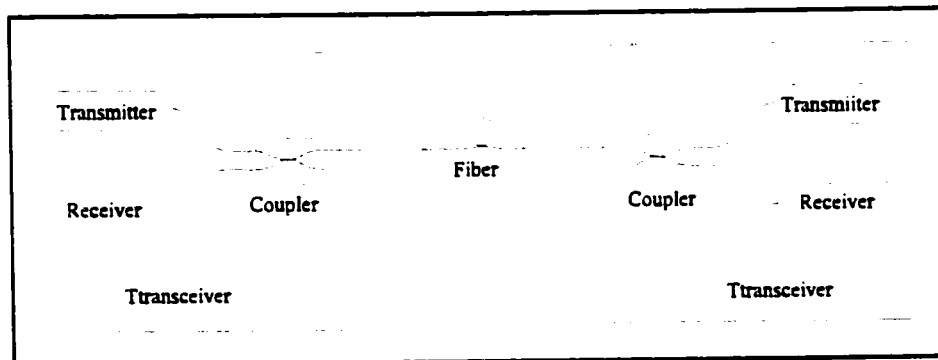


Figure 6.1 Bidirectional Transmission System

Clearly, the bidirectional transmission system can improve the system capacity, and save fiber resources. However, there are some problems which need to be solved in the bidirectional transmission system. The most important limit is the echo which is

caused by the use of a fiber coupler and the existence of Rayleigh backscatter in fiber.

6.1.1 Fiber Coupler

Fig. (6.2) is a basic structure of a four-port fiber coupler [1]. The optical power is launched into port 1, and comes out of ports 3 and 4. A very small part of the launched power is echoed to port 2. The powers in these ports are P_1 , P_2 , P_3 and P_4 .

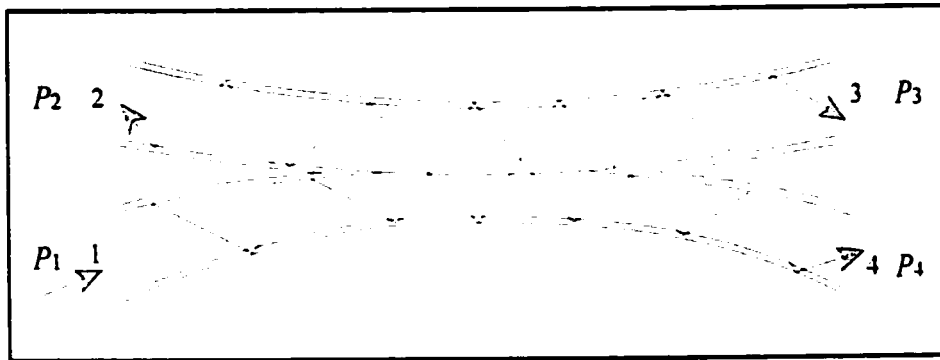


Figure 6.2 Fiber Coupler [1]

The loss parameters of this coupler are defined as follows,

the excess loss, P_{el} , is the ratio of power input to power output,

$$P_{el} = 10 \log_{10} \frac{P_1}{P_3 + P_4}. \quad (6.1)$$

The insertion loss, P_{il} , is the loss obtained for a particular port to port path. For example, the insertion loss of port 1 to port 4, is,

$$P_{il} = 10 \log_{10} \frac{P_1}{P_4}. \quad (6.2)$$

The crosstalk, P_{cr} , is the ratio of the backscatter power received at the second input port to the input power. Crosstalk provides a measure of the directional isolation. It contributes

the echo in the bidirectional transmission,

$$P_{cr} = 10 \log_{10} \frac{P_2}{P_1}. \quad (6.3)$$

Sometimes, directivity, P_{dir} , is used instead of crosstalk,

$$P_{dir} = 10 \log_{10} \frac{P_1}{P_2}. \quad (6.4)$$

The split ratio, P_{sr} , is the percentage division of the optical power between the output ports,

$$P_{sr} = \frac{P_3}{P_3 + P_4} \times 100\%. \quad (6.5)$$

Some typical specifications of WD1515 series, 1538/1558 nm bidirectional couplers from JDS Uniphase are illustrated [69],

Table 6.1 WD1515 series: 1538/1558nm Bidirectional Couplers

Parameter	Specification
Insertion loss	< 2.5 dB bidirectional system
	< 3.2 dB unidirectional system
	< 4.0 dB universal system
Bidirectional directivity	> 60 dB
Return loss	> 55 dB

6.1.2 Rayleigh Backscatter

Rayleigh scattering is a fundamental loss mechanism arising from local

microscopic fluctuations in density [3]. Density fluctuations lead to random fluctuations of the refractive index. Light scattering in such a medium is known as Rayleigh scattering. The backscattered optical power, $P_{rb}(t)$, can be obtained from the relationship [1],

$$P_{rb}(t) = \frac{1}{2} P_i S \gamma_r W_o v_g e^{(-\gamma_a v_g t)}, \quad (6.6)$$

where P_i is the optical power launched into the fiber,

S is the fraction of captured optical power,

γ_r is the Rayleigh scattering coefficient,

W_o is the input optical pulse width, and

γ_a is the attenuation coefficient.

The Rayleigh scatter loss, P_{rsl} is defined as,

$$P_{rsl} = \frac{P_{rb}(0)}{P_i}. \quad (6.7)$$

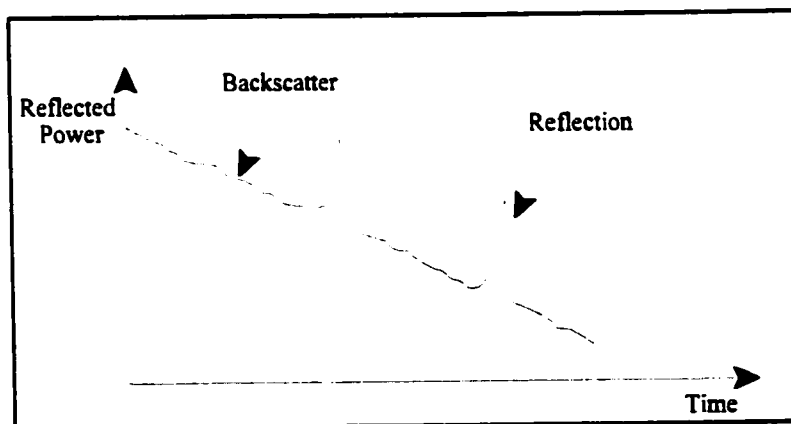


Figure 6.3 A Possible Backscatter Plot

Rayleigh scatter can be measured using OTDR (Optical Time Domain

Reflectometry). The reflected power measured by a OTDR is illustrated in Fig. (6.3).

The slope in this figure represents the loss caused by Rayleigh backscatter, and pulses are caused by reflections. The typical value of Rayleigh scatter loss is -45 dB to -60 dB [1].

6.2 Echo Cancellation

To eliminate the echo due to coupler crosstalk and Rayleigh backscatter, an echo canceller can be used. In this application, the echo canceller is an adaptive electrical filter used between the transmitter and the receiver, which estimates the echo signal from the original signal, then subtracts the estimated echo signal from the received signal. The echo cancellation is illustrated in Fig. (6.4).

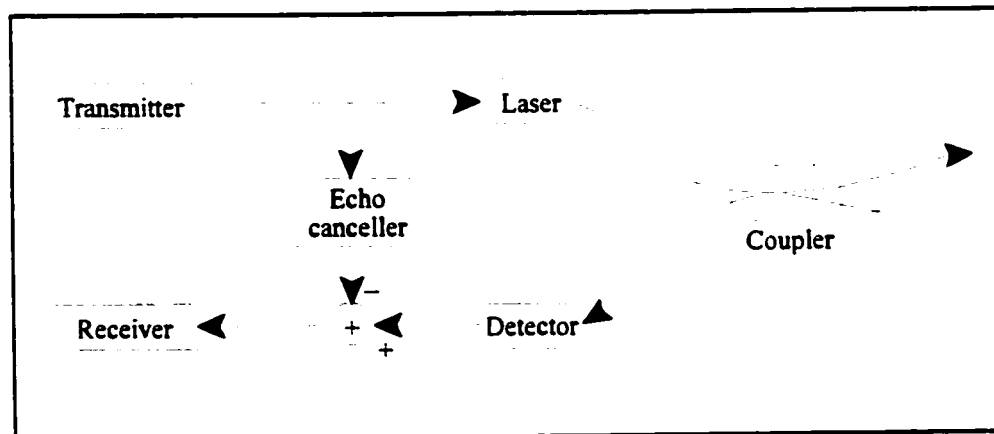


Figure 6.4 Echo Cancellation

The structure of the echo cancellers in the simulation system is shown in Fig. (6.5). The echo cancellers are located after the channel equalizers and CPI cancellers. The structure of the echo cancellers is very similar with that of the channel equalizers and CPI cancellers, and they also use the normalized LMS adaptive algorithm.

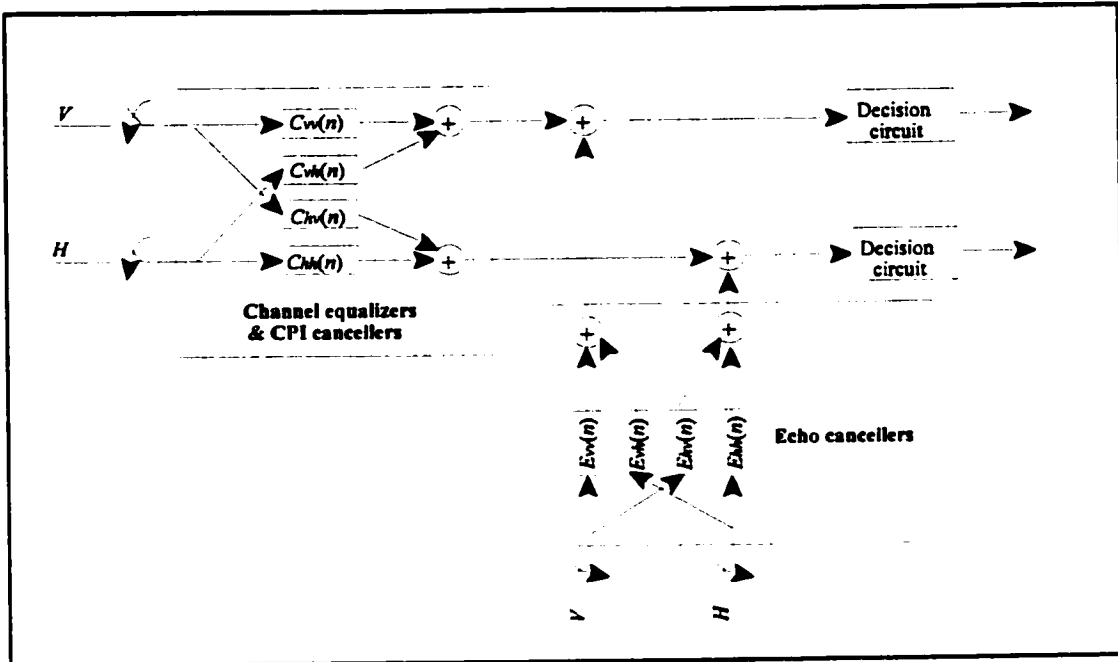


Figure 6.5 Structure of Echo Cancellers

6.3 Power Budget

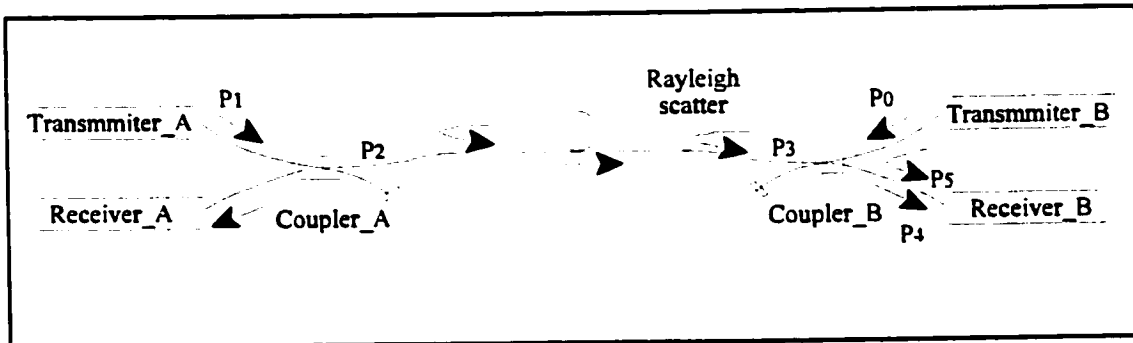


Figure 6.6 Power Budget

A power budget is needed to ensure power will reach the receiver in order to maintain reliable performance, such as a BER being less than 10^{-9} . The power budgets of two bidirectional transmission schemes are discussed, which are the bidirectional

transmission system without echo cancellers and the bidirectional transmission system with echo cancellers.

6.3.1 Power Budget of the System without Echo Cancellers

Fig. (6.6) shows the bidirectional transmission system without echo cancellers.

The power budget of this system is discussed as follows.

Given,

Wavelength: λ $\lambda = 1550 \text{ nm},$

Transmitter_B power: P_0 $P_0 = 0 \text{ dBm},$

Transmitter_A power : P_1 $P_1 = 0 \text{ dBm},$

Coupler insertion loss: P_{il} $P_{il} = 3 \text{ dB},$

Coupler crosstalk: P_{ct} $P_{ct} = -50 \text{ dB},$

Rayleigh scatter loss: P_{rs} $P_{rs} = -50 \text{ dB},$

Fiber loss: α_f $\alpha_f = 0.2 \text{ dB/km},$

System loss: M_s $M_s = 6 \text{ dB},$

Bit rate: B $B = 2.5 \text{ GHz},$

Receiver sensitivity (ASK modulation, heterodyne synchronous detection) [1]: N_p

$N_p = 36$ (average number of photons per bit),

Receiver sensitivity: P_{rec} (dBm)

$$P_{rec} = N_p h f B = N_p h \frac{c}{\lambda} B = 115 \text{ nw} = -49.4 \text{ dBm}, \quad (6.8)$$

where h is Planck's constant, $6.63 \times 10^{-34} \text{ J/Hz}$,

f is optical frequency, and

Fiber length: L , measured in km for these calculations.

Therefore, we can get,

the signal power after coupler_A, P_2 , is,

$$P_2 = P_1 - P_{it} = -3 \text{ dBm.}$$

The signal power received by coupler_B, P_3 , is,

$$P_3 = P_2 - \alpha_f \times L - M_s = -9 - 0.2 \times L \text{ dBm.}$$

The signal power received by receiver_B, P_4 , is,

$$P_4 = P_3 - P_{it} = -12 - 0.2 \times L \text{ dBm,}$$

and the echoed signal due to coupler crosstalk and the Rayleigh scatter is,

$$P_5 = P_0 + P_{ct} + P_{rl} = -47 \text{ dBm.}$$

To detect the signal without the effect of echo, the received signal P_4 should be larger sufficiently than the echo signal P_5 . From Fig. (5.4), to make the BER smaller than 10^{-9} when DGD is 100ps, the SNR is assumed to be 21 dB, that means,

$$P_4 - P_5 \geq 21 \text{ dB.}$$

Thus we have the maximum fiber length is,

$$L = 70 \text{ km.}$$

6.3.2 Power Budget of the System with Echo Cancellers

When the echo canceller is introduced in this bidirectional transmission system, the echo signal will be negligible compared with the received signal, and much smaller than the receiver sensitivity, $P_5 \ll P_{rec}$. Therefore, only the received signal needs only to be larger than the receiver sensitivity. Thus,

$$P_4 = P_{rec}$$

and the maximum fiber length is $L_2 = 187$ km.

The discussion of power budget shows the improvement in transmission distance because of the echo canceller.

6.4 Simulation of Echo Canceller using SIMULINK[®]

The bidirectional transmission system is simulated using SIMULINK[®], as shown in Fig. (6.7). The received signals are U_v and U_h , which include the echo signals. d_v and d_h are desired signals which are used for training. E_v and E_h are transmitted signals which cause the echo.

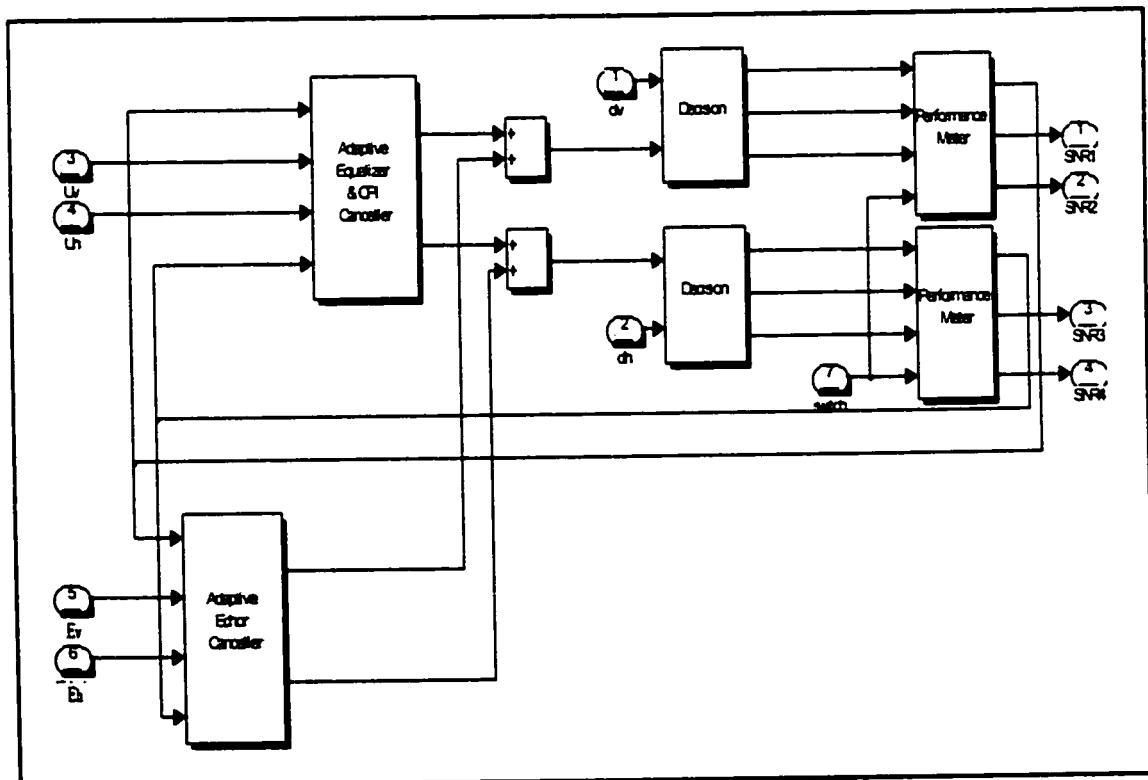


Figure 6.7 Simulation of Echo Cancellers

A 150 km bidirectional optical fiber transmission system is simulated, where

PMD is 100 ps, and the system SNR, γ_s , is 30 dB. The signal bit rate, B, is 2.5 GHz. The number of the adaptive filter taps is 8, step-size, μ is 0.4. The training time is larger than 5×10^{-6} sec. Two schemes, without echo cancellers and with echo cancellers, are investigated. The eye pattern of these two schemes are shown in Figs. (6.8, 6.9). In Fig. (6.8), because there are no echo cancellers, the eye is almost closed, which indicates that the fiber length can not exceed the maximum fiber length, 70 km. In Fig. (6.9), it is a open eye that shows the contributions of echo cancellers.

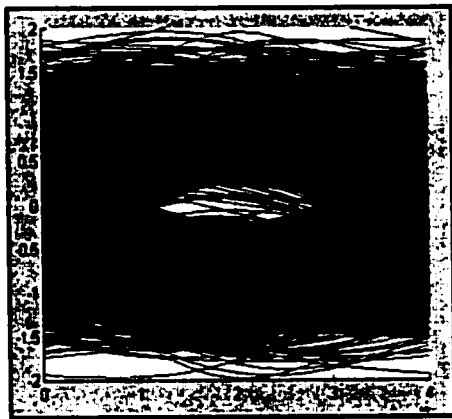


Figure 6.8 Eye Pattern without Echo Cancellers

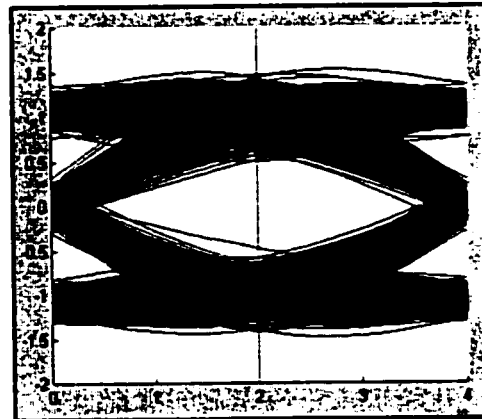


Figure 6.9 Eye Pattern with Echo Cancellers

Chapter 7

Conclusions

7.1 Conclusions

This thesis has presented the simulation of optical fiber communication systems. For the first time, a baseband QAM signal transmission system in dually polarized fiber channels with PMD was simulated. This baseband simulation system included the transmitter, the fiber channel with PMD, the Gaussian noise simulator, the baseband coherent demodulator, channel equalizers, CPI cancellers and echo cancellers.

The waveplate model has been studied to obtain the frequency and impulse responses of the fiber channel with PMD, shown in Figs. (3.4-3.7). The impulse responses showed the broadened pulse, which agree with previous experimental results, in Fig. (3.8).

Through the study of the normalized LMS algorithm applied to adaptive channel equalizers and CPI cancellers, shown in Eqs. (4.48-4.51), for the first time, a PMD compensation technique using the combination of channel equalizers and CPI cancellers was presented. The BER has been calculated when PMD is 10 ps, 100 ps and 500 ps, and the BER plot in Fig. (5.4) showed the contributions of this PMD compensation technique.

Moreover, this thesis presented, for the first time, adaptive echo cancellers applied in a bidirectional optical fiber communication system, with PMD compensation, to overcome the coupler echo and Rayleigh backscatter. For a transmission system with 100-ps PMD, the improvement in fiber length was 117 km when echo cancellers were

used.

7.2 Future Work

In this thesis, only first-order PMD was considered, neglecting chromatic dispersion and second-order PMD. These factors should be considered in future work.

Throughout this thesis, linear adaptive channel equalizers, CPI cancellers and echo cancellers were used. To incorporate nonlinear effects, such as those caused by high transmitter laser power, nonlinear filters should be used. These filters would allow further improvements in bit rate, bit error rate, or fiber length.

With the development of Si/SiGe epitaxial transistors, and other high-speed circuits, experiments to verify the simulation results could be performed. These experiments require optical transmission and reception equipment, a PMD emulator [68], and an integrated circuit design to adapt the tap weights of the adaptive filters. Only such a prototype would allow one to identify all of the complex issues associated with an implementation.

References:

- [1] John M. Senior, *Optical Fiber Communications, Principles and Practice*, 2nd edition, Prentice Hall, 1992.
- [2] Ivan P. Kaminow and Thomas L. Koch, *Optical Fiber Telecommunications IIIA*, Academic Press, 1997.
- [3] Govind P. Agrawal, *Fiber-optic Communication Systems*, New York, Wiley, 1997.
- [4] Edward A. Lee and David G. Messerschmitt, *Digital Communication*, Kluwer Academic Publishers, Boston, 1988.
- [5] Theodore S. Rappaport, *Wireless Communications: Principles and Practice*, N.J., Prentice Hall PTR, 1996.
- [6] Jerry D. Gibson, *Principles of Digital and Analog Communications*, 2nd edition, Macmillan Publishing Company, New York, 1993.
- [7] Simon Haykin, *Adaptive Filter Theory*, 2nd edition, Prentice Hall, 1991.
- [8] John G. Proakis, *Digital Communication*, 3rd edition, McGraw Hill, 1995.
- [9] Sanjit K. Mitra, *Digital Signal Processing, A Computer-Based Approach*, McGraw Hill, 1998.
- [10] *SIMULINK[®] - Dynamic System Simulation for MATLAB[®]*, MathWorks, 1999.
- [11] Weizheng Wang, *SIMULINK[®] - Communications Toolbox*, MathWorks, 1999.
- [12] *DSP Blockset For Use with SIMULINK[®]*, MathWorks, 1999.
- [13] *MATLAB[®] - The Language of Technical Computing*, MathWorks, 1999.
- [14] *Signal Processing Toolbox For Use with MATLAB[®]*, MathWorks, 1999.
- [15] Vinay K. Ingle and John G. Proakis, *Digital Signal Processing using MATLAB[®] V.4*, PWS Publishing Company, Boston, 1997.
- [16] Samuel D. Stearns and Ruth A. David, *Signal Processing Algorithms in MATLAB[®]*, Prentice Hall, New Jersey, 1996.
- [17] Paulo Marques and Fernando Sousa, *Designing an Echo Canceller System Using the TMS320C50 DSP*, TEXAS INSTRUMENTS, 1996.
- [18] David Smalley, *Equalization Concepts: A Tutorial*, TEXAS INSTRUMENTS, 1994.
- [19] *Echo Cancellation Software for the TMS320C54x*, TEXAS INSTRUMENTS, 1997.
- [20] Elliott D. Hoole, *Channel Equalization for the IS-54 Digital Cellular System With the TMS320C5x*, TEXAS INSTRUMENTS, 1994.
- [21] N. Amitay and J. Salz, "Linear Equalization Theory in Digital Data Transmission Over Dually Polarized Fading Radio Channels," *AT&T Bell Lab. Tech. J.*, 63, No. 10, pp. 2215-2259, 1984.
- [22] J. Salz, "Digital Transmission Over Cross-Coupled Linear Channels," *AT&T Bell Lab. Tech. J.*, 64, No. 6, pp. 1147-1159, 1985.
- [23] Michel Borgne, "A New Class of Adaptive Cross-Polarization Interference Cancellers for Digital Radio Systems," *IEEE J. Select. Areas Commun.*, Vol. SAC-5, No. 3, pp. 484-492, 1987.
- [24] L. J. Greenstein, "Analysis/Simulation study of Cross-Polarization Cancellation in

- Dual-Polarization Digital Radio," *AT&T Bell Lab. Tech. J.*, 64, No. 10, pp. 2261-2280, 1985.
- [25] M. Kavehrad and J. Salz, "Cross-Polarization Cancellation and Equalization in Digital Transmission Over Dually Polarized Multipath Fading Channels," *AT&T Bell Lab. Tech. J.*, 64, No. 10, pp. 2211-2245, 1985.
- [26] M. Kavehrad, "Baseband Cross-Polarization Interference Cancellation for M-Quadrature Amplitude- Modulated Signals Over Multipath Fading Radio Channels," *AT&T Bell Lab. Tech. J.*, 64, No. 8, pp. 1913-1926, 1985.
- [27] J. Salz, "A Unified Theory of Data-Aided Equalization," *B.S.T.J.*, Vol. 60, No. 9, pp. 2023-2038, 1981.
- [28] T. L. Lim and M. S. Mueller, "Adaptive Equalization and Phase Tracking for simultaneous Analog/Digital Data Transmission," *B.S.T.J.*, Vol. 60, No. 9, pp. 2039-2063, 1981.
- [29] A. Gersho and T. L. Lim, "Adaptive Cancellation of Intersymbol Interference for Data Transmission," *B.S.T.J.*, Vol. 60, No. 11, pp. 1997-2021, 1981.
- [30] D. D. Falconer, "Jointly Adaptive Equalization and Carrier Recovery in Two-Dimensional Digital Communication Systems," *B.S.T.J.*, Vol. 55, No. 3, pp. 317-334, 1975.
- [31] David G. Messerschmitt, "Minimum MSE Equalization of Digital Fiber Optic Systems," *IEEE Trans. Commun.*, vol. COM-26, No. 7, pp. 1110-1118, 1978.
- [32] David G. Messerschmitt, "Echo Cancellation in Speech and Data Transmission," *IEEE J. Select. Areas Commun.*, Vol. SAC-2, No. 2, pp. 283-297, 1984.
- [33] Kazuo Murano, Shigeyuki Unagami, Fumio Amano, "Echo Cancellation and Applications," *IEEE Communications Magazine*, pp. 49-54, Jan., 1990.
- [34] Hideaki Matsue, Hiroyuki Ohtsuka and Takehiro Murase, "Digitalized Cross-Polarization Interference Canceller for Multilevel Digital Radio," *IEEE J. Select. Areas Commun.*, Vol. SAC-5, No. 3, pp. 493-501, 1987.
- [35] B. L. Kasper, "Equalization of Multimode Optical Fiber Systems," *B.S.T.J.*, Vol. 61, No. 7, pp. 1367-1387, 1982.
- [36] M. Kavehrad, "Cross-Polarization Interference Cancellation and Nonminimum Phase Fades," *AT&T Bell Lab. Tech. J.*, 64, No. 10, pp. 2247-2259, 1985.
- [37] Aly F. Elrefaie, J. Keith Townsend, Malcolm B. Romeiser and K. Sam Shanmugan, "Computer Simulation of Digital Lightwave Links," *IEEE J. Select. Areas Commun.*, Vol. 6, No. 1, pp. 94-104, 1988.
- [38] Donald G. Duff, "Computer-Aided Design of Digital Lightwave Systems," *IEEE J. Select. Areas Commun.*, Vol. SAC-2, No. 1, pp. 171-185, 1984.
- [39] Dietrich Marcuse and Curtis R. Menyuk, "Simulation of Single-Channel Optical System at 100 Gb/s," *Journal of Lightwave Technology*, Vol. 17, No. 4, 1999.
- [40] J. H. Winters and Richard D. Giltin., "Electrical Signal Processing Techniques in Long-haul, Fiber-optic Systems," *IEEE Trans. Commun.*, vol. 38, pp. 1439-1453, 1990.
- [41] J. H. Winters and M. A. Santoro., "Experimental Equalization of Polarization Dispersion," *IEEE Photon. Tech. Lett.*, pp. 591-593, 1990.
- [42] Jack H. Winters, Zygmunt Haas, Mario A. Santoro, and Alan H. Gnauck, "Optical

- Equalization of Polarization Dispersion," *Proc. Soc. Photo-Opt. Instr. Eng.*, vol. 1787, pp. 346-357, 1992.
- [43] Jack H. Winters, "Equalization in Coherent Lightwave Systems Using a Fractionally Spaced Equalizer," *Journal of Lightwave Technology*, Vol. 8, No. 10, 1990.
- [44] A. Elrefaie, R. E. Wagner, D. A. Atlas and D. G. Daut, "Chromatic Dispersion Limitations in Coherent Optical Fiber Transmission Systems," *Electron. Lett.*, Vol. 23, pp. 756-758, 1987.
- [45] Frank Bruyere, "Impact of First- and Second-Order PMD in Optical Digital Transmission Systems," *Optical Fiber Technology 2*, pp. 269-280, 1996.
- [46] Lothar Moller and Herwig Kogelnik, "PMD Emulator Restricted to First and Second Order PMD Generation," *ECOC'99*, pp. 26-30, 1999.
- [47] William K. Burns, Robert P. Moeller and Chin-Lin Chen, "Depolarization in a Single-Mode Optical Fiber," *Journal of Lightwave Technology*, Vol. LT-1, No. 1, pp.44-49, 1983.
- [48] Fabrizio Corsi, Andrea Galtarossa and Luca Palmieri, "Polarization Mode Dispersion Characterization of Single-Mode Optical Fiber Using Backscattering Technique," *Journal of Lightwave Technology*, Vol. 16, No. 10, pp.1832-1843, 1998.
- [49] E. Iannone, F. Matera, A. Galtarossa, G. Gianello and M. Schiano, "Effect of Polarization Dispersion on the Performance of IM-DD Communication Systems," *IEEE Photonics Technology Letters*, Vol. 5, No. 10, pp. 1247-1249, 1993.
- [50] F. Bruyere and O. Audouin, "Assessment of System Penalties Induced by Polarization Mode Dispersion in a 5 Gb/s optically Amplified Transoceanic Link," *IEEE Photonics Technology Letters*, Vol. 6, No. 3, pp. 443-445, pp. 455-468, 1994.
- [51] H. Bulow, R. Ballentin, W. Baumert, G. Maisonneuve, G. Thielecke and T. Wehren, "Adaptive PMD Mitigation at 10Gbit/s Using an Electronic SiGe Equaliser IC," *Proc. ECOC'99, Nice, France*, vol II, pp. 138-139, 1999.
- [52] C.D.Poole, R.E.Wagner, "Phenomenological Approach To Polarisation Dispersion in Long Single-Mode Fibers", *Electron. Lett.*, vol. 22, no. 19, pp. 1029-1030, 1986.
- [53] C. D. Poole and C. R. Giles, "Polarization-Dependent Pulse Compression and Broadening Due to Polarization Dispersion in Dispersion-Shifted Fiber," *Optics Letters*, Vol. 13, No. 2, 1988.
- [54] C. D. Poole, Neal S. Bergano, R. E. Wagner and H. J. Schulte, "Polarization Dispersion and Principal States in a 147-km Undersea Lightwave Cable," *Journal of Lightwave Technology*, Vol. 6, No. 7, pp.1185-1190, 1988.
- [55] C. D. Poole, "Measurement of Polarization-Mode Dispersion in Single-Mode Fibers with Random Mode Coupling," *Optics Letters*, Vol. 14, No. 10, pp. 523-525, 1989.
- [56] C. D. Poole, J. H. Winters and J. A. Nagel, "Dynamical Equation for Polarization Dispersion," *Optics Letters*, Vol. 16, No. 6, pp. 372-374, 1991.
- [57] F. Curti, B. Daino, Q. Mao, F. Matera, and C. G. Someda, "Concatenation of Polarisation Dispersion in Single-mode Fibres," *Electron. Lett.*, vol. 25, pp. 290-292, 1989.
- [58] F. Curti, B. Daino, G. De Marchis and F. Matero, "Statistical Treatment of the Evolution of the Principal States of Polarization In Single-Mode Fibers," *IEEE J. Lightwave Tech*, Vol. 8, pp.1162-1166.

- [59] J. P. Elbers, C. Glingener, M. Duser and E. Voges, "Modelling of Polarisation Mode Dispersion in Single Mode Fibres," *Electron. Lett.*, vol. 33, No. 22, pp. 1894-1895, 1997.
- [60] A. M. Vengsarkar, A. H. Moesle, L. G. Cohen and W. L. Mammel, "Polarization Mode Dispersion in Dispersion Shifted Fibers: A Exact Analysis," *Processings of the OFCC*, ThJ7, 1993.
- [61] A. J. Barlow, J. J. Ramskov-Hansen and D. N. Payne, "Birefringence and Polarization Mode-Dispersion in Spun Single-Mode Fibers," *Appl. Opt.*, Vol. 20, pp. 2962-2968, 1981.
- [62] A. F. Judy, "Improved PMD stability in OptiFibers and Cables," *Processing of 43rd International Wire & Cable Symposium*, pp. 658-664, 1994.
- [63] T. Takahashi, T. Imai and M. Aiki, "Automatic Compensation Technique For Timewise Fluctuating Polarization Mode Dispersion in In-line Amplifier Systems," *Electron. Lett.*, vol. 30, pp. 348-349, 1994.
- [64] D. L. Hareme, J. H. Comfort, J. D. Cressler, E. F. Crabbe, J. Y. -C. Sun, B. S. Meyerson and T. Tice, "Si/SiGe Epitaxial-Base Transistors-Part I: Materials, Physics, and Circuits," *IEEE Transactions on Electron Devices*, Vol. 42, No. 3, pp.455-469, 1995.
- [65] D. L. Hareme, J. H. Comfort, J. D. Cressler, E. F. Crabbe, J. Y. -C. Sun, B. S. Meyerson and T. Tice, "Si/SiGe Epitaxial-Base Transistors-Part II: Process Integration and Analog Applications," *IEEE Transactions on Electron Devices*, Vol. 42, No. 3, pp.469-482, 1995.
- [66] I. P. Kaminow, "Polarization in Optical Fibers," *IEEE J. Quantum Electron.*, QE-17, pp.15-22, 1981.
- [67] R. C. Jones, "A New Calculus For the Treatment of Optical System I.," *J. Opt. Soc. Am.*, Vol. 31., pp. 488-503.
- [68] C. H. Prola Jr., J. A. Pereira da Silva, A. O. Dal Forno, R. Passy, J. P. Von der Weid, N. Gisin. "PMD Emulators and Signal Distortion in 2.48-Gb/s IM-DD Lightwave Systems," *IEEE Photonics Technology Letters*, Vol. 9, No. 6, 1997.
- [69] "WD1515 Series 1538/1558 nm Bi-directional Couplers," JDS Uniphase, http://www.jdsunph.com/html/catalog/products/menu_srch.cfm?fn=wd1515.html.
- [70] James J. Refi, "Optical Fibers for Optical Networking", <http://www.lucent.com/minds/techjournal/jan-mar1999/pdf/paper13.pdf>.

Appendix A. SIMULINK® Simulation Models

A.1 System Model

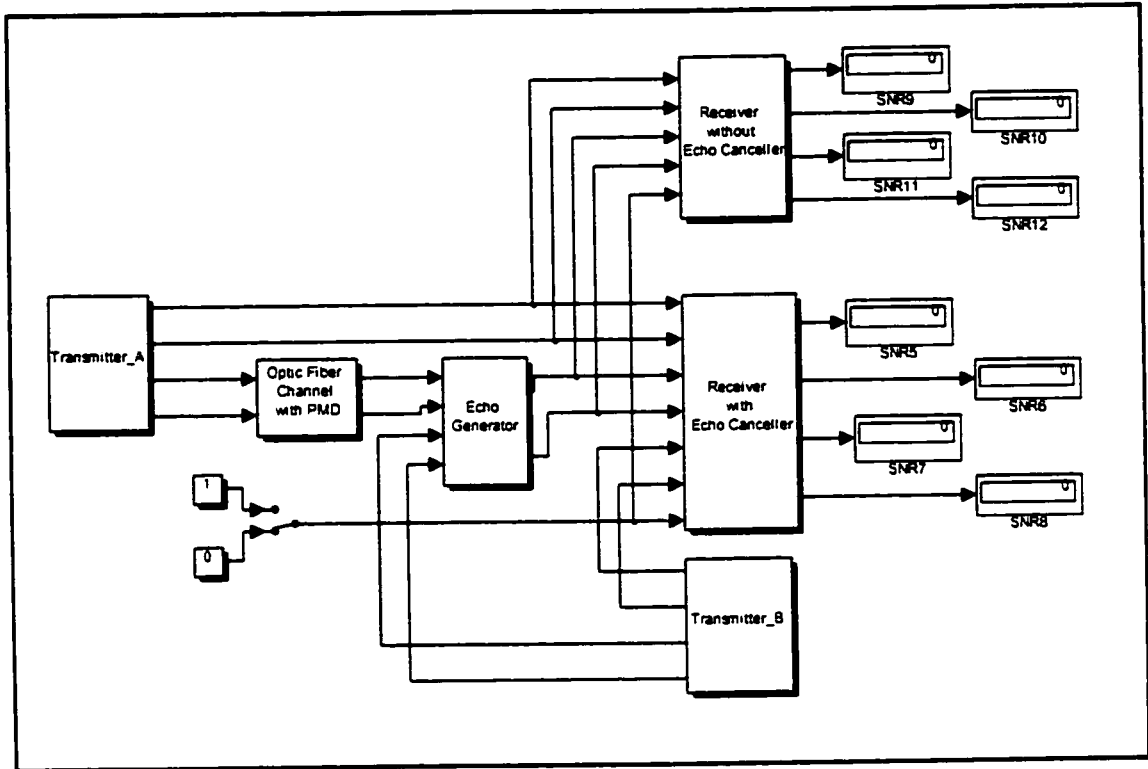


Figure A.1 System Model

Table A.1 Parameters of System Model

Parameters	Symbols	Values
Bit Rate	B	2.5e9
Fiber Segments	K	100
Frequency Points	I	128
PMD	Trms	100e-12
Bit Period	td	1/B
System Sampling Time	ts	td/I
Filter sampling Time	ts1	td/16
Noise level	N0	0.01
QAM State	M	4

A.2 System Model\Transmitter_A(B)

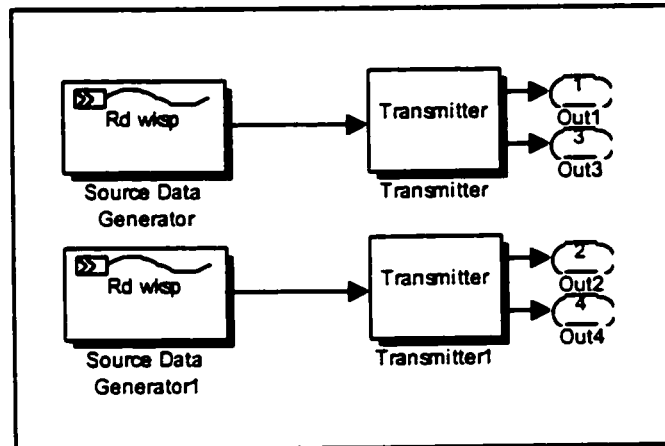


Figure A.2 Transmitter_A(B)

Table A.2 Parameters of Transmitter_A(B)

Block	Parameters	Values
Source Data Generator	Variable	randint(1e5,1,M)
	Data output sampling time (sec)	td
	Cyclic control	1
	Initial output	0

A.3 System Model\Transmitter_A(B)\Transmitter

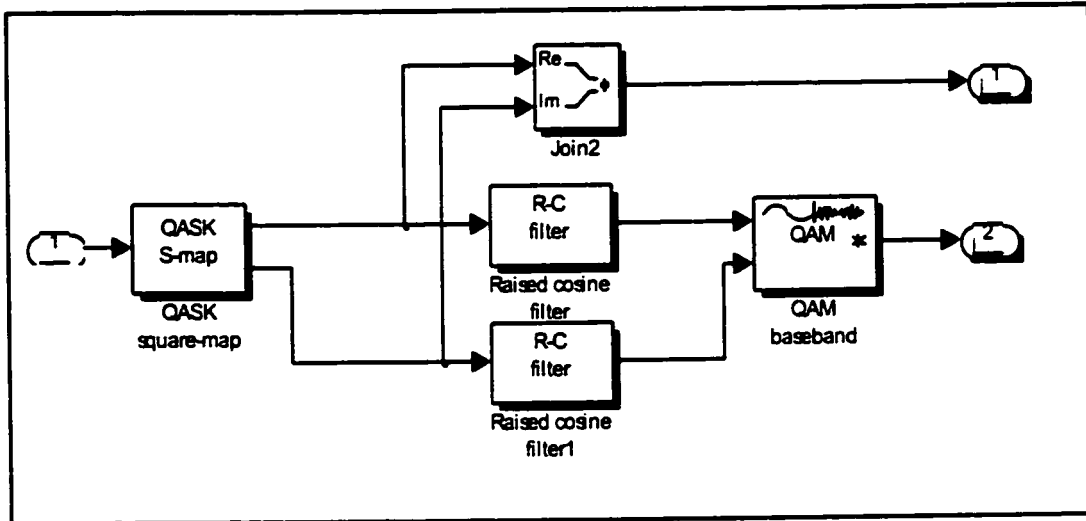


Figure A.3 Transmitter

Table A.3 Parameters of Transmitter

Blocks	Parameters	Values
QASK S-amp	M-ary number	M
	Input symbol interval and offset(sec)	td
Raised-Cosine filter	Symbol interval(sec)	td
	Computation sampling time (sec)	ts1
	Filter rolloff factor	0.8
	Delay step	6
	Filter type	'FIR'
	With or without sinc filter	1
QAM baseband	Initial phase (rad)	0

A.4 System Model\Channel

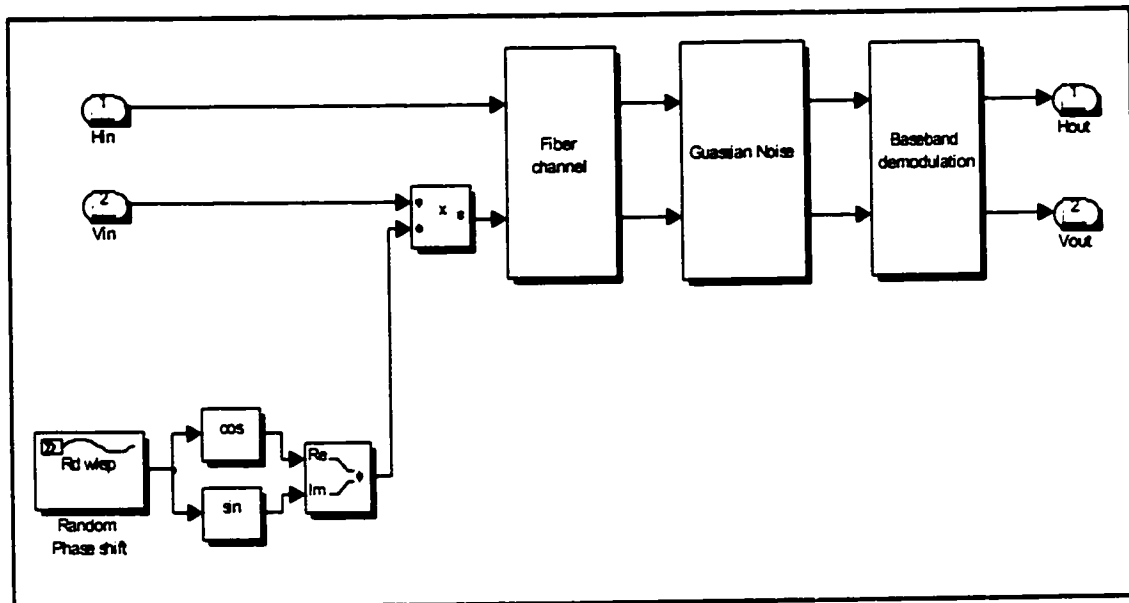


Figure A.4 Channel

Table A.4 Parameters of Channel

Block	Parameter	Value
Random Phase Shift	Variable	$(\text{rand}(1,1)*2-1)*\pi$
	Data output sampling time (sec)	$td*100000$
	Cyclic control	1
	Initial output	0

A.5 System model\Channel\Fiber Channel

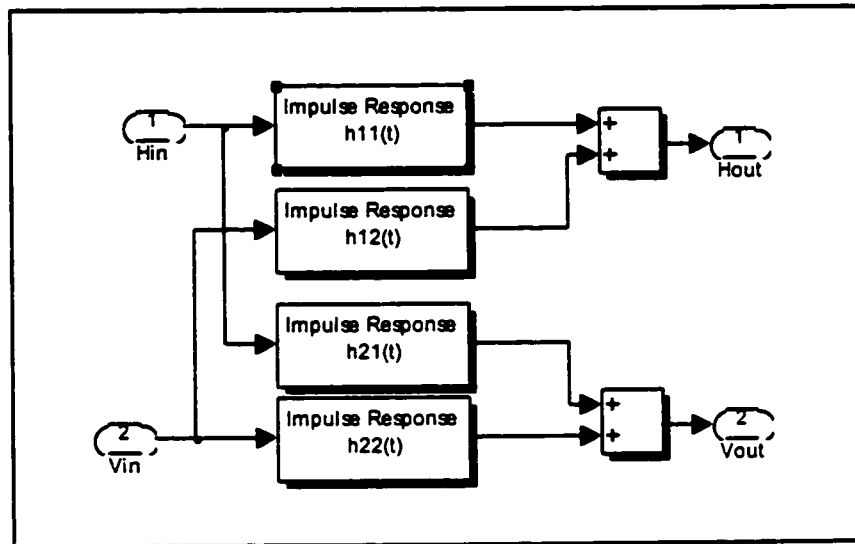


Figure A.5 Optical Fiber Channel with PMD

A.6 System Model\Channel\Fiber Channel\Impulse Response

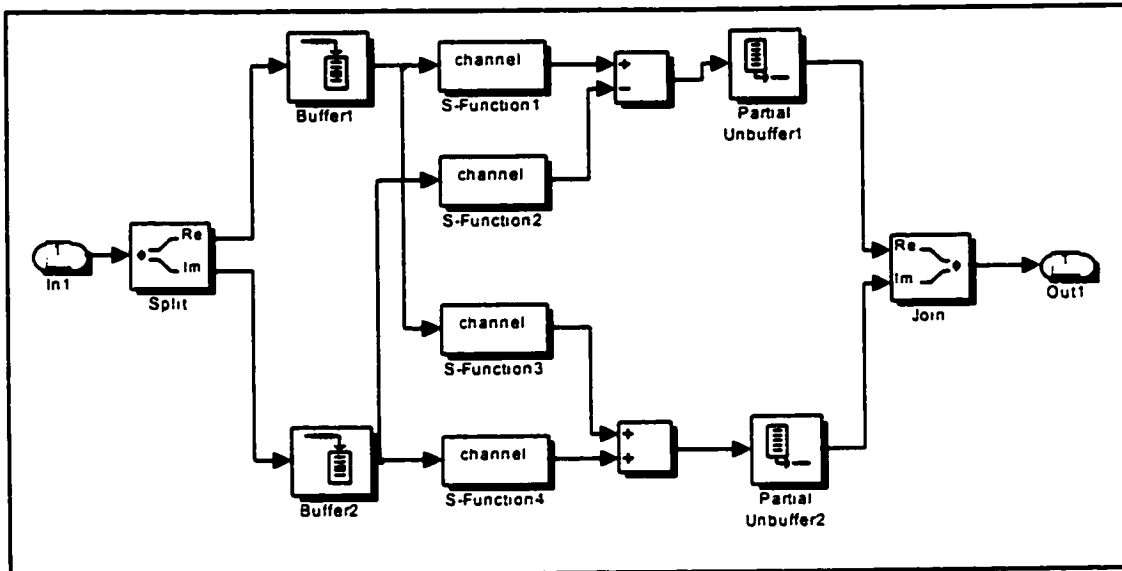


Figure A.6 Impulse Response

Table A.5 Parameters of Impulse Response

Blocks	Parameters	Values
Buffer	Buffer size	$I \cdot K$
	Buffer overlap	1
	Input sampling time	t_s
	Initial condition	0
Partial Unbuffer	Buffer size	$I \cdot K$
	First output index	$I + 1$
	Last output index	$I \cdot K$
	Number of channels	1
	Input sampling time	$t_s \cdot (I \cdot (K - 1))$
S-Function1 & S-Function4	S-function name	channel
	S-function parameters	$I, K, 0, i, t_s \cdot (I \cdot (k - 1))$ $i=1,2,3,4$
S-Function2 & S-Function3	S-function name	channel
	S-function parameters	$I, K, 1, i, t_s \cdot (I \cdot (k - 1))$ $i=1,2,3,4$

A.7 System Model\Channel\Fiber Channel\Gaussian Noise

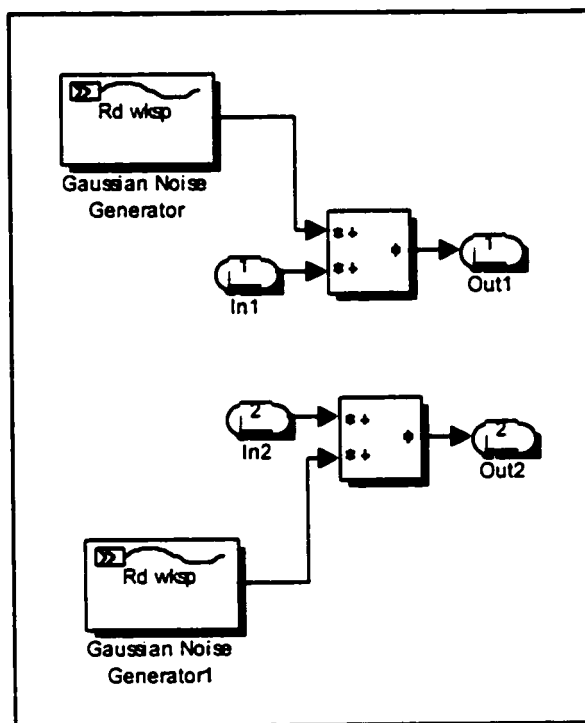


Figure A.7 Gaussian Noise

Table A.6 Parameters of Gaussian Noise

Blocks	Parameters	Values
Gaussian Noise Generator	Variable	$\text{randn}(2,1) \cdot N_0$
	Data output sampling time (sec)	td
	Cyclic control	1
	Initial output	[0 0]'

A.8 System Model\Channel\Fiber Channel\Baseband Demodulation

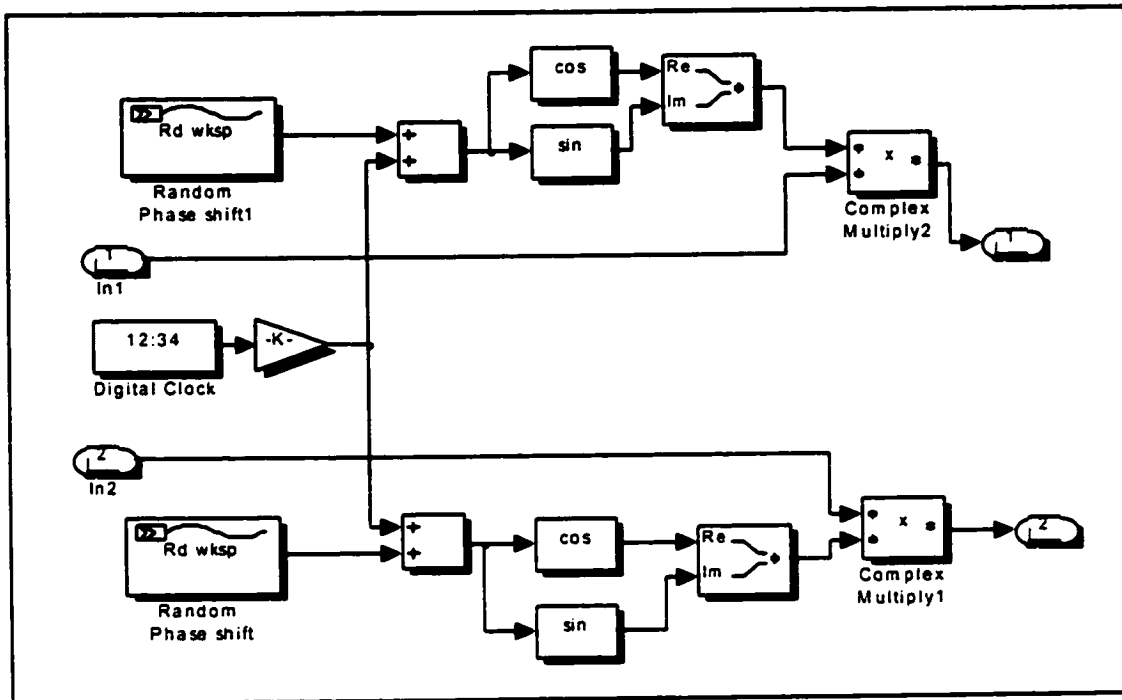


Figure A.8 Baseband demodulation

Table A.7 Parameters of Baseband Demodulation

Blocks	Parameters	Values
Random Phase Shift	Variable	$(\text{rand}(1,1)*2-1)*\pi$
	Data output sampling time (sec)	$\text{td}*100000$
	Cyclic control	1
	Initial output	0
Digital Clock	Sampling time	ts

A.9 System model\Receiver

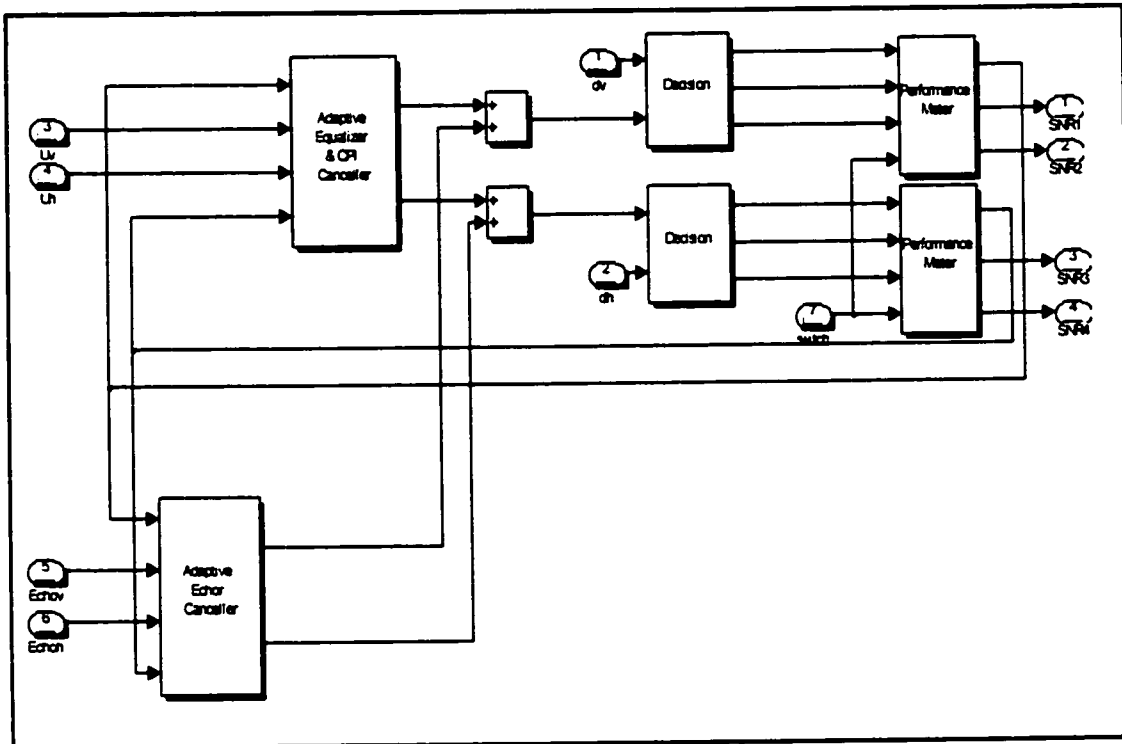


Figure A.9a Receiver with Echo Cancellers

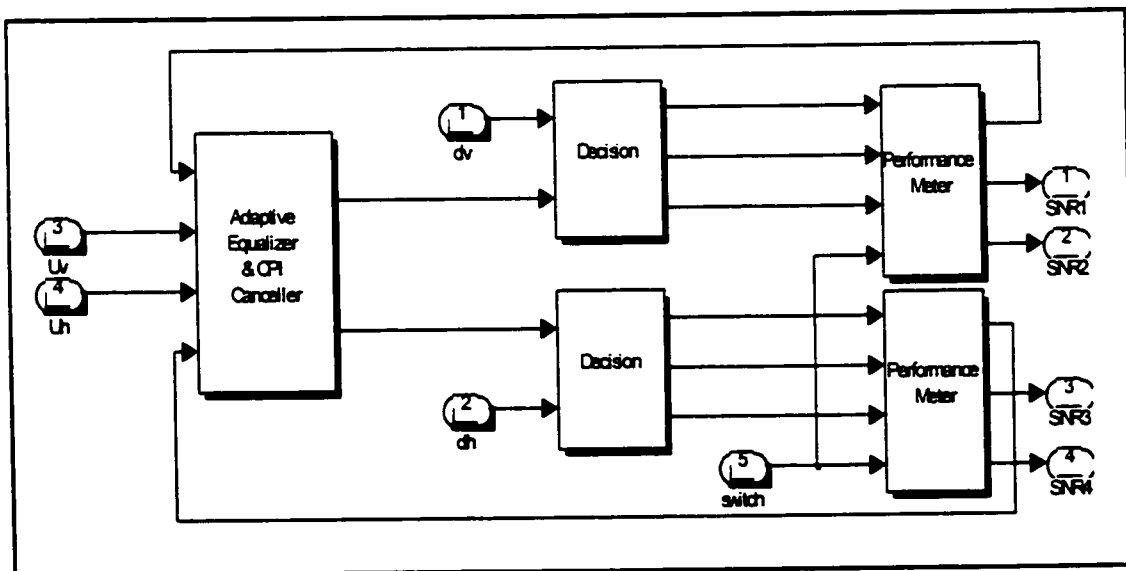


Figure A.9b Receiver without Echo Cancellers

A.10 System model\Receiver\Adaptive Channel Equalizers, CPI Cancellers and Echo Cancellers

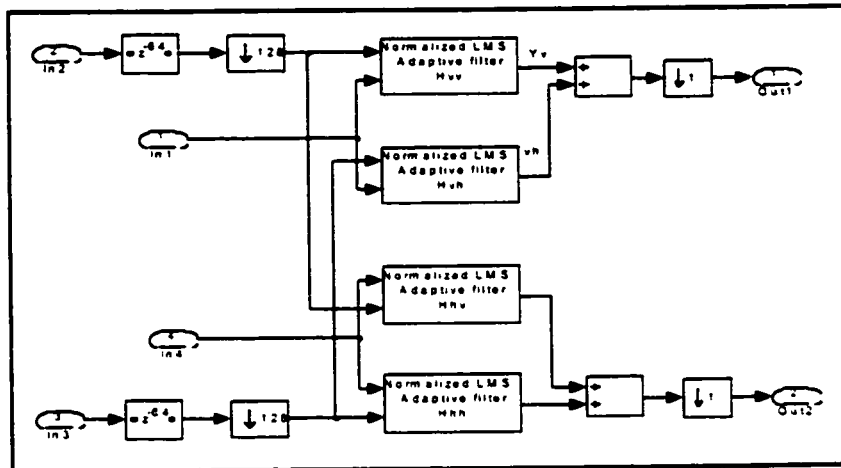


Figure A.10a Adaptive Channel Equalizers & CPI Cancellers

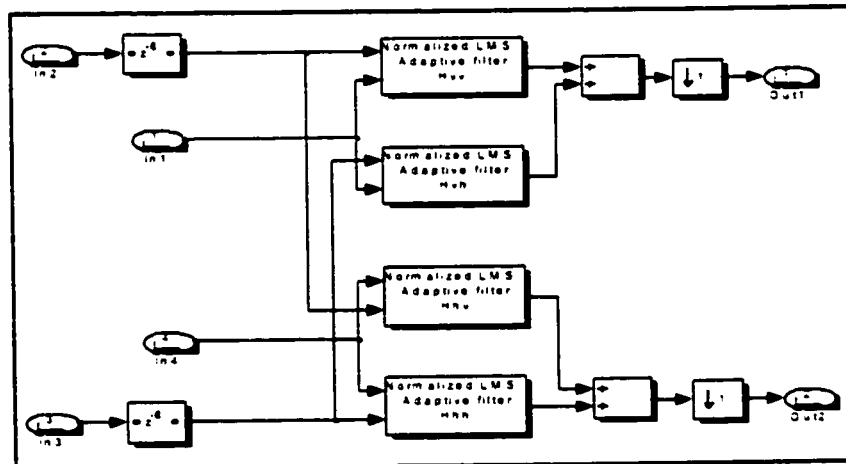


Figure A.10b Echo Cancellers

Table A.8 Parameters of Adaptive Channel Equalizers, CPI Cancellers and Echo Cancellers

Blocks	Parameters	Values
Normalized LMS Adaptive filter	FIR filter length (n)	8
	Step size (mu)	0.4
	Initial value of filter taps (ic)	zeros(1,8)
	sampling time (ts_adp)	td

A.11 System Model\Receiver with Echo Canceller\Adaptive Channel Equalizers, CPI Cancellers and Echo cancellers \Normalized LMS Adaptive Filter

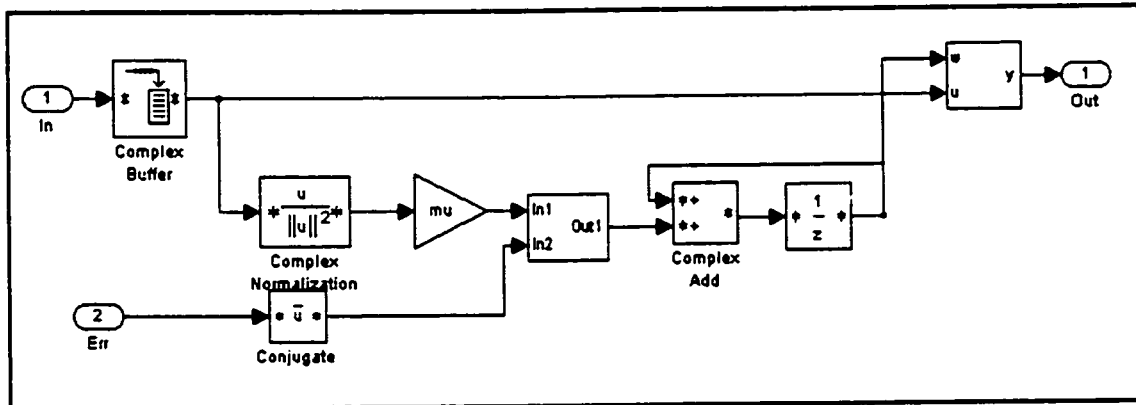


Figure A.11 Normalized LMS Adaptive filter

Table A.9 Parameters of Normalized LMS Adaptive Filter

Blocks	Parameters	Values
Complex Normalization	Norm	Squared 2-norm
	Normalization bias	1e-10
Buffer	Buffer size	n
	Buffer overlap	n-1
	Input sampling time	ts_adp
	Initial condition	0
Gain	Gain	mu
Complex Unit Delay	Initial condition	ic

A.12 System model\Receiver\Decision

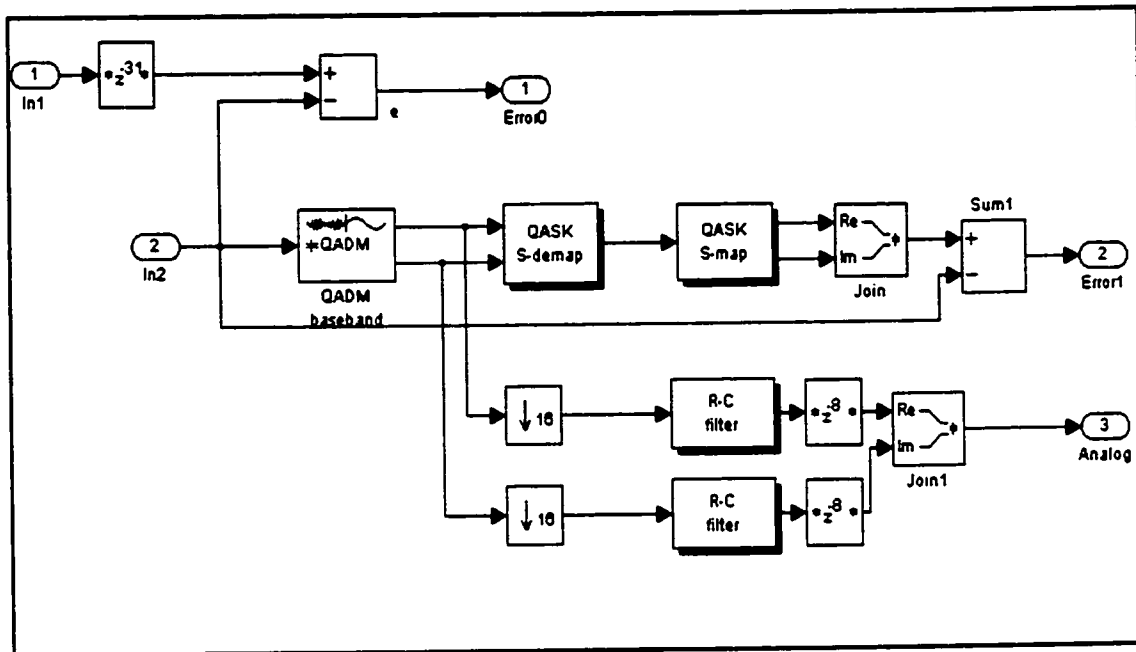


Figure A.12 Decision Circuit

Table A.10 Parameters of Decision Circuit

Blocks	Parameters	Values
Complex delay	Integer sampler delay	$2 * I * (K - 1) * ts / td + 6 + 6 + 1$
	Initial condition	0
QADM baseband	Lowpass filter numerator	1
	Lowpass filter denominator	1
	Initial phase (rad)	0
	Sample time (sec)	ts1
QASK square-demap	QASK M-ary number	M
	Output symbol interval	td
QASK square-map	QASK M-ary number	M
	Input symbol interval	td

A.13 System model\Receiver\Performance meter

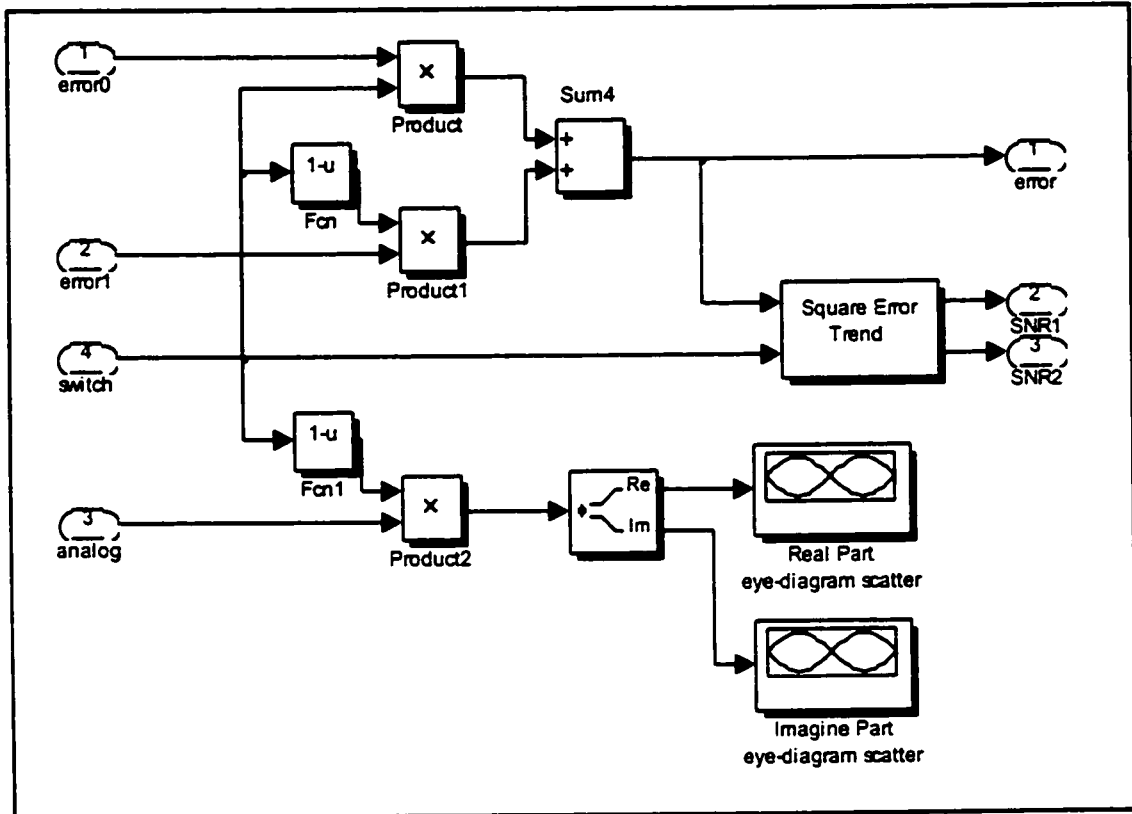


Figure A.13 Performance meter

Table A.11 Parameters of Performance Meter

Blocks	Parameters	Values
Sample time eye-diagram scatter	[Symbol interval, plot offset, decision offset]	[td, td/2, td/2]
	Lower and upper bound in-coming signal	[-1.5 1.5]
	Number of saved traces	5
	Line-type for eye-pattern diagram	'b-/r-'
	Line-type for scatter plot	0
	Plot update sample time	ts1

A.14 System model\Receiver\Performance meter\Square Error Trend

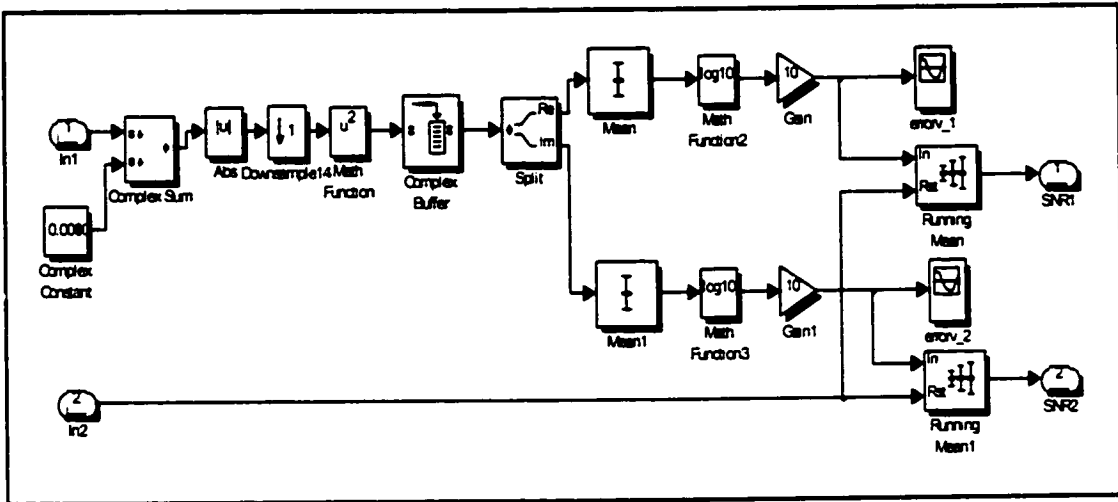


Figure A.14 Square Error Trend

Table A.12 Parameters of Square Error Trend

Blocks	Parameters	Values
Buffer	Buffer size	50
	Buffer overlap	0
	Input sampling time	td
	Initial condition	ones(1,50)+ones(1,50)*i

Appendix B. MATLAB[®] Source Code

B.1 channel.m

```
function [sys,x0,str,ts] = channel(t,x,u,flag,length,num,type,i,Ts)
```

```
%%%%%%%%%%%%%%%%%%%%%%%%%%%%%%%%%%%%%%%%%%%%%%%%%%%%%%%%%%%%%%%%%%%%%%%%%%%%%%  
% Function: channel() %  
% %  
% Purpose: Implements the impulse responses of optical fiber channels %  
% %  
% Parameters: %  
%     length: length of x %  
%     type: real or imagine part of impulse responses %  
%     i: channel bumber %  
%     Ts: sampling time %  
%     u:input signal, %  
% %  
% Copyright (c) 2000 by BIN LU. All Rights Reserved. %  
% Revision: 2.0 %  
% %  
%%%%%%%%%%%%%%%%%%%%%%%%%%%%%%%%%%%%%%%%%%%%%%%%%%%%%%%%%%%%%%%%%%%%%%%%%%%%%%
```

```
switch flag,
```

```
    %%%%%%%%%%%%%%%  
    % Initialization %  
    %%%%%%%%%%%%%%%  
    case 0,
```

```
        [sys,x0,str,ts] = mdlInitializeSizes(length,num,type,i,Ts);
```

```
    %%%%%%%%%%%%%%%  
    % Update %  
    %%%%%%%%%%%%%%%  
    case 2,
```

```
        sys = mdlUpdate(t,x,u);
```

```
    %%%%%%%%%%%%%%%  
    % Output %  
    %%%%%%%%%%%%%%%  
    case 3,
```

```
        sys = mdlOutputs(t,x,u,length);
```

```
    %%%%%%%%%%%%%%%  
    % Terminate %  
    %%%%%%%%%%%%%%%  
    case 9,
```

```

    sys = [];

    otherwise
        error(['unhandled flag = ',num2str(flag)]);
    end

%=====
% mdlInitializeSizes
% Return the sizes, initial conditions, and sample times for the S-
%function.
%=====

function [sys,x0,str,ts]=mdlInitializeSizes(length,num,type,i,Ts)
sizes = simsizes;

sizes.NumContStates = 0;
sizes.NumDiscStates = length;
sizes.NumOutputs = length*num;
sizes.NumInputs = length*num;
sizes.DirFeedthrough = 0;
sizes.NumSampleTimes = 1;

sys = simsizes(sizes);

B=dlmread('c:\FiberImp.dat');

if type==0
    x0=real(B(:,i));
elseif type==1
    x0=imag(B(:,i));
end
x0=abs(x0);
str = [];
ts = [Ts 0];

% end mdlInitializeSizes

%
%=====
% mdlUpdate
% Handle discrete state updates, sample time hits, and major time step
% requirements.
%=====
%
function sys = mdlUpdate(t,x,u)
%end mdlUpdate
sys=x;
%

```

```
%=====
% mdlOutputs
% Return the output vector for the S-function
%=====
%
function sys = mdlOutputs(t,x,u,length)
y=filter(x,1,u);
sys=(y);
```

B.2 FiberImp.m

```
function FiberImp
```

```
%%%%%%%%%%%%%%%%%%%%%%%%%%%%%%%%%%%%%%%%%%%%%%%%%%%%%%%%%%%%%%%%%%%%%%%%%%  
%  
%  
% Function: FiberImp()  
%  
% Purpose: Simulate the channel of optic fiber in the effect of PMD  
%  
% Output: Frequency response H(f) & Impulse response h(n)  
%  
%  
% Copyright (c) 2000 by BIN LU. All Rights Reserved.  
% Revision: 2.0  
%  
%%%%%%%%%%%%%%%%%%%%%%%%%%%%%%%%%%%%%%%%%%%%%%%%%%%%%%%%%%%%%%%%%%%%%%%%%%  
%
```

```
format long
```

```
%%%%%%%%%%%%%%%%%%%%%%%%%%%%%%%%%%%%%%%%%%%%%%%%%%%%%%%%%%%%%%%%%%%%%%%%%% Pre-definition %%%%%%%%%%%%%%%%%%%%%%%%%%%%%%%%%%%%%%%%%%%%%%%%%%%%%%%%%%%%%%%%%%%%%%%%%%%  
C=3e8; %%% Light speed;  
lamda0=1.55e-6;  
f0=C/lamda0;  
  
Trms=100e-12; %%%rms DGD 100ps  
K=100; %%% Segment Number  
B=2.5e9; %%% Bit rate 2.5G/10G  
I=128; %%%freq. points  
T=1/B;  
  
deltaT=T/I; %%%Sampling period;  
t=[-T/2:deltaT:T/2];  
t=t(1:I);  
  
Bw=1/deltaT; %%% Sampling frequency  
f=[-1/2:1/I:1/2]*Bw;  
f=f(1:I);  
f=f+f0;  
w=2*pi*f;  
  
PMD=Trms/(K^0.5);  
  
%%%%%%%%%%%%%%%%%%%%%%%%%%%%%%%%%%%%%%%%%%%%%%%%%%%%%%%%%%%%%%%%%%%%%%%%%% Random parameter %%%%%%%%%%%%%%%%%%%%%%%%%%%%%%%%%%%%%%%%%%%%%%%%%%%%%%%%%%%%%%%%%%%%%%%%%%%
```

```

rand_angle=(rand(2,K)-0.5)*2*pi;  %%%%%%%%% Random angle %%%%%%%%%
rand_phase=(rand(2,K)-0.5)*2*pi; %%%%%%%%% Random phase %%%%%%%%%

```

```

%%%%%%%% time delay in each segment %%%%%%%%%
dgd=DGD(PMD,K);

```

```

M=[];
for i=1:I  %%%% frequency w(i) points I

```

```

    M0=1;
    for k=1:K  %%%%%%%%% fiber segments K %%%%%%%%%

```

```

        M1=[exp(j*rand_phase(1,k))*cos(rand_angle(1,k))
exp(j*rand_phase(1,k))*sin(rand_angle(1,k));
        -exp(-j*rand_phase(1,k))*sin(rand_angle(1,k))  exp(-
j*rand_phase(1,k))*cos(rand_angle(1,k))];

```

```

        Md=[exp(j*dgd(k)/2*w(i))          0          ;
0          exp(-j*dgd(k)/2*w(i))];

```

```

        Mk=M1*Md;

```

```

        M0=M0*Mk;
    end

```

```

    M=[M;M0(1,1) M0(1,2) M0(2,1) M0(2,2)];

```

```

end

```

```

%%%%%%%% Overall frequency response %%%%%%%%%
M=[M(:,1) M(:,2) M(:,3) M(:,4)];

```

```

%%%%%%%% Magnitude of frequency response %%%%%%%%%
figure

```

```

subplot(221),plot(f,abs(M(:,1)))
title('Frequency Response: H11');
ylabel('Magnitude');
subplot(222),plot(f,abs(M(:,2)))
title('Frequency Response: H12');
ylabel('Magnitude');
subplot(223),plot(f,abs(M(:,3)))
title('Frequency Response: H21');
ylabel('Magnitude');
subplot(224),plot(f,abs(M(:,4)))
title('Frequency Response: H22');

```

```
ylabel('Magnitude');
```

```
***** Phase of frequency response *****
```

```
figure
```

```
subplot(221),plot(f,angle(M(:,1)))
```

```
title('Frequency Response: H11');
```

```
ylabel('phase');
```

```
subplot(222),plot(f,angle(M(:,2)))
```

```
title('Frequency Response: H12');
```

```
ylabel('phase');
```

```
subplot(223),plot(f,angle(M(:,3)))
```

```
title('Frequency Response: H21');
```

```
ylabel('phase');
```

```
subplot(224),plot(f,angle(M(:,4)))
```

```
title('Frequency Response: H22');
```

```
ylabel('phase');
```

```
***** Real part of frequency response *****
```

```
figure
```

```
subplot(221),plot(f,real(M(:,1)))
```

```
title('Frequency Response: H11');
```

```
ylabel('real');
```

```
subplot(222),plot(f,real(M(:,2)))
```

```
title('Frequency Response: H12');
```

```
ylabel('real');
```

```
subplot(223),plot(f,real(M(:,3)))
```

```
title('Frequency Response: H21');
```

```
ylabel('real');
```

```
subplot(224),plot(f,real(M(:,4)))
```

```
title('Frequency Response: H22');
```

```
ylabel('real');
```

```
***** Imagine part of frequency response *****
```

```
figure
```

```
subplot(221),plot(f,imag(M(:,1)))
```

```
title('Frequency Response: H11');
```

```
ylabel('imagine');
```

```
subplot(222),plot(f,imag(M(:,2)))
```

```
title('Frequency Response: H12');
```

```
ylabel('imagine');
```

```
subplot(223),plot(f,imag(M(:,3)))
```

```
title('Frequency Response: H21');
```

```
ylabel('imagine');
```

```
subplot(224),plot(f,imag(M(:,4)))
```

```
title('Frequency Response: H22');
```

```
ylabel('imagine');
```

```

***** Covert frequency responses to impulse responses *****
M=[M(I/2+1:I,:); M(1:I/2,:)];
m=ifft(M);
m=[m(I/2+1:I,:); m(1:I/2,:)];

```

```

***** Magnitude of impulse response *****

```

```

figure
subplot(221),plot(t,abs(m(:,1)))
title('Impluse Response: H11');
ylabel('Magnitude');
subplot(222),plot(t,abs(m(:,2)))
title('Impluse Response: H12');
ylabel('Magnitude');
subplot(223),plot(t,abs(m(:,3)))
title('Impluse Response: H21');
ylabel('Magnitude');
subplot(224),plot(t,abs(m(:,4)))
title('Impluse Response: H22');
ylabel('Magnitude');

```

```

***** Phase of impulse response *****

```

```

figure
subplot(221),plot(t,angle(m(:,1)))
title('Impluse Response: H11');
ylabel('phase');
subplot(222),plot(t,angle(m(:,2)))
title('Impluse Response: H12');
ylabel('phase');
subplot(223),plot(t,angle(m(:,3)))
title('Impluse Response: H21');
ylabel('phase');
subplot(224),plot(t,angle(m(:,4)))
title('Impluse Response: H22');
ylabel('phase');

```

```

***** Real part of impulse response *****

```

```

figure
subplot(221),plot(t,real(m(:,1)))
title('Impluse Response: H11');
ylabel('real');
subplot(222),plot(t,real(m(:,2)))
title('Impluse Response: H12');
ylabel('real');
subplot(223),plot(t,real(m(:,3)))
title('Impluse Response: H21');
ylabel('real');
subplot(224),plot(t,real(m(:,4)))
title('Impluse Response: H22');
ylabel('real');

```

```

***** Imagine part of impulse response *****
figure
subplot(221),plot(t,imag(m(:,1)))
title('Impluse Response: H11');
ylabel('imagine');
subplot(222),plot(t,imag(m(:,2)))
title('Impluse Response: H12');
ylabel('imagine');
subplot(223),plot(t,imag(m(:,3)))
title('Impluse Response: H21');
ylabel('imagine');
subplot(224),plot(t,imag(m(:,4)))
title('Impluse Response: H22');
ylabel('imagine');

***** save filter coefficients *****
dlmwrite('FiberImp.dat',m);

```


B.3 DGD.m

```

function z=DGD(delta,N)
%%%%%%%%%%%%%%%%%%%%%%%%%%%%%%%%%%%%%%%%%%%%%%%%%%%%%%%%%%%%%%%%%%%%%%%%
%
% Function: DGD()
% Purpose: Generate Maxwellian random DGDs
%
%
% Copyright (c) 2000 by BIN LU. All Rights Reserved.
% Revision: 2.0
%%%%%%%%%%%%%%%%%%%%%%%%%%%%%%%%%%%%%%%%%%%%%%%%%%%%%%%%%%%%%%%%%%%%%%%%

%%%%%%%% variance %%%%%%%%%
delta=((delta*1e12)^2/3)^0.5;

%%%%%%%% Gaussian distributed dispersion %%%%%%%%%
x=[0:N];
almaga=randn(3,N)*delta;

%%%%%%%% Maxwellian distributed DGD %%%%%%%%%
y=almaga.^2;
z0=(y(1,:)+y(2,:)+y(3,:)).^0.5;
z1=[];
for l=0:N
    z1=[z1 sum(z0(l,:)>1 & z0(l,:)<l+1)/N];
end
z=z0*1e-12;

rms=delta;
t=x;
z2=((2/pi)^0.5).*(t.^2)/(rms^3).*exp(-t.^2/(2*rms^2));

%%%%%%%% draw the output figure %%%%%%%%%
figure
stem(x,z1);
hold on
plot(x,z2,'r');
return

```